CHEMICAL REVIEWS

pubs.acs.org/CR

Review

Progress and Prospects in Transition-Metal Dichalcogenide Research Beyond 2D

Tomojit Chowdhury,[§] Erick C. Sadler,[§] and Thomas J. Kempa*

Cite This: *Chem. Rev.* 2020, 120, 12563–12591

Read Online

ACCESS | Metrics & More | Article Recommendations

ABSTRACT: This review discusses recent advances and future research priorities in the transition-metal dichalcogenide (TMD) field. While the community has witnessed tremendous advances through research conducted on two-dimensional (2D) TMD crystals, it is vital to seek new research opportunities beyond developed areas. To this end, in this review we focus principally on articulating areas of need in the preparation and analysis of TMD crystals encompassing dimensionalities and morphologies beyond 2D. Ultimately, the development of new synthetic methods to control key structural features of low-dimensional TMD crystals (*e.g.*, dimensionality, morphology, and phase) will afford access to a broader range of breakthrough properties for this intriguing material class. We begin with a brief overview of the evolution of 2D TMD research, discussing both the synthetic methods that have enabled the preparation of these materials and the manifold properties they possess. We focus the bulk of our review on discussion of recent advances associated with 1D TMD crystals, which are often referred to as TMD nanoribbons, and include a discussion of recent efforts in 0D systems. We discuss synthetic strategies that have been developed to prepare such beyond 2D crystals and highlight their unique physical and chemical properties. After reviewing the host of analytical tools available for characterization of TMD materials, we identify future analytical instrumentation needs. We conclude with a discussion of the prospects of beyond 2D TMD crystals in optoelectronics, catalysis, and quantum information science.

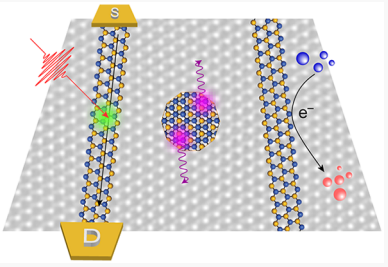

CONTENTS

Received: May 22, 2020
Published: September 22, 2020

https://dx.doi.org/10.1021/acs.chemrev.0c00505
Chem. Rev. 2020, 120, 12563–12591

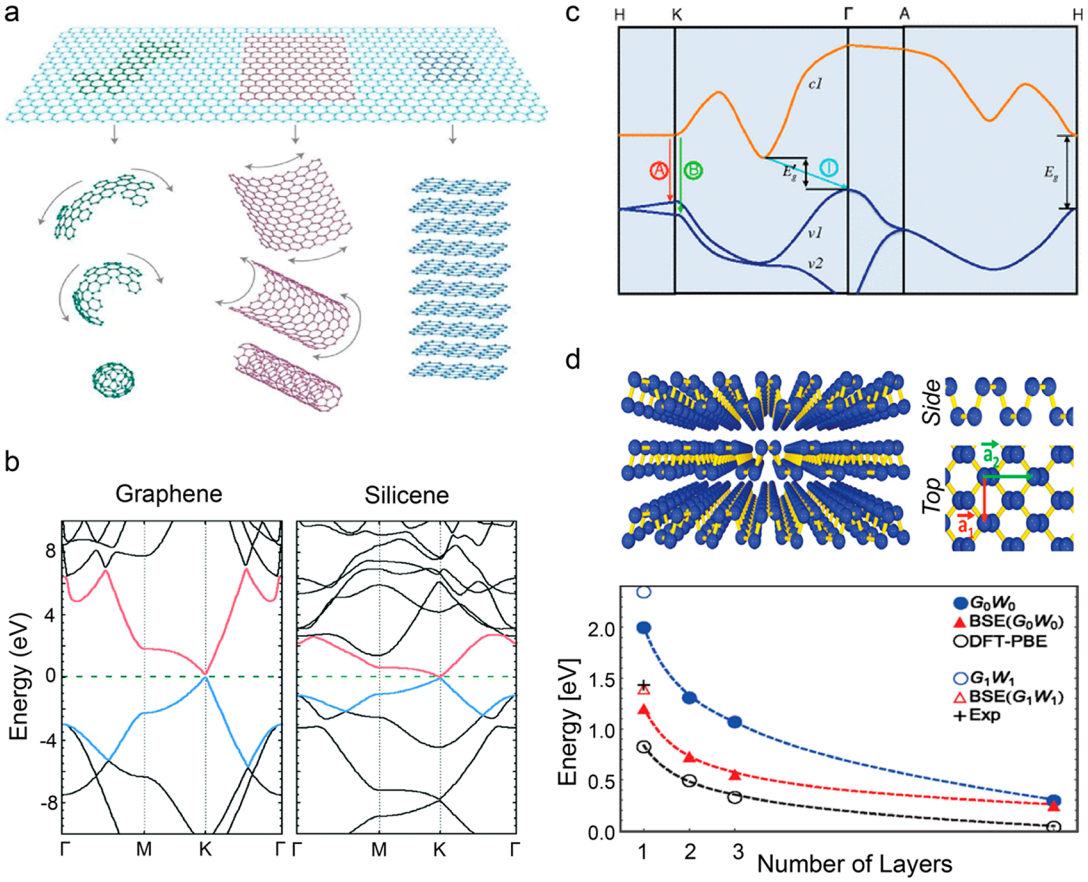

Figure 1. Two-dimensional materials. (a) Visual representation of the fullerene, nanotube, and graphene allotropes of carbon. Reproduced with permission from ref 19. Copyright 2007 Nature Publishing Group. (b) Band structures for graphene and silicene with the conduction band and valence band highlighted red and blue, respectively. Reproduced with permission from ref 11. Copyright 2014 Royal Society of Chemistry. (c) Illustration of the band structure of MoS_2 illustrating its direct and indirect band edge transitions. Reproduced with permission from ref 1. Copyright 2010 American Physical Society. (d) Illustration of vertically stacked phosphorene layers with axial and planform views of the lattice. Experimental and theoretical data of the band gap energy in phosphorene as a function of the number of layers. Reproduced from ref 25. Copyright 2014 American Chemical Society.

1. INTRODUCTION

1.1. Scope and Outline of this Review

This review chronicles key developments in the transition-metal dichalcogenide (TMD) field and advances several priorities and goals for future research.

The goal of this review will be to curate recent efforts and continuing areas of need in the preparation and exploration of TMD crystals encompassing dimensionalities and morphologies beyond 2D. Of particular importance, we feel, is the need to develop new synthetic methods to control the principal structural features of low-dimensional TMD crystals, including, (i) dimensionality, (ii) morphology, (iii) phase, (iv) layer number, and (v) layer orientation. Through controlled manipulation of these features one could elicit unique optical and electronic responses, valley-spin coupling, and moiré effects.[1−4] In general, having direct and atom-precise mastery over these and other low-dimensional materials will provide full access to their breakthrough properties and technological potential.

We begin with a brief history of the recent surge in research effort in two-dimensional (2D) TMD materials and then provide an overview of the status of the field from the standpoint of the scientific impact that 2D TMD crystals have had on the physics, chemistry, and materials science communities. We briefly discuss the synthetic methods that have enabled the preparation of 2D TMDs and review the manifold properties these materials possess. By design, our discussion of 2D TMDs will be short and we direct the reader to a number of other excellent reviews focused on crystal growth and property studies of these 2D materials.[5−11]

Our review pivots to focus on a discussion of recent advances in the area of TMD nanoribbons, or nominally 1D TMD crystals. We discuss unique synthetic strategies that have been developed to prepare such crystals and highlight their intriguing physical properties. We also discuss research in the area of 0D TMDs to further highlight the many efforts devoted to realizing low-dimensional TMD platforms beyond 2D.

Finally, our review takes a holistic view of the research prospects and priorities in the TMD field. Besides emphasizing the need for breakthroughs in synthesis, we identify critical needs in characterization capabilities which will fuel future property discovery and analysis. We then discuss priority research areas for TMD materials by highlighting how future studies can build on the vast body of effort in optoelectronics, catalysis, and quantum information science that has thus far focused on 2D TMDs. The intent in this latter section is to acknowledge the great strides made to-date while providing a focused view of research opportunities unique to 1D TMDs.

https://dx.doi.org/10.1021/acs.chemrev.0c00505
Chem. Rev. 2020, 120, 12563−12591

2. 2D TMDs: IMPACT, SYNTHESIS, AND PROPERTIES

2.1. Scientific Impact of 2D TMDs

Chemists, physicists, and materials scientists have been captivated by two-dimensional (2D) materials for more than a decade. After the discovery of an ambipolar electric field effect in graphene in 2004,[12] researchers spent the ensuing years uncovering many other exceptional, and potentially technologically relevant, features of this material, including its unique electronic structure, high electronic mobility, high thermal conductivity, and optical transparency.[11,13−20] Geim and coworkers envisioned a scenario where graphene could in principle serve as the parent material from which numerous graphitic forms of varying dimensionality can be derived, including fullerene, nanoribbons, and nanotubes (Figure 1a).[19] Inspired by the impressive research progress in the graphene field, scholars began to search for other 2D materials that could serve as platforms for the investigation of new physical and chemical phenomena. In short order, the 2D materials field expanded through seminal reports and investigations of crystals of transition metal dichalcogenides (TMDs), hexagonal boron nitride (h-BN),[21−23] silicene,[11,24] phosphorene,[25,26] and other 2D graphene analogs.[27−30] Band structure calculations identifying unique changes in bandgap as a function of material dimensionality and layer number in silicene, TMDs, and phosphorene motivated the rapid expansion of research into 2D materials beyond graphene (Figure 1b−d).[1,11,25]

The last ten years have seen preparatory methods for 2D TMDs evolve from simple bulk exfoliation to advanced bottom-up approaches involving solution- and gas-phase synthesis. The discovery that MoS_2 manifests as a direct band gap semiconductor when isolated as a single 2D layer spurred a focus on band engineering in 2D TMD materials through doping, electrostatic gating, compositional grading, and the formation of heterostructures.[1] In addition to having a layer-dependent, and therefore tunable, electronic structure, 2D TMDs exhibit strongly bound excitons,[31−35] enhanced catalytic activity of their edge states,[36−41] and novel spin/pseudospin degrees of freedom.[3,42,43] Suppressed screening interactions in 2D TMDs facilitate large exciton binding energies that are an order of magnitude greater than in conventional semiconductors and are linked with the diverse optoelectronic properties of these materials.[2] The edge sites and activated basal planes of 2D TMDs have been shown to be highly active toward catalysis of the hydrogen evolution reaction (HER).[37,44]

The diversity of properties explored and exploited within the family of 2D TMDs bodes well for future studies on TMDs involving further synthetic manipulation to yield new crystal morphologies, compositions, and dimensionalities.

2.2. Synthesis and Properties of 2D TMDs

The most widely used methods for synthesis of 2D TMDs include mechanical exfoliation,[45] solution exfoliation,[46] chemical vapor deposition (CVD),[47] metal−organic chemical vapor deposition (MOCVD), and molecular beam epitaxy (MBE).[48] Mechanical exfoliation of TMD monolayers can be accomplished through the use of scotch tape or through the adhesion of deposited polymer (*e.g.*, poly methyl-methacrylate) thin films to TMD crystals followed by etching of the growth substrate to release said crystals.[49] Though relatively straightforward and effective at yielding large amounts of transferred TMD crystals, mechanical exfoliation frequently induces damage to crystals through tearing or unwanted buckling and can introduce surface impurities. Solution exfoliation utilizes surfactants and ionic species to disrupt the weak van der Waals forces holding together the layers of the bulk TMD. Though it is a rapid preparatory route for 2D TMDs, the resulting crystals typically exhibit significant dispersity in size and quality and disordered edges.[45,46,50] In contrast, gas-phase synthetic techniques such as CVD and MOCVD typically yield 2D TMD crystals with low defect densities and more uniform size dispersions. However, these methods are generally more laborious than exfoliation for the production of single monolayers of 2D crystals. While MBE techniques generally produce 2D TMD materials of excellent quality, long synthesis times and the use of complex instrumentation present challenges and some reports have suggested that MBE-grown materials contain defects and disorder that degrade electrical performance.[51−54] Nevertheless, recent advances in MOCVD have enabled wafer-scale growth of uniform MoS_2 monolayers that exhibit high electrical performance when integrated within field effect transistor devices.[55]

Quantum size effects owing to the restricted dimensionality of 2D TMDs are central to the exceptional properties these materials exhibit. Notably, the fact that the atoms of a TMD monolayer are highly exposed offers exceptional opportunities to tune the materials' phase, composition, and electronic structure through chemical doping, surface functionalization, or through application of electrostatic potentials.[10] For example, while the 2H phase is the primary MoS_2 polymorph, with a unit cell having trigonal prismatic symmetry about the Mo atom, intercalation by alkali metals can convert this phase to the so-called 1T phase whose unit cell has octahedral symmetry about the Mo atom. Such phase changes are notable because they can be used to switch MoS_2 between semiconducting (2H phase) and metallic (1T phase) states. In addition, 2D TMD materials can be doped with guest transition metal or chalcogen atoms. Finally, crystallite morphology (*e.g.*, triangle, ribbon, and tube) plays a powerful role in determining TMD properties.

Given their diverse array of unique chemical and physical properties, and the potential to tune these properties finely, 2D TMDs have served as a rich platform for investigation of a multitude of research questions in optics, electronics, spintronics, valleytronics, and electrochemistry. Eda et al. reported photoluminescence (PL) from chemically exfoliated single-layer MoS_2 flakes that was similar to that reported previously in mechanically exfoliated films of MoS_2.[1,56,57] Scuri et al. demonstrated that single-layer $MoSe_2$,[58] when passivated by h-BN, can function as an electrically switchable reflective surface or "mirror". Such electrically tunable reflectance enables the use of such 2D layered architectures as building blocks for active optical cavities, modulators, and meta-surfaces. Wang et al. have also demonstrated the precise confinement and manipulation of electronic and excitonic excitations in a TMD monolayer by controlling electronic disorder in a 2D MoS_2 film,[59] with attendant implications for quantum computing devices. In yet another demonstration of the importance of controlling structural features of 2D TMDs, groups have shown that grain boundaries in 2D TMDs can regulate transistor channel current as a function of gate voltage and that such structure−property relations can be harnessed to yield novel field-programmable architectures.[60,61] Demonstrating the chemical relevance of 2D materials, Voiry et al. reported the enhanced activity of 1T phase WS_2 nanosheets toward catalysis of the hydrogen evolution reaction (HER).[62] This performance was attributed to the presence of strain-induced lattice distortions.

https://dx.doi.org/10.1021/acs.chemrev.0c00505
Chem. Rev. 2020, 120, 12563−12591

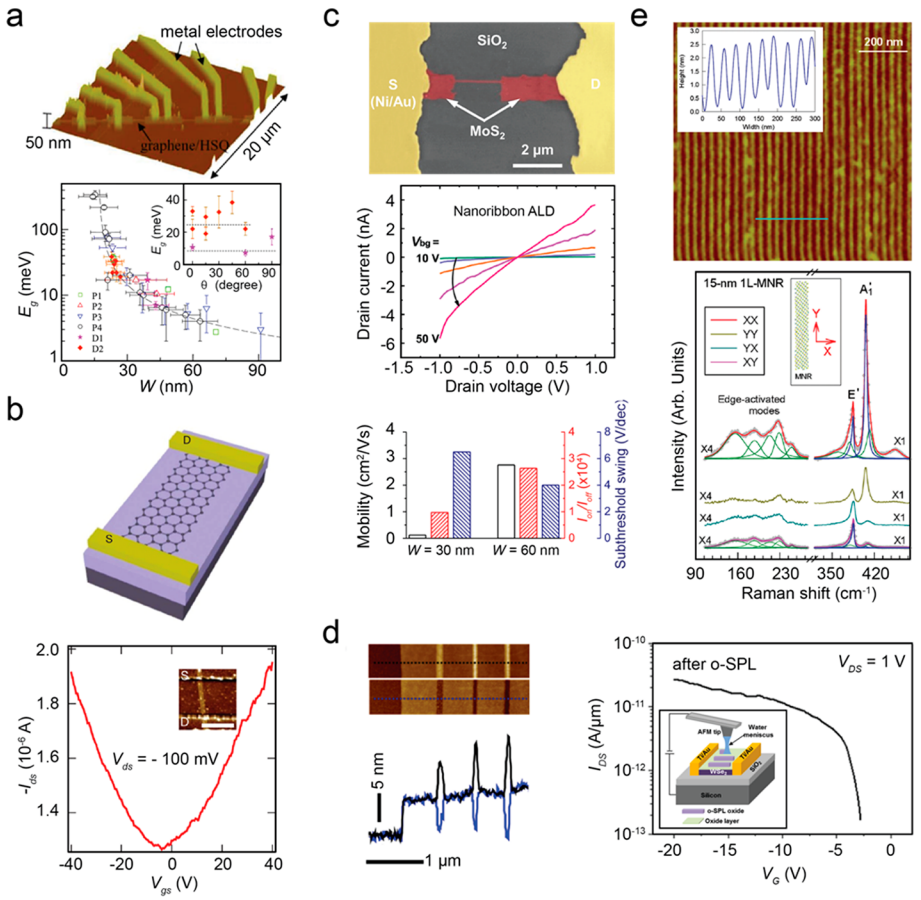

Figure 2. 1D/nanoribbon crystals prepared by top-down methods. (a) Graphene nanoribbon (GNR) device and plot showing the dependence of GNR band gap on nanoribbon crystal width. Reproduced with permission from ref 79. Copyright 2007 American Physical Society. (b) GNRs obtained from carbon nanotubes (CNTs) exhibit a "V"-shaped $I_{ds} - V_{gs}$ transport characteristic. Inset: AFM map of device; scale bar: 200 nm. Reproduced with permission from ref 82. Copyright 2009 Nature Publishing Group. (c) Monolayer MoS_2 nanoribbons obtained through scanning probe lithography (SPL) exhibit appreciable field effect mobilities. Reproduced from ref 96. Copyright 2019 American Chemical Society. (d) *p*-type doped few-layer WSe_2 nanoribbons obtained by oxidation scanning probe lithography (o-SPL). Reproduced from ref 94. Copyright 2018 American Chemical Society. (e) Single layer MoS_2 nanoribbons patterned through helium ion-beam milling exhibit noticeable anisotropy in their Raman signatures. Reproduced with permission from ref 95. Copyright 2016 Wiley-VCH.

The diverse structure−property relationships encompassed by 2D TMDs motivates continued investments in the development of synthetic strategies for control of the size, morphology, phase, and nature of interfaces within these crystals.

3. 1D TMDs: ACHIEVEMENTS AND FEATURES

3.1. Overview

It is well established that control over the dimensionality of semiconducting materials provides an important pathway toward unlocking new physical and chemical phenomena.[63] Transitioning from 2D to lower dimensionality (*e.g.*, 1D) can elicit quantum confinement effects that in turn dictate key material properties.[64,65] For example, previous efforts have demonstrated that 1D semiconductors (*e.g.*, nanowires) can be prepared using bottom-up chemical approaches and tailored to exhibit a panoply of unique properties relevant to photonics, electronics, spintronics, catalysis, biophysics, and photovoltaic energy conversion.[66−76] Moreover, shortly after graphene took the condensed matter physics community by storm,[19] many leading research groups directed their efforts to the preparation and study of dimensionally restricted variants of graphene, notably graphene nanoribbons (GNRs).[77−84] In 2007, Han et al. observed that the band gap energy in lithographically patterned GNRs can be systematically tuned by changing the GNR width, thereby setting in motion a broad-based effort focused on discovery of new low-dimensional condensed matter systems (Figure 2a).[79] Soon after, Dai and co-workers demonstrated a highly tunable field-effect mobility in GNR devices (Figure 2 (b)).[78,80,82]

Following the discovery that a single monolayer of 2D MoS_2 exhibits a direct band gap,[1] many research groups developed a keen interest in producing and examining nanoribbon-like structures of TMDs. While the number of reports on the direct synthesis of 1D TMD nanoribbons is significantly smaller as compared to reports on preparation of 2D TMDs, several theoretical analyses have indicated that 1D TMDs harbor unique features that distinguish them from their 2D analogs. These features result from the contribution and interplay of a number of structural effects unique to 1D systems, including lateral confinement effects, the strong influence of edge states that can mediate key electronic transitions, and strain fields. These structure-specific features have direct consequences on the mechanical, electronic, optical, magnetic, and thermoelectric properties of TMD nanoribbons. For example, Li et al. described armchair MoS_2 nanoribbons as nonmagnetic,[85] similar to single

https://dx.doi.org/10.1021/acs.chemrev.0c00505
Chem. Rev. 2020, 120, 12563−12591

crystal bulk MoS_2. In contrast, 1D MoS_2 nanoribbons with zigzag edges exhibit metallic behavior,[86] as seen in 2D MoS_2 sheets.[87] Notably, while 2D TMDs exhibit stable ferromagnetic ground states, 1D TMD nanoribbons elicit an edge-dependent magnetic behavior that renders the nanoribbons highly tunable and therefore potentially more compelling as a platform for magnetoresistive devices. A weak ferromagnetism has been observed in multilayer 2D TMDs, with reports suggesting that this magnetic behavior can be enhanced for single layers and small grain sizes.[87,88] In light of these results, further investigation of the magnetic features of 1D crystals is warranted. Pan et al. demonstrated that hydrogen saturation enhances magnetic states at zigzag MoS_2 nanoribbon edges and that this strategy could be used to render the material *n*- or *p*-type through systematic passivation of dangling bonds with H.[89] While zigzag edge-terminated MoS_2 nanoribbons were found to be interesting for their tunable magnetic and electronic properties, semiconducting armchair 1D MoS_2 nanoribbons have been shown to exhibit impressive thermoelectric performance as judged by a high thermoelectric figure of merit (ZT) value of 3.4.[90−92] Aside from the unique edge-dependent properties that manifest in TMD nanoribbons, the observation of dimension-dependent phase transitions in 1D TMD nanostructures further motivates research on this class of material. For example, Zan et al. demonstrated that the crystallographic 1T polytype, while metastable in 2D TMDs, is the thermodynamically favored phase in TMDs that assume a 1D morphology.[93] The 1T phase is favored in 1D TMDs because the higher coordination of edge metal atoms in this phase reduces edge dangling bonds, whose role in increasing the crystal energy is particularly apparent in 1D systems.

3.2. Synthesis and Fabrication Challenges

The aforementioned studies show that if crystal edge-structure and/or dimensionality can be experimentally controlled reliably and to atom-levels of precision, then 1D TMD nanoribbons could emerge as a promising material testbed for electrocatalytic, optoelectronic, magnetoresistive, and thermoelectric device applications. It is important to note that the preparation, manipulation, and investigation of nanoscale wide and atomically thin 1D crystals is inherently challenging. The following is a brief survey of the existing methods for fabrication and synthesis of TMD crystals.

Top-down. Top-down processing methods involving direct patterning,[94−97] etching,[97,98] and intercalation have been used to prepare TMD nanoribbons and other nongraphene 2D materials with tunable properties (Figure 2c,d).[94,96,99] We direct our readers to the review of Stanford et al. concerning progress toward and challenges in top-down nanofabrication and patterning of 2D materials beyond graphene.[100] Lithographically patterned MoS_2 nanoribbons with widths ranging from 30 to 400 nm showed width-dependent field-effect mobilities and on/off ratios of approximately 10^6.[96,97] In addition, FETs fashioned from MoS_2 nanoribbons prepared through traditional top-down methods exhibited a clear transition from depletion-mode to the enhancement-mode operation upon careful manipulation of their channel width.[97] MoS_2 nanoribbons (width: ∼50 nm) obtained through plasma etching exhibited field-effect mobilities and on/off ratios comparable to those measured in nanoribbons prepared lithographically.[98] Helium ion milled TMD nanoribbons showed tunable light emission and a substantial Raman spectral anisotropy as a function of their width (Figure 2e).[95]

Although top-down techniques can achieve sub-50 nm nanoribbon widths through the systematic removal of material from a parent 2D TMD, there are notable challenges with traditional processing methods. Electron-beam lithography (EBL) and photolithography have intrinsic resolution limits that prevent patterning of materials with the atomic precision that is ultimately desired. Moreover, the production of large quantities of nanoscale crystals is hampered by the intrinsically low-throughput of electron-beam lithography. Finally, the quality of crystal edges and basal planes can be adversely affected by the liquid- or gas-phase etching conditions the crystals are subjected to during top-down processing.

Bottom-up. Though bottom-up synthetic approaches are a highly desirable alternative for the preparation of low-dimensional crystals, there is a notable dearth of such methods for explicitly controlling the size, shape, phase, and dimensionality of nanoribbon structures. Bottom-up methods offer several advantages compared to top-down processes. Critically, direct synthesis can, in principle, overcome the resolution limits, fidelity issues, and low throughput of lithography-based approaches. Furthermore, synthesis offers a plausible approach toward creating in-plane heterostructures and crystals with complex hierarchies. Notably, recent efforts on the synthesis of TMD nanoribbons have demonstrated ribbons with high-quality edges (< ∼3 nm edge deviations) that are superior to those found on ribbons (∼10−30 nm edge deviations) fabricated via lithography and etching.[94,96,101−104]

The preparation, manipulation, and investigation of nanoscale wide and atomically thin 1D crystals is inherently challenging. Nevertheless, opportunities abound, and it is the goal of this review to provide perspective on these challenges and on the mandates for future research. In addition, the shortage of mechanistic insights into the highly asymmetric and often nonequilibrium growth modes responsible for such anisotropic ribbon structures mandates the development of new analytical and theoretical tools. The small lateral size of 1D TMD crystals restricts the efficacy of some existing ex situ measurement techniques that are widely utilized for 2D TMDs. Insights into the critical nucleation processes and substrate interactions that take place during synthesis of 1D materials are also lacking. For example, Cheng et al. reported that $MoSe_2$ nanoribbons with spatially modulated edges can be synthesized in a ultrahigh vacuum (UHV) chamber on Au(100) surfaces, thereby articulating the importance of considering the role of substrates in dictating the growth of low-dimensional crystals.[101] Continued development of *in situ* analytical methods will be vital for improved measurement, and perhaps even modulation, of the growth mechanism of such 1D crystals in real time. For example, Cho et al. have utilized an UHV reaction chamber equipped with a quadrupole mass spectrometer (QMS) to monitor the dissociative adsorption of gaseous species on surfaces, the evolution of substrate morphology, and the kinetics of film growth.[105]

Despite recent progress in the TMD nanoribbon community, there is still an extensive need for new crystal growth methods and characterization tools that will enable the fashioning of crystals beyond 2D sheets, the subsequent exploration of their unique mechanical, optical, and electrical properties, and their integration into high-performance devices.

3.3. New Synthetic Strategies for 1D TMDs

Recently a number of creative strategies have been developed for synthesis of 1D TMD crystals.

https://dx.doi.org/10.1021/acs.chemrev.0c00505
Chem. Rev. 2020, 120, 12563−12591

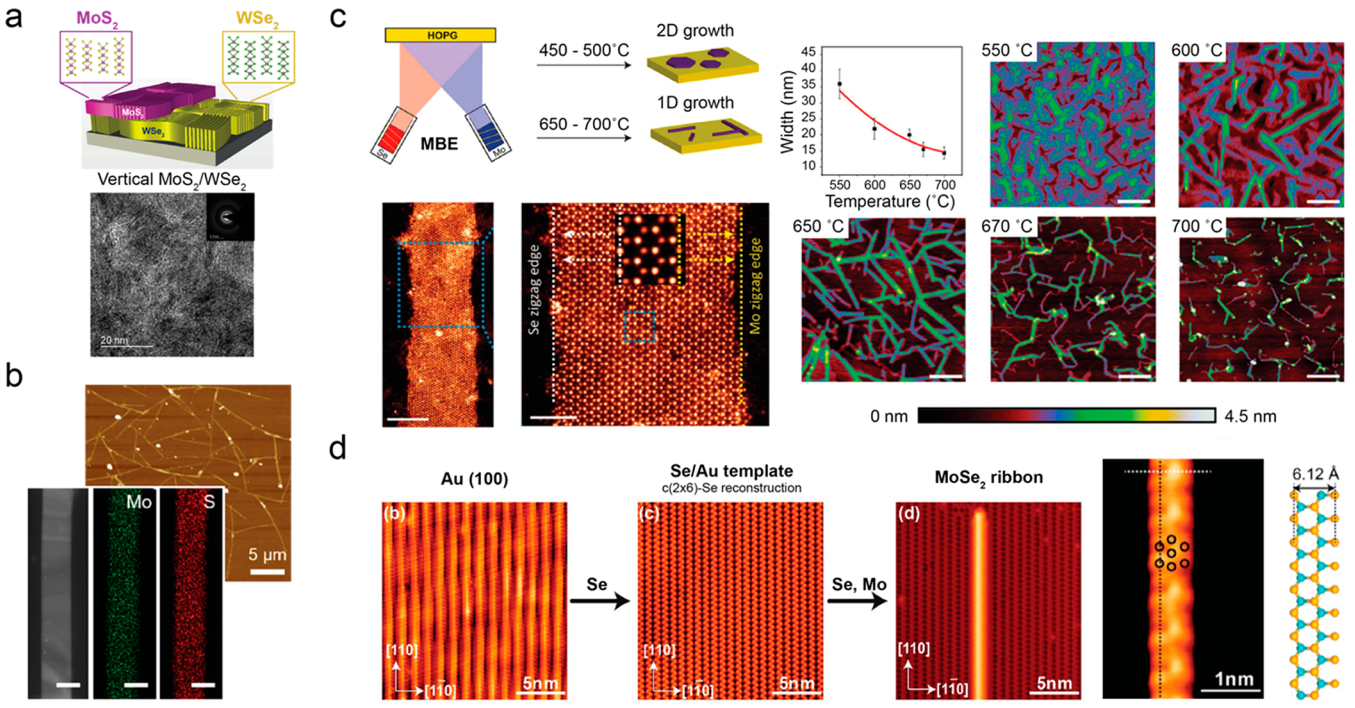

Figure 3. TMD nanobelts and wires prepared by bottom-up methods. (a) Vertically oriented MoS_2/WSe_2 heterostructures synthesized via sequential growth of WSe_2 and MoS_2. Reproduced from ref 108. Copyright 2015 American Chemical Society. (b) MoS_2 nanobelts synthesized by an atmospheric CVD process. Scale bars: 100 nm. Reproduced from ref 109. Copyright 2018 American Chemical Society. (c) Growth of $MoSe_2$ nanoribbons whose widths can be tuned through adjustment of the substrate temperature during molecular beam epitaxy (MBE). Scale bars (left to right): 5, 2, and 200 nm (panels to the right). Reproduced with permission from ref 103. Copyright 2017 Wiley-VCH. (d) Growth of ultranarrow $MoSe_2$ nanoribbons on Au(100) substrates in an ultrahigh vacuum (UHV) chamber with corresponding characterization by high-resolution scanning tunneling microscopy (STM) at ∼0.4 K. Reproduced from ref 101. Copyright 2017 American Chemical Society.

3.3.1. Vertically Oriented TMD Crystals. Early efforts explored new deposition modalities and the use of substrate templates to effect control over the morphology, dimensionality, and activity of TMD materials. In 2013, Kong et al. demonstrated that vertically oriented MoS_2 and $MoSe_2$ nanobelts can be grown on a range of substrates through a kinetically gated growth method.[106] When oriented perpendicular to their substrate, the TMD layers provide an entirely edge-terminated surface that contributes to the high catalytic activity of these films toward the hydrogen evolution reaction (HER).[106,107] Following this study, Yu et al. reported the synthesis of vertical TMD heterostructures comprised of MoS_2 and WSe_2 and characterized the resulting diode properties of devices fabricated from these heterostructures (Figure 3a).[108] Recently, one-dimensional MoS_2 nanobelts were obtained via an alternative atmospheric CVD growth process and were subsequently shown to support enhanced light scattering (Figure 3b).[109] It is important to note that the aforementioned vertically oriented crystals consist of slabs containing many laterally clustered layers[106−109] and that the properties of such ensembles can differ substantially from those of single-layer 2D TMD crystals oriented parallel to the substrate plane.[61] Moreover, vertically- and horizontally oriented TMD crystals typically grow via substantially different mechanisms. Adding to researchers understanding of the synthetic parameter space for TMD growth, it has been shown that the transition metal (Mo, W) seed layer plays a crucial role in determining the growth direction of TMD crystals. For example, while thick (>3 nm) metal (Mo, W) seed layers initiate vertical growth, thinner (1−3 nm) seed layers yield predominantly horizontal growth.[110] Apart from seed layer thickness, there are other factors that can be responsible for determining crystal growth directions. For example, the high intrinsic strain of a TMD nucleosome can give rise to vertically aligned nanosheets.[111] Moreover, in a demonstration of how reaction conditions can significantly alter crystal geometry, it has been shown that a large chalcogen:metal ratio and high chalcogen evaporation temperature (to provide high chalcogen flux) yields vertically aligned TMD flakes, while a lower ratio and lower temperature favors the growth of horizontal TMD sheets.[112]

3.3.2. Horizontally Oriented TMD Crystals. More recently, researchers have focused on the synthesis of horizontally oriented 1D TMD crystals with exceptionally narrow widths in order to examine the unique electrical, optical, and magnetic properties such dimensionally restricted crystals may support. Recent results by Cheng et al. have shown that high aspect ratio (>100:1) $MoSe_2$ nanoribbons with tunable widths can be grown on Au(100) substrates.[101] This growth process involved an initial step of selenium (Se) deposition onto pristine Au (100) to furnish a Se/Au (100) surface template. Following this, codosing the template surface with molybdenum (Mo) and selenium (Se) resulted in the formation of $MoSe_2$ nanoribbons of ∼1 nm width. The highly anisotropic surface reconstruction of the Se/Au (100) template was implicated in guiding the formation of the high aspect ratio $MoSe_2$ nanoribbons (Figure 3d).[101] Notably, high-resolution scanning tunneling microscopy and spectroscopy (STM/STS) studies revealed a crossover from metallic to semiconducting behavior when traversing the STS probe from the edge to the center, respectively, of an ∼2−4 nm wide 1D $MoSe_2$ nanocrystal. Meanwhile, ultranarrow (∼0.7 nm) nanoribbons displayed predominantly metallic behavior. Finally, Poh et al. demon-

https://dx.doi.org/10.1021/acs.chemrev.0c00505
Chem. Rev. 2020, 120, 12563−12591

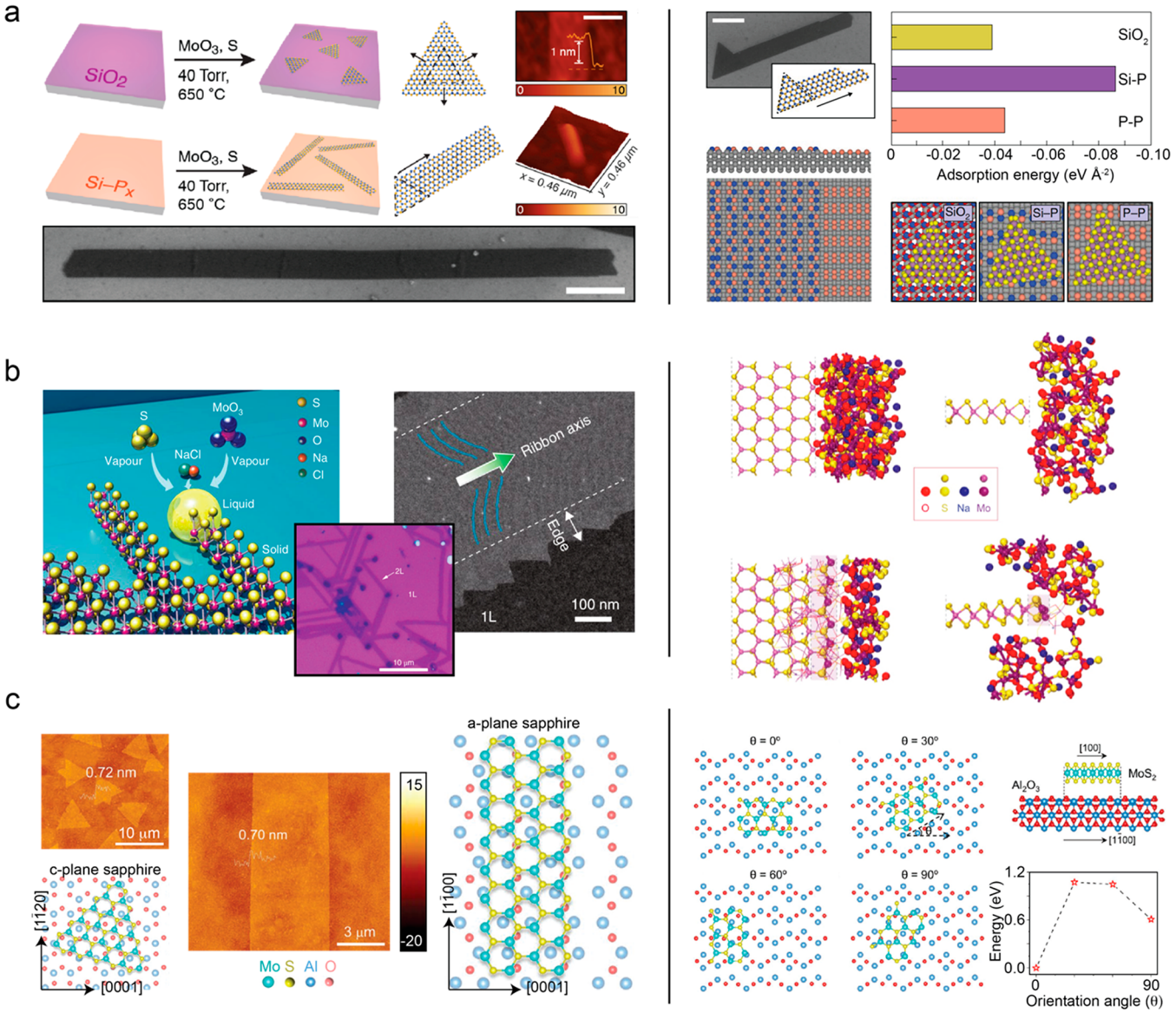

Figure 4. 1D/nanoribbon TMD crystals prepared by bottom-up methods. (a) (Left) Anisotropic and width-tunable MoS_2 nanoribbons grown on a Si−P designer growth substrate showing exceptional height and width uniformity. Scale bars: 250 nm (top), 500 nm (bottom). (Right) Experimental data and DFT calculations supporting a novel growth mode for TMD nanoribbons on Si−P surfaces. 1D crystals grow following a heterogeneous nucleation process from nanoscale 2D seeds, which are selectively stabilized on the Si−P designer surface. Blue, gray, salmon, pink, yellow, and red spheres are Si (surface), Si (bulk), P, Mo, S, and O atoms, respectively. Scale bar: 500 nm. Reproduced with permission from ref 104. Copyright 2020 Nature Publishing Group. (b) (Left) Vapor−liquid−solid (VLS) growth of MoS_2 nanoribbons from NaCl catalyst droplets. (Right) DFT-MD simulation results showing the initial (top) and the final (bottom) stages of the MoS_2 precipitation process from the catalyst droplet. Reproduced with permission from ref 115. Copyright 2018 Nature Publishing Group. (c) (Left) Gas phase synthesis of MoS_2 on *c*-plane and *a*-plane sapphire substrates yields anisotropic growth of rectangular (ribbon-like) MoS_2 domains. (Right) DFT calculated structures of MoS_2 seeds oriented at different angles with respect to the *a*-plane sapphire substrate. A calculation of seed crystal adsorption energy as a function of orientation with respect to sapphire substrate reveals the 0° orientation to be the most stable configuration from whence MoS_2 grains grow. Reproduced with permission from ref 122. Copyright 2020 Wiley-VCH.

strated the large-area synthesis of 1D $MoSe_2$ nanoribbons with atomically sharp zigzag edges by using molecular beam epitaxy (MBE) (Figure 3c).[103] Collectively, these and other studies on the synthesis of 1D $MoSe_2$ nanoribbons,[102,113] exemplify the burgeoning interest in the development of novel synthetic methods for preparation of high-quality nanoribbons.

The preparation of nanobelts and few-atom-wide wires of TMDs spurred the development of other novel methods for the preparation of tailored low-dimensional crystals. Kempa and co-workers recently introduced the concept of using designer surfaces, which are prepared through chemical treatment of known substrates, to control the morphology and dimensionality of TMD materials.[104] The authors showed that a Si(001) substrate pretreated with phosphine (PH_3) facilitates the rapid unidirectional growth of MoS_2 nanoribbons with high aspect ratios of ∼10:1 (Figure 4a).[104] The presence of Si−P surface dimers is instrumental to the process of stabilizing incipient and nanosized TMD seed crystals from whence heterogeneous nucleation takes place to yield the 1D crystals.[105] Notably, the widths of the MoS_2 nanoribbons can be systematically

https://dx.doi.org/10.1021/acs.chemrev.0c00505
Chem. Rev. 2020, 120, 12563−12591

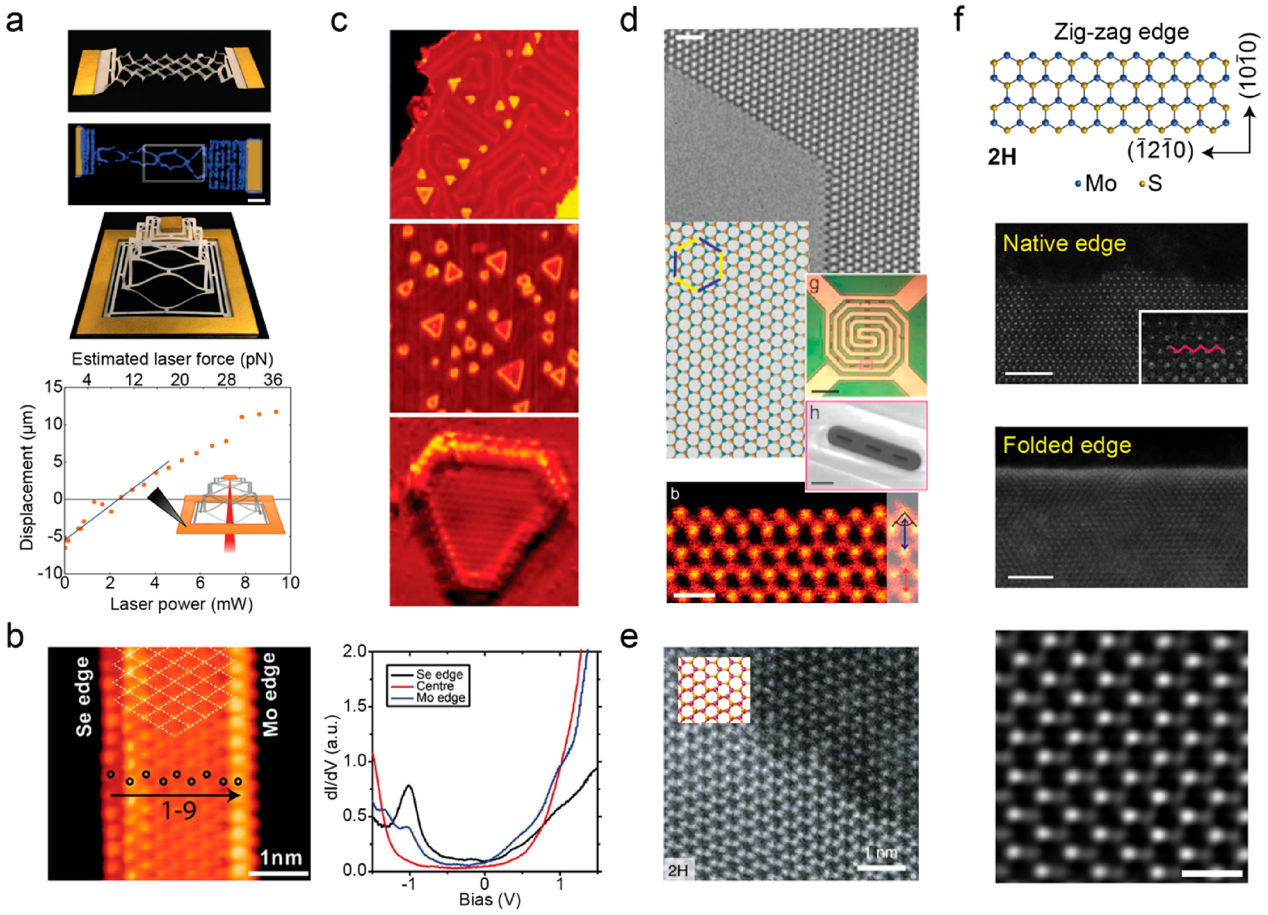

Figure 5. Physical properties of 1D/nanoribbon crystals: edges and defects. (a) Graphene kirigami involving interconnected graphene ribbons, which were prepared through top-down fabrication from graphene sheets. Scale bar: 10 μm. Reproduced with permission from ref 128. Copyright 2015 Nature Publishing Group. (b) Scanning tunneling microscopy (STM) and spectroscopy (STS) suggest that the edges of $MoSe_2$ nanoribbons are metallic, while the interior is predominantly semiconducting. Reproduced from ref 101. Copyright 2017 American Chemical Society. (c) STM images of MoS_2 clusters on Au(111) reveal conducting edge states. Field of view (top to bottom): 470 × 470 Å^2, 470 × 470 Å^2, and 60 × 60 Å^2. Reproduced with permission from ref 37. Copyright 2007 American Association for the Advancement of Science. (d) Thermal annealing of single-layer MoS_2 performed *in situ* within an ac-STEM creates atomically sharp zigzag edges. Scale bars: (top to bottom) 1 nm, 0.1 mm, 5 μm, and 0.5 nm. Reproduced from ref 137. Copyright 2017 American Chemical Society. (e) MoS_2 nanoribbons grown by VLS adopt type 2H-stacked bilayers. Purple and yellow spheres represent Mo and S atoms, respectively. Scale bar: 1 nm. Reproduced with permission from ref 115. Copyright 2018 Nature Publishing Group. (f) MoS_2 nanoribbons grown on Si−P designer substrates exhibit edges with the zigzag atomic configuration and occupy the 2H crystallographic phase. Notably, the nanoribbons can fold along their longitudinal edges and form visible moiré interference patterns. Scale bars: (top to bottom) 2 nm, 2 nm, 5 Å. Reproduced with permission from ref 104. Copyright 2020 Nature Publishing Group.

controlled in the range of 50 nm to over 1 μm by altering the concentration of PH_3 introduced during the Si surface pretreatment step. The synthesis was shown to be general for the growth of other TMD ribbons. Because of the reduced dimensionality of 1D MoS_2 crystals, the nanoribbons exhibited photoluminescence that is blue-shifted by ~50 meV with respect to that of 2D MoS_2 crystals.[1,55,114] Other notable features included the fact the crystals exhibited edges which were nearly 1 order of magnitude sharper than those obtained through conventionally processed (*i.e.*, with lithography and etching) TMD nanoribbons. The broad range over which the dimensions of the crystals could be controlled exceeded levels demonstrated through previous efforts. More broadly, the development of new classes of designer surfaces has the potential to demonstrate unprecedented levels of low-dimensional crystal growth control with attendant benefits to basic science and technology.

Demonstrating an alternative approach to growth of TMD nanoribbons, Li et al. showed that the vapor−liquid−solid (VLS) growth mechanism can be harnessed to prepare MoS_2 ribbons on crystalline surfaces.[115] This method involves the crystallization of MoS_2 nanoribbons from molten catalyst droplets comprised of NaCl, MoO_3, and dissolved sulfur (Figure 4b).[115] Na and MoO_3 readily form a eutectic under the authors' reaction conditions thus facilitating VLS growth of the MoS_2 nanoribbons.[116] This study found a strong correlation between the alignment of the nanoribbons and the orientation of the underlying growth substrate,[115] much like previous demonstrations of in-plane VLS growth of nanotubes and nanowires[117,118] and of gas-phase synthesis of graphene nanoribbons (GNRs) on germanium substrates.[119−121]

Returning to the subject of using substrate interactions to tailor the growth of TMD crystals, Ma et al. recently reported that gas-phase synthesis of MoS_2 on *a*-plane sapphire substrates yields rectangular MoS_2 grains, while growth on the *c*-plane sapphire produces typical triangular MoS_2 crystals (Figure 4c).[122] Growth temperature was found to play a critical role in the morphological evolution of the crystals and their alignment with respect to the *a*-plane sapphire substrate. Additionally,

https://dx.doi.org/10.1021/acs.chemrev.0c00505
Chem. Rev. 2020, 120, 12563−12591

photoluminescence (PL) arising from the as-grown rectangular MoS_2 crystals was weaker relative to the PL from triangular MoS_2 grains and this effect was attributed to strong crystal−substrate coupling.

3.4. Physical Properties of 1D TMDs

3.4.1. Role of Edges and Defects. 1D crystals and nanoribbons obtained via bottom-up synthetic or top-down processing methods can support mechanical, optical, electronic, and magnetic properties that are distinct from those that manifest in their 2D crystal counterparts. Before utilizing these dimensionally restricted materials for new applications in nanoscience and nanotechnology their physical properties must be enumerated.

Though the term 1D TMD could be used to encompass both nanoribbons and nanotubes, our review focuses on the chemistry and physics of nanoribbons. Nanoribbons are essentially atomically thin 2D TMD sheets wherein one lateral dimension has been reduced substantially enough to give rise to confinement phenomena. Given this definition, we will use the terms 1D TMD and nanoribbon interchangeably through this review and aim to differentiate nanoribbons as a class of 1D TMD from TMD nanotubes, which are cylindrical cage-like structures, akin to carbon nanotubes. Seminal work from Tenne et al. has elaborated on the structure and properties of TMD nanotubes, many of which can be prepared through annealing of 2D TMD films under reducing atmospheres[123,124] to yield multiwalled tubes whose diameters typically range between 30 to 150 nm.[125] The structural distinctions between nanoribbons and nanotubes can be expected to endow each material with unique properties and uniquely accessible phenomena. Because of their open structure, nanoribbons, unlike closed cylindrical TMD nanotubes, can present "free" and well-defined crystalline edges (*e.g.*, zigzag or armchair) that impose interesting edge-dependent chemical and physical properties. Furthermore, nanoribbons are, in principle, capable of showing both 1D and 2D confinement effects as a result of their significantly restricted lateral dimensions and atomically thin nature. Though TMD nanotubes predominantly reveal only 1D confinement, they can exhibit intriguing chirality and curvature-dependent correlated properties (*e.g.*, superconductivity) and hence serve as a distinct model system for studying pairing mechanisms in non-centrosymmetric systems.[126,127]

The micro/nanostructure and dimensionality of layered materials has been shown to play a crucial role in determining many of their physical properties. For example, the structure and ordering of edge sites influences the selectivity and activity of TMD catalysts. Moreover, the size and shape of 2D materials dictates how readily they may undergo folding or other mechanical distortion. As an example of the unique mechanical properties encompassed by 1D crystals derived from 2D materials, Blees et al. used top-down fabrication to prepare graphene ribbon-based devices that could be remotely actuated to induce reversible crumpling (Figure 5a).[128] This study demonstrated how mechanical folding of low-dimensional crystals can be harnessed and, more broadly, motivates the search for strategies to create functional devices whose properties are responsive to externally applied optical, thermal, magnetic, or chemical gradients.

The edges of nanoribbons can assume zigzag or armchair configurations, each of which endows the nanoribbon with distinct electrical and magnetic properties.[40,85,129−132] In addition, the higher stability of nanoribbons relative to 2D layers offers advantages for studying nanoribbon properties under a wide range of experimental conditions.[129] Interestingly, calculations suggest that few unit-cell wide TMD nanoribbons having zigzag edges are of metallic character, whereas bulk 2D TMD crystals are predominantly semiconducting.[129] This calculation agrees well with the experimental findings of Cheng et al., who showed that the electrical properties of $MoSe_2$ nanoribbons switch from metallic to semiconducting character as a function of ribbon width (Figure 5b).[101] Edge sites also participate in and define the catalytic activity of low-dimensional atomic crystals. Jaramillo et al. demonstrated that the edge sites in MoS_2 nanocrystals are catalytically more potent than are terrace sites, and that the extent of hydrogen evolution is directly proportional to the number of edge sites (Figure 5c).[37,38] Given the non-negligible fraction of edge to basal plane sites in nanoribbons, especially ultranarrow nanoribbons, it is reasonable to assume that TMD nanoribbons could serve as attractive catalysts for HER.[36,101,104]

In addition, it has been shown that the magnetic behavior of TMD nanoribbons can be systematically tuned by altering their width. Density functional theory (DFT) calculations carried out by Chen et al. predicted that ferromagnetism can be induced in 1T'-phase MoS_2 nanoribbons through the incorporation of edge reconstructions.[133] Importantly, the magnetic moment in these nanoribbons has been predicted to vary between 0.1 and 1.2 μ_B (μ_B: Bohr magneton) as a function of the nanoribbon width. Moreover, a recent study showed through calculation that monolayer 1T'-phase MoS_2 exhibits insulating behavior arising from topological and excitonic phenomena that cooperatively increase the bulk gap by breaking crystal inversion symmetry.[134] More research is needed to flesh out the extent to which the optical absorption and emission spectra of TMD nanoribbons exhibit a topological dependence.

Given the importance of using edge modification as a route toward manipulation of a 1D crystal's mechanical, electronic, and magnetic properties, recent efforts have focused on demonstrating exceptional control over the structure, uniformity, and composition of these crystal edges. Already, researchers have demonstrated the sensitivity of the physical properties of phosphorene nanoribbons on their edge termination.[135,136] Chen et al. used aberration corrected scanning transmission electron microscopy (ac-STEM) to confirm that atomically abrupt zigzag edges are formed when MoS_2 nanoribbons are subjected to annealing at 800 °C on an *in situ* heating stage within the microscope.[137] This study revealed that the zigzag edge exists in a unique Mo-terminated configuration that may be exploited to further tune quantum mechanical phenomena extant in such nanoribbons (Figure 5d).[137]

Increased focus on direct synthesis of atom-precise TMD crystals has led to experimental work showing that $MoSe_2$ and MoS_2 ribbons with nearly atomically sharp zigzag edges can be synthesized through gas-phase methods (Figure 5e,f).[35,101,104,115,137] Future research efforts would benefit enormously from having not only a detailed structural and electronic understanding of edge terminations within 1D crystals but also the means to manipulate these edges at will using physical and/or chemical means.

Defects in 2D TMDs play an important role in determining their electronic,[60,138] optical,[139,140] magnetic,[141] and electrochemical features, and it is anticipated that the defects will play an equal potent role in defining and modulating the properties of lower dimensionality (*e.g.*, 1D) crystal systems.[39,142] Intrinsic

https://dx.doi.org/10.1021/acs.chemrev.0c00505
Chem. Rev. 2020, 120, 12563−12591

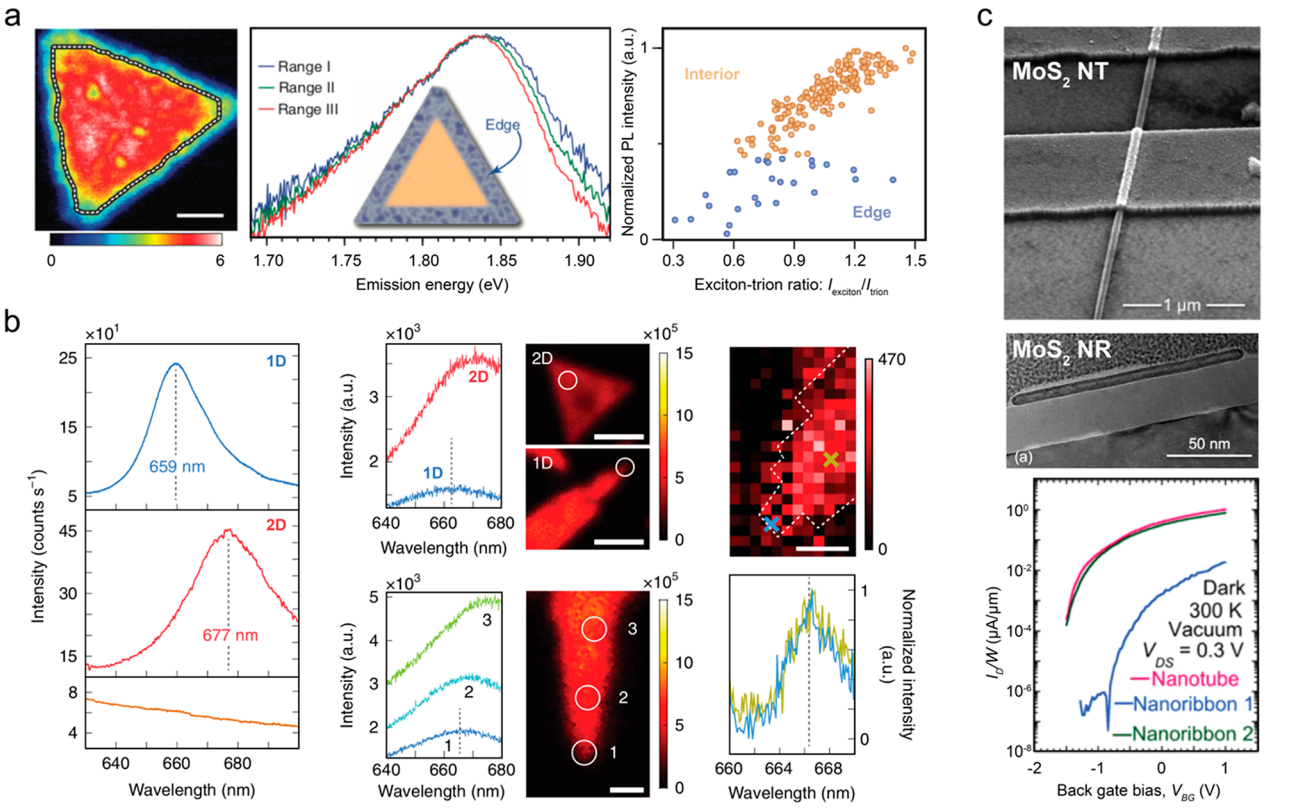

Figure 6. Physical properties of 1D/nanoribbon crystals: optical and electronic effects. (a) Near-field photoluminescence (PL) map and spectra collected from the edge region of a single-layer 2D MoS_2 crystal. The data reveal the relative excitonic and trionic contributions to the total PL emission. Scale bar: 1 μm. Reproduced with permission from ref 156. Copyright 2015 Nature Publishing Group. (b) Far-field and near-field PL maps and spectra obtained from 1D MoS_2 crystals and tapered 1D MoS_2 crystals all of which were grown on Si−P designer surfaces. The data identify that MoS_2 nanoribbons exhibit an emission that is blue-shifted relative to the 2D MoS_2 crystals and can be tuned by adjusting the nanoribbon width. Scale bars (PL maps): (top left) 2 μm, (bottom left) 1 μm, and (top right) 100 nm. Reproduced with permission from ref 104. Copyright 2020 Nature Publishing Group. (c) Multiwall MoS_2 nanotubes and nanoribbons exhibiting substantial field effect mobilities. Reproduced with permission from ref 163. Copyright 2015 American Institute of Physics.

structural defects, such as point defects, dislocations, edges, and grain boundaries have been shown to enhance the optical and electronic responsivity of a number of devices based on 2D TMDs. Sangwan et al. showed that the resistance of specifically oriented grain boundaries in single-layer MoS_2 memristors can be tuned through application of set voltages in an electroforming process.[60] Interface and defect engineering have been utilized to modulate the electrical and optoelectronic properties of layered TMD materials,[143,144] including the realization of enhanced photoluminescence in single-layer MoS_2.[139]

Interface Engineering. Various strategies, such as surface charge transfer doping (SCTD), TMD-metal contact engineering, and dielectric−TMD interface engineering have been utilized to develop high performance, functional TMD devices. SCTD involves the manipulation of quasi-Fermi levels at metall semiconductor junctions through charge transfer between a donor species and the surface to which it is attached.[145] Some degree of contact engineering is required in order to lower the Schottky barrier at metal−TMD interfaces and, thereby, to enhance device performance. As usual, metal electrodes having appropriate work functions must be chosen in order to allow for facile electron and hole injection.[146−149] Notably, Cui et al. reported on the use of cobalt in conjunction with monolayer h-BN as a contact to MoS_2 and showed that this contact architecture exhibits two distinct properties: (i) it modifies the work function of Co, and (ii) it yields a flat-band Schottky barrier of 16 meV and a carrier density of $5.3 \times 10^{12}/cm^2$.[148] It should be noted that in other MoS_2 devices utilizing h-BN as a buffer layer, Coulomb impurities could be attributed to charge carrier scattering.[150]

Defect Engineering. Point defects, line defects, and phase transitions also play a crucial role in tuning the optical and electronic properties of 2D TMD crystals.[144,151] Chalcogen and transition metal vacancies are the origins of point defects leading to *n*-type (cf. MoS_2) and *p*-type (cf. WSe_2) doping, respectively.[152,153] In addition, 1D line defects and phase transitions were found to be responsible for dramatic changes in the optical, electronic, and catalytic properties of CVD-grown layered TMDs. Chen et al. recently reported the use of ion implantation to introduce lattice defects into CVD-grown MoS_2.[142] The resulting lattice defects modify the electronic energy levels in MoS_2, rendering the material a more active catalyst for HER. In a similar approach, Zhang et al. have shown that potassium ion (K^+) incorporation into single-layer WSe_2 leads to the formation of midgap defect states.[154] Moreover, their calculations suggested that charge transfer from K to surrounding W and Se atoms influences the local magnetic moment with attendant implications for the design and implementation of gate-programmable magnetic moments at defect sites. Finally, Voiry et al. demonstrated that phase engineering of monolayer TMDs can be achieved through covalent functionalization and that this process yields an intense and tunable photoluminescence in metallic 1T MoS_2 crystals.[155]

https://dx.doi.org/10.1021/acs.chemrev.0c00505
Chem. Rev. 2020, 120, 12563−12591

Future research must likewise examine what defects principally manifest in and how they are responsible for inducing exotic physical and chemical properties in 1D TMDs.

3.4.2. Optical and Electronic Effects. Single layer thick TMDs are direct bandgap semiconductors with optical and electronic characteristics distinct from their bulk counterparts.[1] Nanoribbons provide an additional, namely lateral, level of confinement for excitons. Several attempts have been made to study the consequence of lateral confinement on the optical and electronic properties of TMDs. Bao et al. utilized a Campanile nano-optical probe to perform subwavelength imaging of exciton recombination in monolayer MoS_2.[156] Interestingly, nano-optical PL mapping of single 2D MoS_2 crystals identified two distinct regions: an ordered region in the interior of the crystal with an edge length of ∼1−4 μm and an energetically disordered region of width ∼300 nm localized at the edge of the crystal (Figure 6a).[156] The PL quantum yield was found to be weaker in the peripheral edge region relative to that in the interior region and was attributed to increased nonradiative Auger recombination arising from enhanced formation of trions in the edge region.[31] In this work, it was reported that exciton quenching takes place within ∼150 nm of the periphery of the 2D MoS_2 crystal, suggesting that crystals with widths approaching this length-scale will be subject to similar effects on their PL.[156] Recently, Chowdhury et al. reported that as-grown and transferred MoS_2 nanoribbons (width: ∼150 nm) exhibit PL at 660 nm, which represents a substantial blue-shift of PL energy relative to 2D MoS_2 crystals (Figure 6b).[104] In this work, far-field PL mapping revealed a monotonic increase in the PL energy as a function of decreasing nanoribbon width. Near-field optical characterization revealed that this blue-shifted PL emanates uniformly from the entire sub-200 nm width of the MoS_2 nanoribbons, implicating the aforementioned mechanism of edge-boundary exciton quenching.

Besides single-layer TMDs, multilayer TMDs are a promising platform on which to exert unique control of excitonic states. The demonstration by Zhang et al. that top-down fabricated multilayer WS_2 resonators intrinsically support both excitonic and photonic cavity modes opens up possibilities for the use of such architectures in the integration of various emitting media.[157,158] Notably, multilayer TMD nanoribbons obtained via bottom-up synthesis displayed comparable PL behavior to that of monolayer ribbons under ambient conditions, which should stimulate future research efforts investigating the interplay between exciton-polariton modes, photonic cavity modes, and decay channels in 1D crystals.[104]

The electrical transport properties of TMD nanoribbons are also anticipated to be a sensitive function of the degree of lateral confinement within them. For context, confinement effects in graphene nanoribbons (GNRs) with widths of less than 5 nm have been well documented.[84,159−161] However, unlike graphene, which hosts massless Dirac Fermions recalcitrant to confinement due to high probability of Klein tunneling through potential barriers, TMDs host massive Dirac Fermions which are amenable to in-plane quantum confinement. It has been proposed that isolating a few-nm wide TMD "dot" within the matrix of another 2D TMD monolayer could afford such in-plane confinement.[162] Realizing lateral confinement and heterostructuring with the requisite atom-level precision will require substantial synthetic advances. To-date top-down methods have been used routinely to generate narrow ribbons that are then integrated into devices. Recent work demonstrated MoS_2 and WSe_2 nanoribbon-based field effect transistors (FETs) showing high field-effect mobilities (Figure 6c).[94,96,163] Chen et al. fabricated FETs from *p*-type MoS_2 nanoribbons of widths and lengths ranging from 30 to 370 nm and 0.16 to 2.1 μm, respectively, and showed field-effect mobilities in the range of 0.36−8.53 $cm^2/(V\ s)$, with on/off ratios on the order of $\sim 10^3-10^6$.[96] Similarly, few-layer WSe_2 nanoribbon-based FETs showed predominantly *p*-channel behavior following oxygen plasma treatment.[94] It is important to note that while the aforementioned top-down methods yielded *p*-type TMD nanoribbons, efforts using bottom-up synthetic approaches were able to produce MoS_2 nanoribbons with *n*-type behavior.[104,115] These results reinforce the key role that preparatory routes can play in dictating material electronic properties through the, sometimes unintentional, introduction of sulfur-vacancies, impurities, or strain.[164]

As discussed earlier, lateral confinement of parent 2D TMD crystals has the potential to unearth a multitude of hybrid 1D−2D confinement modes and dimensionality is progressively reduced. The imposition of lateral confinement and hetero-structuring with finesse and at atom-levels of precision is a profound synthetic challenge that should inspire continued research and development. Although top-down techniques are customarily used to obtain TMD nanoribbons, the spatial resolution limits and harsh etching conditions associated with these methods impose significant restrictions on the quality of the obtained nanoribbons, especially with regard to realizing atomically sharp edges (cf. section 3.2). Consequently, researchers are developing bottom-up synthetic methods better suited to producing TMD nanoribbons with well-defined clean edges that dictate key electronic properties of these low-dimensional materials. In this vein, Loh and co-workers used a specialized scanning probe technique to prepare <5 nm wide TMD nanoribbons under ultrahigh vacuum conditions and at extremely low temperatures.[101] Moreover, bottom-up synthesis affords unique opportunities to manipulate crystalline quality and environment through the passivation of surface and edge states, through doping, and through the imposition of strain during crystal growth.[165,166]

Realizing the full optoelectronic potential of 1D TMDs will require addressing and/or mitigating the stability issues of these and indeed all low-dimensional crystals. The highly exposed surfaces and edges of TMD nanoribbons are susceptible to degradation (*e.g.*, oxidation, molecular contaminant adsorption to under-coordinated atoms) under ambient conditions. These issues can not only give rise to unwanted artifacts which would confound attempts to identify the intrinsic properties of these materials but also hamper the reliability of devices. Recent efforts have made progress in overcoming synthetic bottlenecks toward achieving precise lateral confinement, while producing chemically stable, high-quality, width-tunable TMD nanoribbons.[101,103,104,115] We are confident that the development of new designer synthetic methods will progress alongside new strategies targeting improved crystal stability through surface passivation, edge modification, and encapsulation.

4. PROSPECTS AND PRIORITIES FOR TMDS: 2D AND BEYOND

Section 2 of our review summarized the diverse structure−property relationships encompassed by 2D TMDs and set the stage for our subsequent discussions. Section 3 of our review sought to highlight some of the exciting research efforts underway in beyond 2D TMDs with a focus on 1D (nanoribbon) motifs. A significant portion of this section was

https://dx.doi.org/10.1021/acs.chemrev.0c00505
Chem. Rev. 2020, 120, 12563−12591

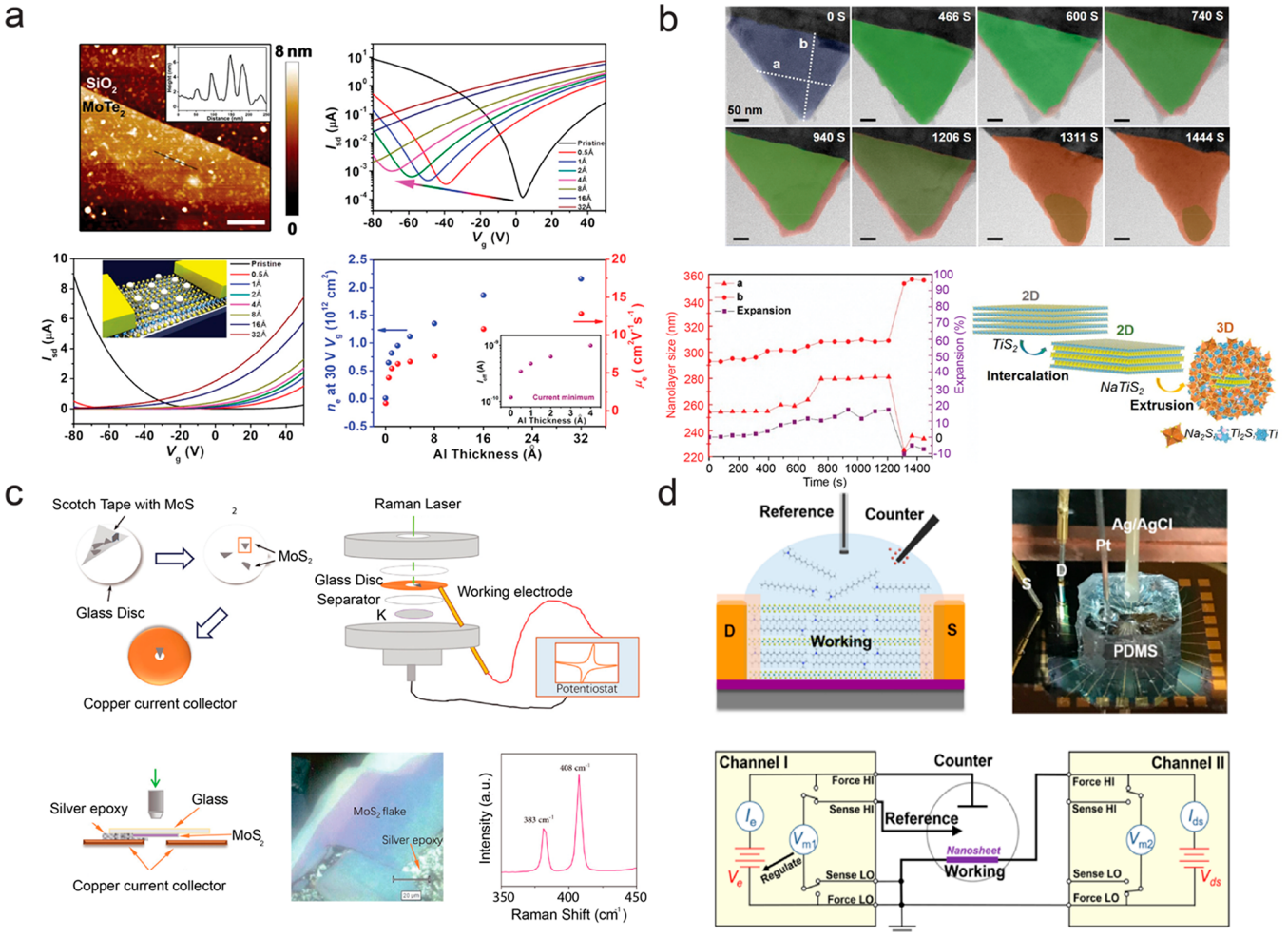

Figure 7. *In situ* observation of TMD properties and their evolution. (a) AFM micrograph of a $MoTe_2$ layer on SiO_2. Scale bar: 200 nm. *I*–*V* characteristics were collected *in situ* during deposition of Al metal on the surface of the $MoTe_2$ FET, and these data were used to determine the electron mobility as a function of Al thickness. Reproduced from ref 175. Copyright 2019 American Chemical Society. (b) False-colored STEM images showing the *in situ* evolution of TiS_2 to $NaTiS_2$ (green) and Na_2S + Ti (orange). These data were used to construct a plot of the expansion of the nanoflake under Na^+ intercalation and a proposed model for this process. Reproduced from ref 176. Copyright 2019 American Chemical Society. (c) Schematic of the experimental setup for *in situ* optical and electronic characterization; optical micrograph of a MoS_2 flake and its characteristic Raman spectrum. Reproduced from ref 178. Copyright 2019 American Chemical Society. (d) Schematic and optical image of the experimental setup for *in situ* electrical characterization of MoS_2 during the intercalation of CTAB. Reproduced from ref 179. Copyright 2019 American Chemical Society.

devoted to a discussion of synthetic breakthroughs. We reached the critical conclusion that while the preparation, manipulation, and investigation of nanoscale wide and atomically thin 1D crystals is challenging, the mechanical, magnetic, electronic, and optical phenomena that uniquely manifest in these beyond 2D TMDs is well worth the future scientific investment required. From a synthetic standpoint, the grail would be to have a method that affords selective control over the crystal dimensionality, edge morphology, and phase with atom-levels of precision and at a scale to render device fabrication practical. Moreover, our discussion suggested a number of distinct features of 1D TMDs that contribute to the exceptionally tunable and in some cases anomalous properties these materials exhibit. These features include (i) a lateral confinement potential that can influence electron and/or exciton transport, (ii) a non-negligible contribution of edge states to the total material response, and (iii) mechanical properties providing for new strain/defect modes.

As discussed in our introduction, the principal goal of this review is to provide perspective on the challenges in and mandates for future research in TMDs. Therefore, section 4 will now take a holistic view of the research prospects and priorities in the TMD field. Besides again emphasizing the need for breakthroughs in synthesis, we identify critical needs in analytical tools. New instruments and methods are needed to fuel future property discovery and analysis. We then discuss priority research areas for TMD materials by highlighting how future studies can build on the vast body of effort in optoelectronics, catalysis, and quantum information science that has thus far focused on 2D TMDs. The intent in this latter section is to acknowledge the great strides made to-date while providing a focused view of research opportunities unique to 1D TMDs.

4.1. Analytical Tools for Characterizing and Manipulating TMDs

4.1.1. Current Status of Probe-Based Techniques. The manifold dimension-dependent optical and electronic phenomena exhibited by TMD nanoribbons motivate the need for continued development of powerful analytical tools. We note that the tools discussed in this section are equally applicable to

https://dx.doi.org/10.1021/acs.chemrev.0c00505
Chem. Rev. 2020, 120, 12563−12591

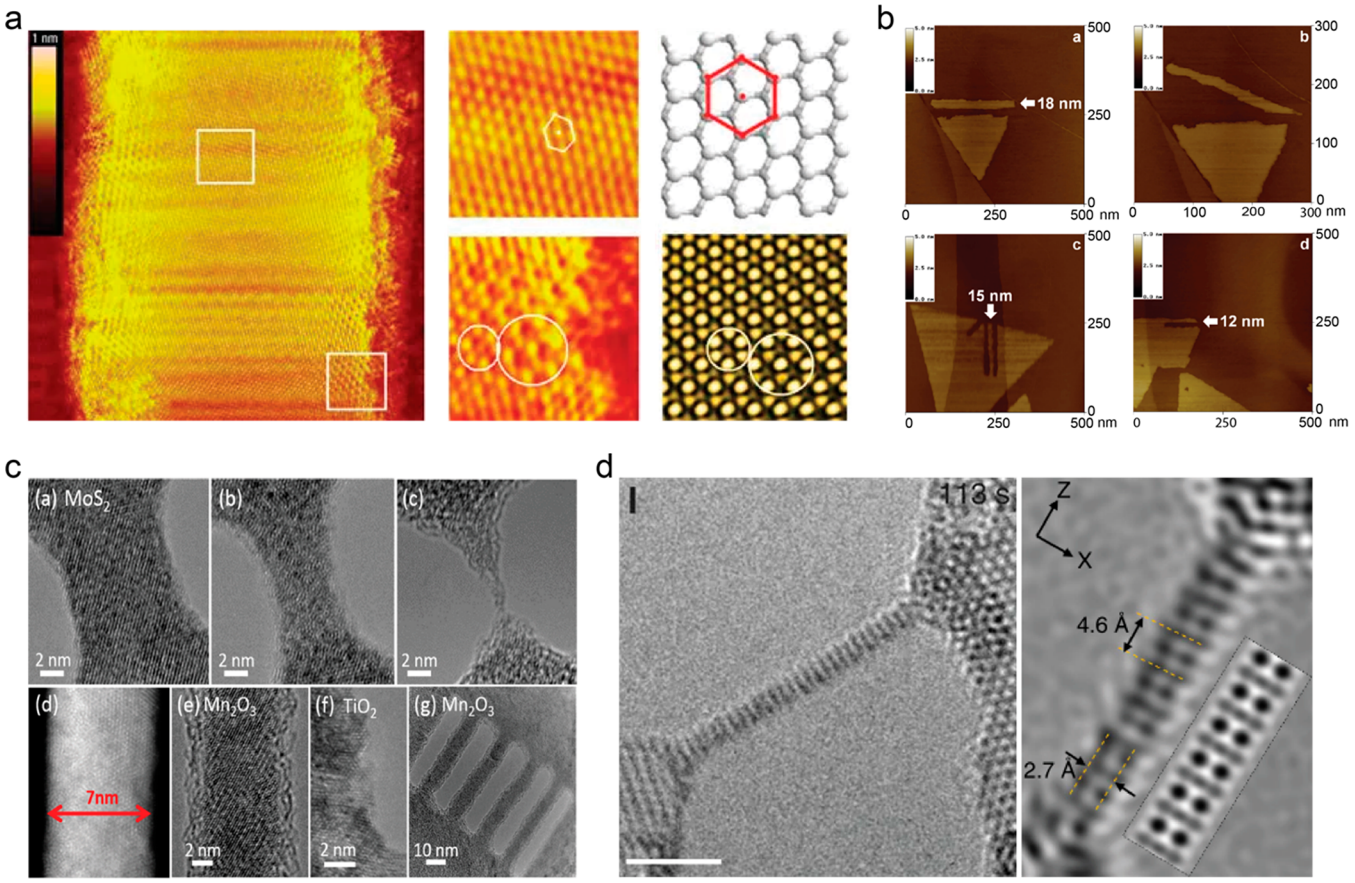

Figure 8. Tailoring 1D materials through top-down fabrication. (a) STM micrographs of a graphene nanoribbon. Reproduced with permission from ref 184. Copyright 2008 Nature Publishing Group. (b) STM images of a two-dimensional MoS_2 flake which was cut with an STM probe to form extremely narrow one-dimensional channels. Reproduced with permission from ref 185. Copyright 2016 Elsevier. (c) TEM micrographs of several materials, including MoS_2, which have been thinned into narrow one-dimensional nanoribbons through He^+ ion beam milling. Reproduced from ref 187. Copyright 2015 American Chemical Society. (d) TEM images of a MoS_2 flake that underwent *in situ* thinning under electron irradiation. Scale bar: 2 nm. High-resolution TEM image of a sub-nm wide MoS_2 channel formed as a result of electron-beam induced thinning. Reproduced with permission from ref 188. Copyright 2013 Nature Publishing Group.

all classes of TMDs. The most commonly used characterization techniques for identifying the morphology, chemical composition, physical and electronic structure, and optical properties of TMD crystals include atomic force microscopy (AFM), scanning electron microscopy (SEM), transmission electron microscopy (TEM), Raman spectroscopy, photoluminescence (PL) mapping and spectroscopy, energy dispersive X-ray spectroscopy (EDS), and X-ray photoelectron spectroscopy (XPS).[15,57,58,167−169] We note that other advanced microscopy techniques, such as scanning atomic electron tomography, will aid in the investigation of TMD materials.[170]

The imaging and spectroscopy of 1D TMDs does present unique challenges.[103,171] First, the smaller size and, in some cases, greater mechanical flexibility of nanoribbons may render them more susceptible to electron beam damage or Joule heating during prolonged TEM or energy loss spectroscopy (EELS) sessions. Second, methods (*e.g.*, Raman and PL mapping and XPS) relying on optical means to seek out TMD samples or sample areas prior to detailed spectroscopic investigation will be limited in their utility for investigating nanoribbons. Besides these challenges, we envision new tools that could leverage recent breakthroughs in *in situ* TEM, cathodoluminescence techniques, and real-time surface analysis methods to enable high-resolution monitoring of a TMD nanocrystal's structure and property evolution during synthesis.[172−174] Such methods may not only provide powerful insights into TMD crystal growth mechanisms but also lead to the discovery of new properties that may emerge during the course of material formation. Another intriguing possibility is to use such *in situ* probes to directly manipulate crystal growth in real time.

4.1.2. *In Situ* Probes to Monitor TMDs. In recent years there has been increased attention focused on the application of *in situ* methods to monitor the formation and evolution of TMD materials and their heterostructures. *In situ* electron microscopy has been used not only to reveal the effects of electron irradiation on the phase and structure of TMDs but also to investigate the temporal evolution of heterointerfaces and dopant distributions within these materials.[84] *In situ* experiments utilizing optical and electrical probes have also been carried out. Studies have focused on understanding the morphological and optical changes that TMDs undergo when intercalated with alkali metals, as is commonly done to transform TMDs from their semiconducting 2H phase to their metallic 1T phase. Demonstrating the potential of *in situ* techniques to modulate the properties of TMD crystals in real-time, Qi et al. showed that *in situ* evaporation of Al onto $MoTe_2$ FETs leads to significant modulation of the character (*p*- to *n*-type) and magnitude of their electronic transport properties (Figure 7a).[175] Complementing these *in situ* electronic property measurements within

https://dx.doi.org/10.1021/acs.chemrev.0c00505
Chem. Rev. 2020, 120, 12563−12591

their high-vacuum system, the authors also monitored the composition of their materials through *in situ* XPS and UPS. *In situ* electron microscopy was used by Wang et al. to identify a cascade of intermediate phase changes in TiS_2 nanoflakes subjected to intercalation by Na^+ ions (Figure 7b),[176] while Ren et al. showed that *in situ* optical absorption measurements can likewise yield insights regarding the rate of electrically driven Li^+ (de)intercalation within similar TiS_2 nanoflakes.[177] *In situ* Raman spectroscopy was used by Li et al. to determine the degree of reversibility of K^+ intercalation into MoS_2 flakes (Figure 7c).[178] Other studies have expanded on these ion intercalation studies to examine the intercalation of molecular species into layered TMD crystals. For example, He et al. investigated the intercalation kinetics of cetyltrimethylammonium cations (CTA^+) within MoS_2 through *in situ* electrical measurements and also monitored phase transitions during the intercalation process (Figure 7d).[179] In another study, Kumar et al. used *in situ* spectro-electrochemical techniques to monitor the thinning of TMD flakes during electroablation.[180] The authors monitored changes in the extinction spectra of TMD crystals as a function of applied electrochemical potential. Finally, Sang et al. used scanning transmission electron microscopy (STEM) to observe changes in the edge structure of 2D TMDs subjected to *in situ* heating within the microscope.[181] The authors observed characteristic reconstructions at the edges of pores formed within $Mo_{1-x}W_xSe_2$ monolayers subjected to various thermal treatments.

The foregoing examples of *in situ* characterization reinforce the importance of having techniques that can provide insight into the evolution of TMD materials as they respond to external stimuli or potentials. Crucially, as more attention shifts to the synthesis and characterization of 1D and hierarchically structured TMD crystals, it is hoped that many existing, and newly developed, *in situ* tools will be applied to uncover their unique growth mechanisms and mechanical, optical, and electronic properties.

4.1.3. *In Situ* Probes to Manipulate TMDs. Researchers have also used the optical and microprobe techniques otherwise employed for *in situ* characterization to manipulate the structure and phase of TMD materials. Beams of electrons, ions, and photons, in addition to scanning probes, have been used to alter TMD materials into 1D (*e.g.*, nanoribbon) morphologies. Chen et al. combined thermal treatment with irradiation by a focused electron beam to produce an array of 5 nm wells in bilayer WS_2 through removal of a single layer of WS_2.[182] Though these wells did not assume significant aspect ratios, the technique could be used to create arrays of highly confined 1D−2D vertical heterostructures. A KrF laser was used by Vasu et al. to unzip TMD nanotubes into nanoribbons.[183] Such control over intradimensional material transitions must be expanded to build a more complete repertoire of methods for the manipulation of TMD and other low-dimensional materials. Tapasztó et al. utilized STM probes to directly tailor graphene nanoribbons (GNRs) into aspect ratios suitable for their integration into devices and other architectures (Figure 8a).[184] Though the fine structural alterations realized with GNRs have not yet been accomplished with TMDs, Koós et al. did use a STM-based method to carve 1D regions out of 2D TMD materials (Figure 8b).[185] The exceptionally small probe sizes realizable in STM allow for the creation of extremely narrow nanoribbons with Å level precision. Besides lasers and scanning probes, ion beams have been used to sculpt 2D materials into other morphologies, including 1D or nanoribbon forms. Abbas et al. employed a helium ion beam to trim graphene into sub-5 nm graphene nanoribbons.[186] Fox et al. likewise used He^+ beam milling to manipulate a variety of 2D TMDs into materials of significantly reduced dimensionality (Figure 8c).[187] It was found that He^+ irradiation induces significant changes in the composition and phase of the irradiated TMD material, causing it to convert from the semiconducting to metallic state. Moreover, ion beam milling can be used to modify the edge structure of low-dimensional materials. Liu et al. demonstrated the formation of subnanometer wide nanoribbons from electron beam irradiation of a 2D MoS_2 nanosheet and noted that these irradiation conditions alter the TMD structure from the nominal MoS_2 to Mo_5S_4 (Figure 8d).[188] In a related approach, Huang et al. used electron beam irradiation to selectively modify the edges of a MoS_2 2D sheet to form a 1D chain of Mo_6S_6.[189] In a more recent study by Kumar et al., aberration-corrected electron microscopy was utilized to obtain real-time insights into the nonequilibrium structural transformations of 2D TMD films, with concomitant identification of crystalline quantum-confined regions in the 2D crystals.[190] These studies point out that the use of highly energetic *in situ* probes to tune crystal morphology may be accompanied by substantial structural and compositional changes.

Though the aforementioned methods reveal the promise of using nonchemical probes to alter the structure of TMD materials, the development of solely chemical or hybrid chemical-physical methods to effect control over the morphology, dimensionality, phase, and order of low-D materials is of great interest. Ultimately, the realization of highly selective and massively parallel strategies to exert such control is desired. Moreover, the integration of *in situ* probe-based measurement and manipulation techniques within reactors would offer the tantalizing opportunity to observe and control crystal growth in real-time. Such approaches may allow for the identification and stabilization of complex metastable phases currently overlooked due to the prevalence of postsynthetic characterization methods. High-resolution probes compatible with a range of gas-phase synthetic conditions will be crucial in order to uncover principal intermediates (*e.g.*, incipient crystal growths) formed on pathway to the growth of complex phases, such as 1D materials.

4.2. 0D TMDs: Emerging Synthetic Routes and Properties

In keeping with the theme of exploring TMD crystals beyond 2D, significant effort has recently been devoted to study of 0D or quantum dot TMDs because of the strong light absorption and, in some instances, single photon emission these materials can exhibit.[191,192] To maintain the cohesion and focus of our review, we define 0D TMDs as predominantly atomically thin TMD crystals which have been restricted substantially in their dimension with respect to their 1D counterparts.

Mechanical sonication is currently the primary method for production of 0D TMD crystals. Zhang et al. demonstrated the versatility of sonication by using it to isolate a range of 0D TMD quantum dot (QD) materials.[193] Though the authors succeeded in achieving cluster diameters of generally less than 5 nm, size dispersity within this range was still a concern. Tan et al. used ball-milling in conjunction with Li-intercalation to prepare TMD quantum dots and demonstrated enhanced electrochemical activity for HER catalysis.[194] $MoSe_2$ QDs dispersed on MoS_2 and WSe_2 monolayers exhibited modified photoluminescence and Raman spectra consistent with QD-to-monolayer charge transfer.[195] After exploiting sulfur vacancies in $ZnIn_2S_4$ monolayers to seed growth of MoS_2 QDs within the

https://dx.doi.org/10.1021/acs.chemrev.0c00505
Chem. Rev. 2020, 120, 12563−12591

parent monolayer, Zhang et al. showed that the resulting 0D/2D heterostructure produces more electrocatalytic hydrogen as compared to bulk $ZnIn_2S_4$.[196] Such mixed-dimensional hybrids of 0D with 1D and/or 2D TMDs may prove a viable route toward realizing more complex functional materials. Laser ablation is another route toward production of 0D TMDs. In this vein, Wu et al. prepared fullerene-like MoS_2 nanoparticles between 20−100 nm in diameter by pulsed laser ablation of pressed MoS_2 powder pellets in water.[197] These materials were shown to be biocompatible in cell viability studies. Finally, pushing the limits of laser ablation, Ou et al. prepared less than 3 nm wide MoS_2 quantum dots, which exhibited enhanced electrocatalytic activity toward hydrogen production due to their high surface area and conductivity.[198]

0D features confined within 2D TMD crystals have attracted interest as possible quantum emitter sources. Srivastava et al. identified 0D regions in monolayer WSe_2 that exhibited quantum emission characteristics (*e.g.*, photon antibunching) and suggested that these emissive sites may be associated with defects or vacancies.[199] Reports by Chakraborty et al., He et al., and Koperski et al. show both 0D defect and edge features in 2D WSe_2 that are associated with quantum emission.[200−202] More recently, Lu et al. were able to induce optically a spin-valley within a charged WSe_2 quantum dot, providing important progress toward use of beyond 2D TMD crystals in valleytronics.[203] These reports indicate the promise of utilizing 0D defect centers as optically active emitters in 1D and 2D TMDs. Going forward, we emphasize the need to not just identify and exploit adventitious 0D defects in TMDs but to develop the means to control their size, boundary conditions, and location explicitly.

4.3. Research Areas and Opportunities

As discussed in the opening to this section, 1D TMDs or nanoribbons offer a multitude of favorable chemical and physical attributes that render them an attractive platform for studies in catalysis, optoelectronics, and quantum information science (Figure 9). For example, the combination of a large ratio of edge-to-basal sites in TMD nanoribbons, especially ultranarrow nanoribbons, with the propensity for these materials to support unique edge reconstructions is likely to increase the catalytic activity of these crystals. Moreover, new approaches to controlled growth of 1D TMDs on designer substrates raises the prospect for direct synthesis of complex in-plane and out-of-plane heterostructures with intriguing optoelectronic properties. Furthermore, through judicious tuning of edge states, atomic defects, and dislocations in strained 1D TMDs, one may be able to engineer spectrally pure emitters and perhaps even photostable single photon emitters (SPE). Such a result would hold tremendous promise for future quantum information processing technologies.

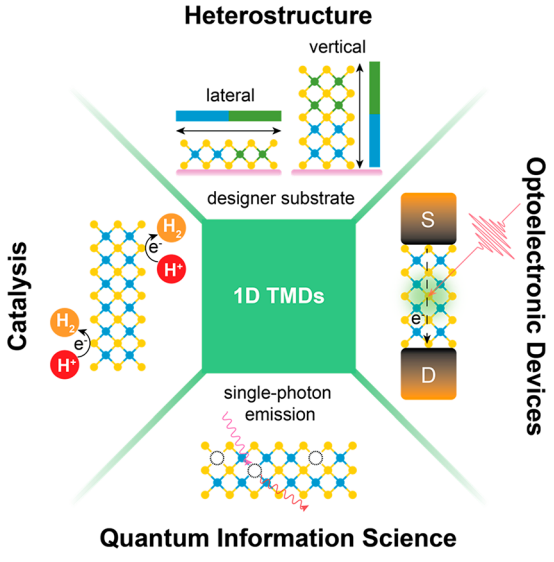

Figure 9. Potential research areas involving 1D TMDs. Schematic illustrating some of the many application opportunities for 1D TMDs. Dimensionally restricted and atomically thin TMD crystals are compelling candidates to advance studies in catalysis, optoelectronics, and quantum information science (QIS).

This section discusses four possible research directions, catalysis, heterostructures, optoelectronics, and quantum information science, for TMD crystals beyond 2D. We note that while the majority of optoelectronic and quantum information applications have to-date utilized 2D materials as their platform, we nevertheless discuss them here to motivate the reader to recognize the many opportunities available if related studies are performed with beyond 2D crystals. As highlighted in earlier sections, there are also many research opportunities unique to 0D and 1D TMDs that are waiting for the willing and courageous scholar.

4.3.1. Catalysis. The catalytic performance of a low-dimensional material can be substantially tuned by controlling the extent of strain, defects, and vacancies in the material and by employing phase engineering and heterostructuring strategies to further alter the parent lattice.[204−207] TMDs exhibit appreciable activity toward catalysis of the hydrogen evolution reaction (HER).[208,209] The catalytic role of TMD edge sites was established through STM experiments conducted by Jaramillo et al.[37]

While 2D TMDs present with competitive catalytic activity for HER and for the hydrodesulfurization reaction, their basal plane, the majority of the material surface area, is catalytically inert. This drawback has been overcome by introducing defects into the basal plane of TMD and mixed transition metal crystals through doping, strain, and defect- and hole-engineering.[210−214] There has been ample work on the activation of edge sites in 2D TMDs.[38] For example, Voiry et al. strained WS_2 nanosheets to induce their conversion to the more catalytically active 1T metallic polymorph (Figure 10a).[62] This result is a canonical example of the use of strain to modulate material phase in a manner that manifests in improved catalytic performance.

One can intuit that TMDs with reduced dimensionality, such as 1D nanoribbons, could exhibit enhanced catalytic performance because of the greater ratio of edge-to-basal plane atoms they contain and also because of their inherently higher flexibility and therefore susceptibility to modification by applied strain. Nevertheless, efforts to explore the catalytic features of 1D TMDs have lagged behind those focused on 2D TMDs. Early efforts focused on preparing heterostructures comprised of TMDs alongside their corresponding TM oxides. For example, Chen et al. prepared MoO_3/MoS_2 nanowires wherein the two materials are disposed in a core/shell arrangement.[215] They found that this geometry, with the core providing a conductive scaffold for the MoS_2 catalyst shell, yielded an architecture with appreciable stability during HER catalysis (Figure 10b).[215] Finally, Li et al. prepared MoS_2 nanoparticles on a reduced graphene oxide (RGO) support.[209] The electronic and chemical coupling of the RGO and MoS_2 was found to yield improved electrocatalytic activity toward the HER when compared to

https://dx.doi.org/10.1021/acs.chemrev.0c00505
Chem. Rev. 2020, 120, 12563−12591

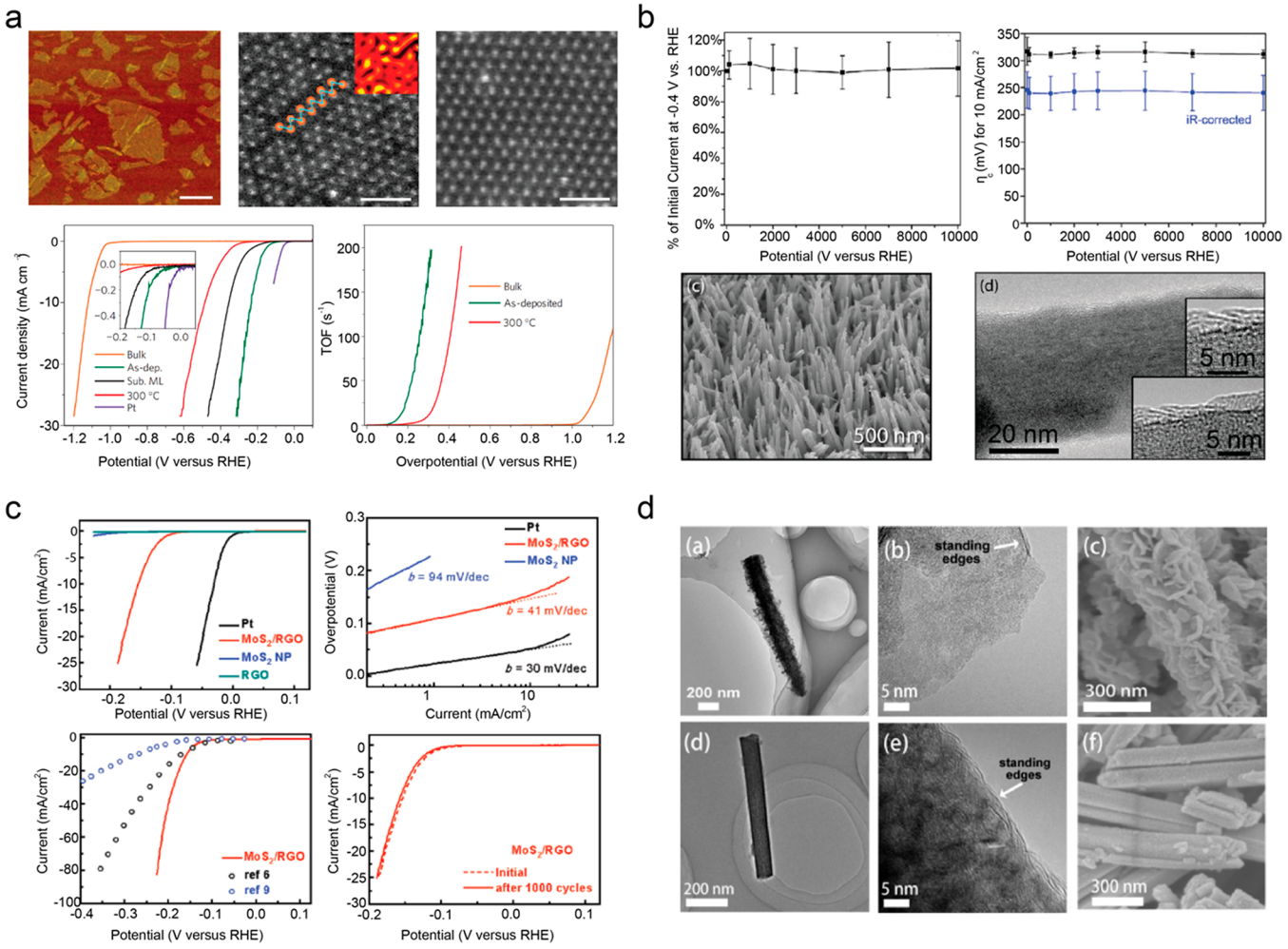

Figure 10. Catalytic properties of TMD materials. (a) AFM topographical map of WS_2 flakes. Scale bar: 500 nm. STEM-HAADF images of 2D WS_2 crystals are used to identify their 1T (left) and 2H (right) phases. Scale bars: 1 nm. Plots of current-density versus applied voltage and turnover frequency (TOF) versus applied voltage for a set of WS_2 electrodes prepared under different conditions. These data reveal an ~900 mV lower overpotential (for onset of HER catalysis) and higher TOF for as-deposited WS_2 material compared to bulk WS_2. Reproduced with permission from ref 62. Copyright 2013 Nature Publishing Group. (b) Electron microscopy images of MoO_3 (core)−MoS_2 (shell) nanowires and plots showing the excellent stability of these heterostructured nanowires during HER catalysis over 10,000 cycles. Reproduced from ref 215. Copyright 2011 American Chemical Society. (c) Current−voltage plots attesting to the lower overpotential and smaller Tafel slope of MoS_2 crystals when supported on reduced graphene oxide. Reproduced from ref 209. Copyright 2011 American Chemical Society. (d) Micrographs of layered WS_2 decorating WO_2 nanorods (top) and layered MoS_2 decorating MoO_2 nanorods. Reproduced from ref 216. Copyright 2016 American Chemical Society.

either MoS_2 nanoparticles or the RGO alone (Figure 10c).[209] The solvothermal synthesis method used in this study allowed the one-dimensional structures to retain their porosity and conductivity while maintaining the catalytic activity of the TMD. Wang et al. prepared porous nanorods incorporating MS_2/MO_2 (M: W or Mo) heterointerfaces and found that these materials show a reduced overpotential and increased current density when operated as catalysts for HER, as compared to nanorods comprised solely of MoO_2 or WO_2 (Figure 10d).[216]

Besides creating heterostructures, researchers have consistently employed doping of 1D TMD materials as a strategy toward increasing their catalytic activity. Recent work has shown that P atom doped WS_2 requires only −98 mV (versus the reversible hydrogen electrode) of overpotential to generate a current density of -10 mA cm^{-2} during HER catalysis, a result which is comparable to the performance seen in corresponding 2D TMD materials.[217] Li et al. prepared WTe_2 nanoribbons with a distorted octahedral (1T') phase and observed that these materials exhibit a lower overpotential and smaller Tafel slopes for HER catalysis as compared to other WX_2 (X = S, Se) TMDs with the naturally occurring 2H phase.[218] It was argued that the higher conductivity of the 1T' phase over the 2H phase facilitates higher charge-transfer rates through the nanoribbons. Explicit phase selection by doping has also been explored to introduce electronic states more activating for HER catalysis. The native cubic structure of $CoSe_2$ shifts under the influence of P doping to an orthorhombic phase yielding a coordination environment that facilitates enhanced catalytic activity toward HER.[219]

The strategies discussed here represent some of the diverse approaches toward utilizing or improving 1D or nearly-1D TMDs for catalysis. However, the catalytic properties of high quality, single-layer, nanoribbon-like morphologies have yet to be investigated in detail.

4.3.2. Heterostructures. Heterostructuring is a broadly employed strategy for incorporating new functional interfaces in multicomponent TMD materials. Laterally[220−222] and vertically[108,220,223] disposed heterostructures have been realized in

https://dx.doi.org/10.1021/acs.chemrev.0c00505
Chem. Rev. 2020, 120, 12563−12591

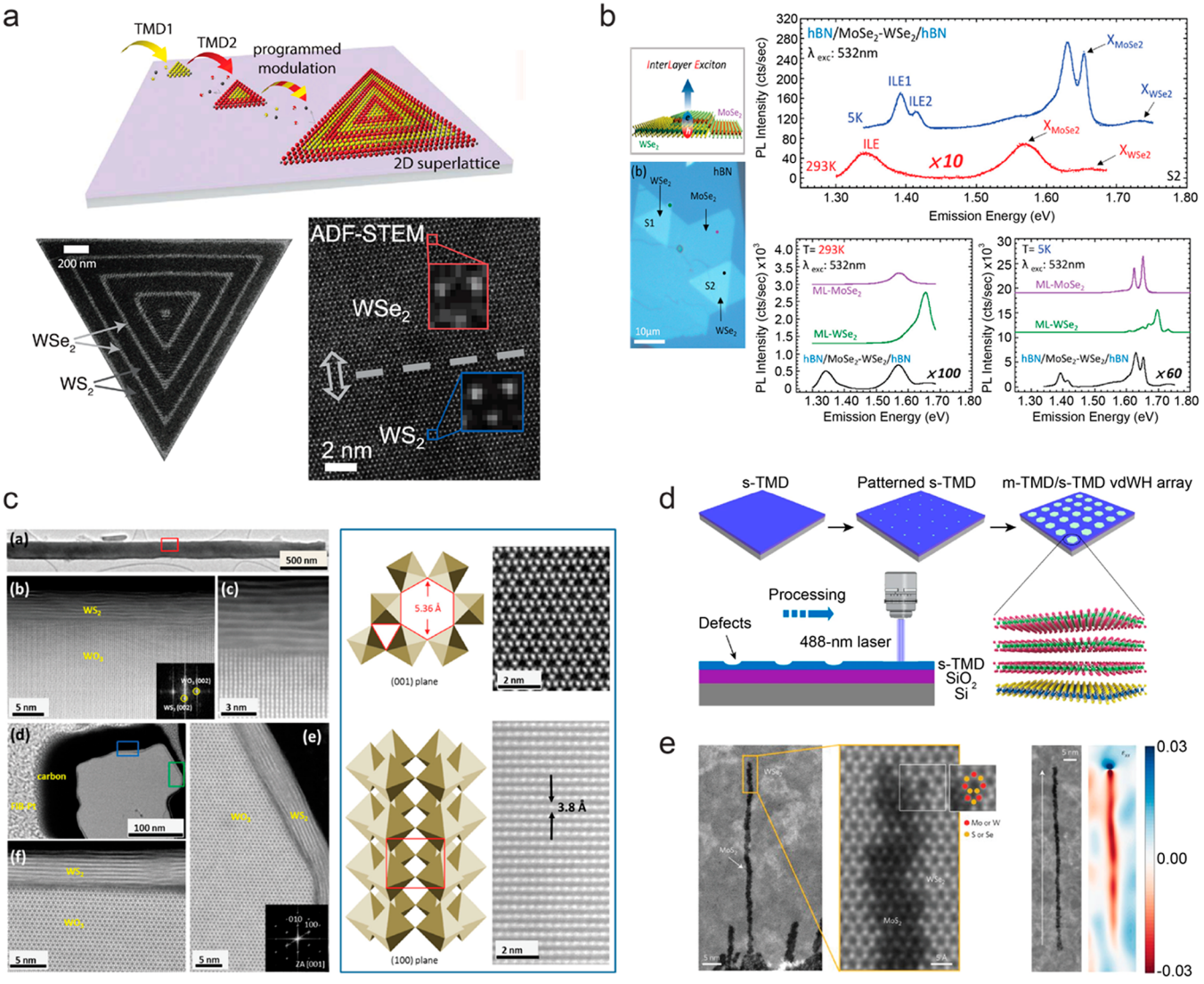

Figure 11. Heterostructure assemblies of 2D and 1D TMDs. (a) Generalized schematic for the synthesis of 2D TMD lateral superlattices and STEM image of a heterostructured 2D lateral superlattice comprised of WSe_2 and WS_2 segments. Reproduced with permission from ref 236. Copyright 2018 American Association for the Advancement of Science. (b) Optical image of a vertical heterostructure comprised of stacked $MoSe_2$ and WSe_2 layers and photoluminescence spectra highlighting emission from interlayer excitons of this vertical assembly. Reproduced from ref 33. Copyright 2018 American Chemical Society. (c) TEM and STEM images identifying the discrete core-WO_3 and shell-WS_2 domains in a mixed-dimensional heterostructure. Schematic illustrations and STEM images of a WO_3 nanowire under axial and longitudinal perspectives. Reproduced from ref 239. Copyright 2016 American Chemical Society. (d) Schematic of the fabrication process of metallic-semiconducting TMD heterostructures. Periodically spaced defects are formed by laser etching. These defects then seed the growth of metallic TMDs. Reproduced with permission from ref 227. Copyright 2020 Nature Publishing Group. (e) TEM micrographs of dislocation-catalyzed filaments of MoS_2 within WSe_2. Reproduced with permission from ref 240. Copyright 2018 Nature Publishing Group.

2D TMD crystals through the application of diffusion-mediated techniques,[221] sequential edge-epitaxy,[224] sequential vertical growth,[223] thermal annealing,[225,226] and sequential lateral growth.[108,220−223] While most TMD heterostructures prepared to-date constitute a homologous series wherein the transition-metal or chalcogen is altered (*e.g.*, $MoS_2/MoSe_2$ and $WSe_2/MoSe_2$), mixed van der Waals heterostructures (*e.g.*, those comprised of graphene and a TMD) are also common.[9,21] van der Waals heterostructures comprised of 2D metallic and semiconducting TMDs (*e.g.*, $NiTe_2/WSe_2$) have also been realized.[227]

The primary goal of heterostructuring is to impart new properties or functions through the combination and interplay of multiple 2D layered materials such as TMDs, h-BN, graphene, or any of the extensive family of group IV graphene-analogs. The features often targeted through heterostructuring include increased catalytic performance,[228,229] the introduction of interlayer exciton transport physics,[33,34,230] and the realization of unique quantum-engineered transistor architectures.[48,231,232] In the context of 1D TMD crystals, it has been proposed that compositionally heterogeneous nanoribbons of MoSSe could support enhanced thermoelectric performance raising the possibility that nanoribbons bearing explicit heterointerfaces may likewise exhibit improved *ZT* values.[233] Electron transport and other device figures of merit may be rendered highly tunable by utilizing heterostructured 2D and quasi 1D TMDs.[163,232,234,235]

Given that 1D TMD crystals are the topological analog of a wire, and that they can support unique transport physics because of their restricted dimensionality, they represent a compelling

https://dx.doi.org/10.1021/acs.chemrev.0c00505
Chem. Rev. 2020, 120, 12563−12591

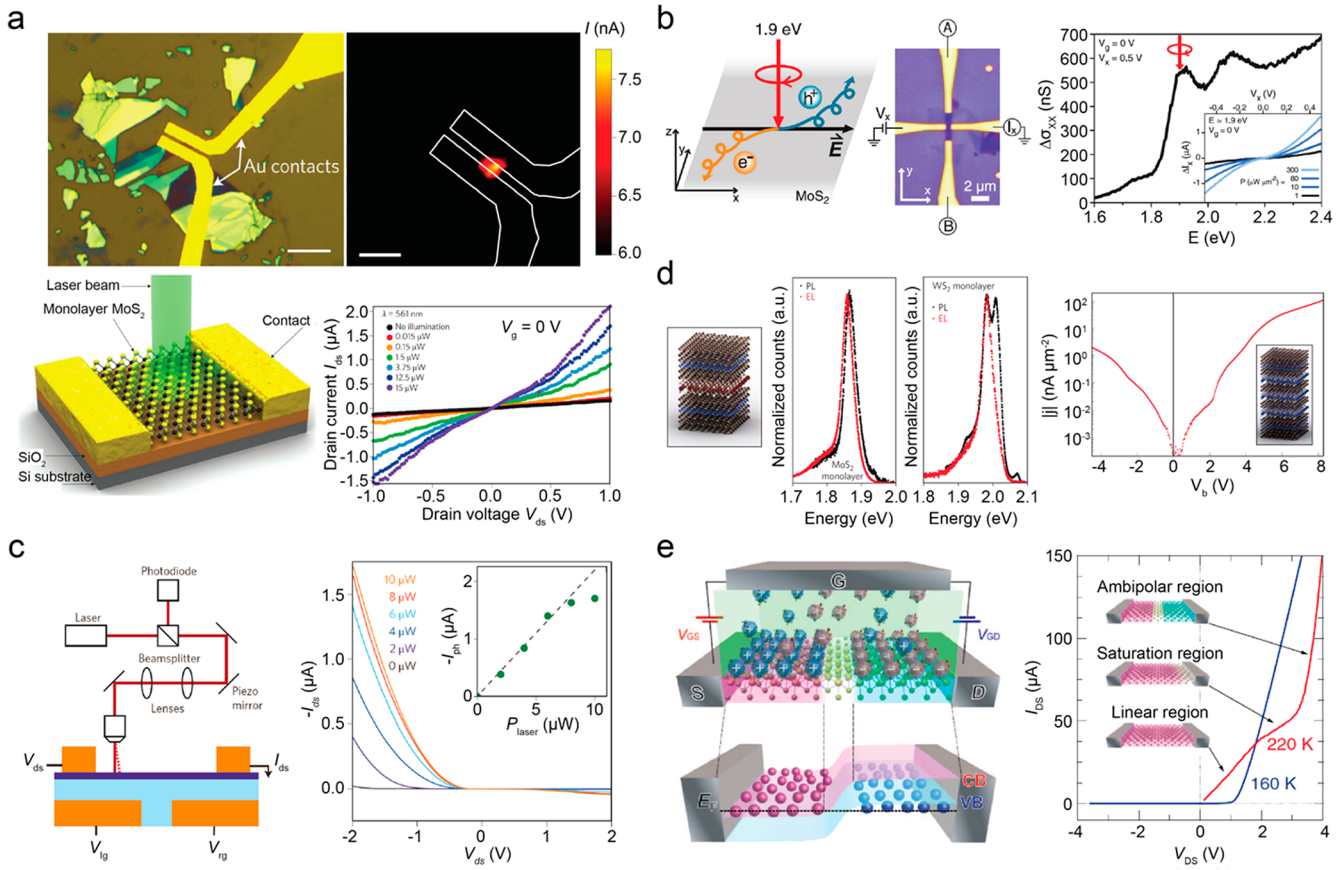

Figure 12. Optoelectronic devices based on TMDs. (a) Optical images of a single-layer MoS_2 photodetector and its current−voltage transport characteristics under different illumination powers. Scale bars: (left) 10 μm, (right) 5 μm. Reproduced with permission from ref 250. Copyright 2013 Nature Publishing Group. (b) Schematic illustration of the photoinduced anomalous Hall effect (AHE) driven by valley polarization (left). Singe-layer MoS_2 Hall bar device (middle). Plot of the change in conductivity as a function of incident photon energy. Reproduced with permission from ref 43. Copyright 2014 American Association for the Advancement of Science. (c) Photodetection in a single-layer WSe_2 device. Schematic illustration of a typical scanning photocurrent instrument setup and the TMD device. Plots of drain current as a function of drain-source bias ($V_{\text{left-gate}} = +10$ V, $V_{\text{right-gate}} = -10$ V) for the WSe_2 device while illuminated with a 532 nm laser diode at powers of 0−10 μW. Reproduced with permission from ref 253. Copyright 2014 Nature Publishing Group. (d) Single- and multiple-quantum well devices comprised of stacked layers of MoS_2 and WS_2 exhibit substantial photo- and electro-luminescence (PL and EL). Reproduced with permission from ref 264. Copyright 2015 Nature Publishing Group. (e) Schematic illustration of a TMD-based electric double-layer transistor (EDLT) subject to ambipolar charge accumulation (left). $I-V$ characteristics of a WSe_2 EDLT. Reproduced with permission from ref 265. Copyright 2014 American Association for the Advancement of Science.

platform on which to explore new quantum and optoelectronic device concepts, provided that advances in heterostructure synthesis continue apace.

Rational heterostructure synthesis requires precise control of the extent, structure, and composition of TMD domains. There is significant precedent for controlled growth of lateral and vertical heterostructures of 2D TMDs. For example, Zhang et al. used CVD techniques to achieve several lateral heterostructures, such as WS_2/MoS_2 and $WSe_2/MoSe_2$,[222] while Xie et al. demonstrated WS_2/WSe_2 lateral 2D superlattices with coherent heterointerfaces (Figure 11a).[236] Hanbicki et al. utilized CVD and transfer techniques to assemble $WSe_2/MoSe_2$ heterostructures on h-BN and probed the interlayer exciton response in the heterostructures (Figure 11b).[33] Zhang et al. demonstrated doping of MoS_2 with Re at high concentrations using a powder vaporization technique and showed that the Re-doped material exhibited optical properties substantially different from those of the parent material.[237] These advances highlight progress toward exerting exceptional control over crystal growth and present a path toward the realization of more complex and functional 2D TMD heterostructures.

Though the preparation of laterally heterostructured 1D TMD crystals presents unique growth challenges, for example the maintenance of an asymmetric growth front, the growth of mixed-dimensional materials (*e.g.*, hybrids of 2D and 1D crystals) has captured attention. For example, Chen et al. demonstrated seeded growth of 2D TMD nanosheets (*e.g.*, MoS_2 and $MoSe_2$) from nanowires of $Cu_{2-x}S$, a typical transition metal monochalcogenide (TMM).[238] Work by Choudhary et al. prepared mixed-dimensional composites comprised of WO_3 nanowires sheathed by WS_2 nanosheets and noted the superlative charge−discharge retention of these supercapacitor architectures (Figure 11c).[239] Tang et al. used CVD techniques to synthesize graphene-WS_2 heterostructures for use in transistors and noted an enhancement in the on−off current ratio and unipolar electrical characteristic.[48] Li et al. patterned semiconducting 2D TMD layers to seed the growth of periodic arrays of mixed semiconducting−metallic TMD vertical heterostructures (Figure 11d).[227] In an interesting example of self-driven heterostructure formation, Han et al. identified that dislocations in 2D WSe_2 can catalyze the growth of 1D-like MoS_2 filaments (Figure 11e).[240] This method yields in-plane

https://dx.doi.org/10.1021/acs.chemrev.0c00505
Chem. Rev. 2020, 120, 12563−12591

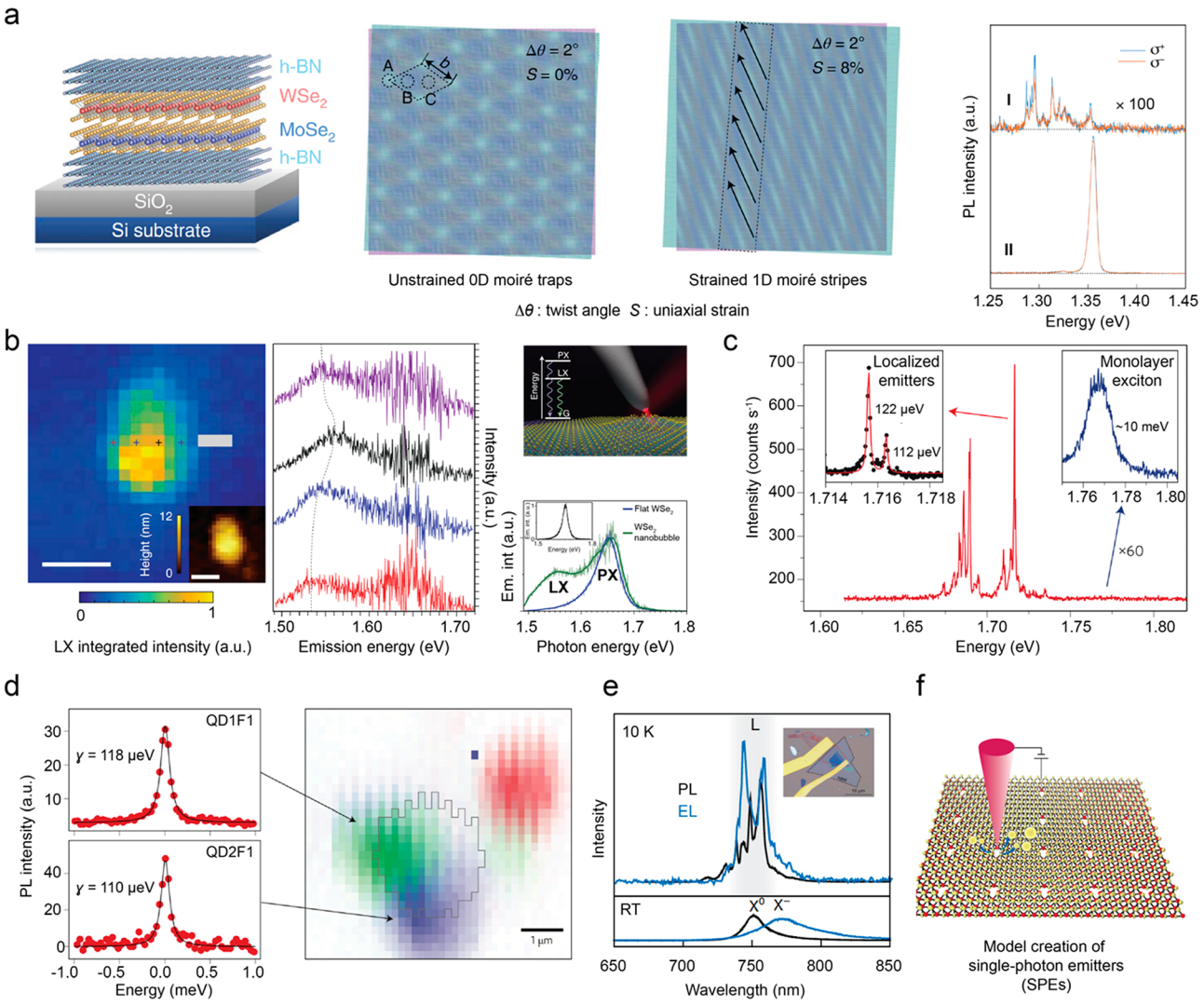

Figure 13. Applications in quantum information science (QIS). (a) Hexagonal (unstrained) and quasi-1D (strained) moiré patterns in a twisted (twist angle = 2°) $WSe_2/MoSe_2$ heterobilayer assembly. Polarized PL spectra obtained at $T = 4$ K divulge sharp PL peaks. Reproduced with permission from ref 270. Copyright 2020 Nature Publishing Group. (b) Nano-PL imaging and spectroscopy revealing distinct localized excitonic (LX) states within a WSe_2 nanobubble. Scale bars: 100 nm. Schematic of the nano-PL imaging setup with simple energy-level diagram illustrating energy ordering (top right and inset). Relative peak position and intensity of localized and primary exciton (LX and PX) states (bottom right). Reproduced with permission from ref 272. Copyright 2020 Nature Publishing Group. (c) Single quantum emitter (SQE) behavior in single-layer WSe_2 is characterized by ultrasharp spectral line features. Reproduced with permission from ref 201. Copyright 2015 Nature Publishing Group. (d) Photoluminescence from single-layer WSe_2 flakes exhibits intense peaks with a narrow energy spread. These features are typical of quantum emitters. Reproduced with permission from ref 199. Copyright 2015 Nature Publishing Group. (e) PL and EL spectral peaks obtained from monolayer WSe_2 flakes exhibit narrow bandwidths. Reproduced with permission from ref 273. Copyright 2016 Nature Publishing Group. (f) Schematic of a strategy to create well-defined single-photon emitters through the introduction of atom-precise defects by scanning probe lithography. Reproduced with permission from ref 276. Copyright 2019 Nature Publishing Group.

grown 1D TMDs that remain confined within a 2D parent crystal. Although the emergence of significant lattice mismatch is necessary to catalyze the formation of the 1D filaments, this method is capable of producing impressively narrow nanoribbons with widths below 2 nm. Calculations by Deng et al. suggest that heterostructures comprising graphene interfaced with compositionally alloyed MoSSe nanoribbons can support a higher ZT at higher temperatures.[233] These reports suggest the need for continued development of mixed dimensional TMD heterostructures.

Explicit preparation of heterostructured axial 1D TMD crystals has not been realized. Though Guo et al. did realize axially modulated CdS/CdS_xSe_{1-x} nanowires as high performance photodetectors, these TMM architectures can be best described as quasi-1D in nature.[241] Theoretical predictions of anomalous electronic transport and possible spin filtering in laterally heterostructured TMD nanoribbons has spurred interest in such architectures.[232,234,235,241] In this context, we envision that recent breakthroughs in direct synthesis of width-tunable TMD nanoribbons may be adapted to prepare 1D crystal platforms with prescribed heterointerfaces.

The preparation and study of truly 1D crystals with atomically sharp and finely controlled heterojunctions merits serious future effort.

4.3.3. Optoelectronic and Neuromorphic Devices. As discussed above, single-layer TMD crystals hold significant promise for use in novel optoelectronic devices due to their diverse exciton physics and broken in-plane inversion

https://dx.doi.org/10.1021/acs.chemrev.0c00505
Chem. Rev. 2020, 120, 12563−12591

symmetry.[3] Moreover, the substantial mechanical flexibility and electronic structure tunability of 2D TMDs bodes well for their integration into flexible and reconfigurable devices. Most 2D material-based devices take the form of photodetectors or light emitting diodes (LEDs) fashioned from graphene[18,242−245] or TMD crystals.[246−255] In this section, we will limit our discussion to 2D TMD-based optoelectronic devices.

2D TMD photodetectors function primarily through the photovoltaic effect and exhibit a high responsivity and low dark current.[256] A single-layer MoS_2 transistor with responsivities as high as 880 A W^{-1} when subjected to electric fields of ∼4 V μm^{-1} was demonstrated by Lopez-Sanchez et al. (Figure 12a).[250] In a seminal study, Mak et al. first reported a 2D MoS_2 transistor operating in photoconduction mode, in which photoexcited carriers enhanced the device conductance (Figure 12b).[43] In this study, the authors illuminated their MoS_2 Hall bar device with circularly polarized light to break time-reversal symmetry and generate a valley polarization that contributed to the enhanced photoconduction observed. This and many other studies have since nucleated the field of valleytronics. Nearly concurrently, photodetectors operating in photocurrent mode, wherein photoexcited carriers are subjected to drift in the presence of a built-in electric field, were demonstrated. Single-layer WSe_2 devices with electrostatically induced $p-n$ junctions were shown to exhibit ambipolar transport characteristics.[247,253,254] Baugher et al. demonstrated that WSe_2 diodes illuminated with a 532 nm laser exhibit a photodetection responsivity of 210 mA W^{-1} (Figure 12c).[253] Although these devices perform well under large bias, their comparatively low external quantum efficiency is a consequence of their low optical absorption and unoptimized device geometry. Improvements in the latter would require efficient exciton migration and eventual dissociation in the presence of the large built-in electric fields supported within these diode devices.[257] In contrast to the foregoing examples of $p-n$ junctions disposed in the in-plane direction, out-of-plane charge separating junctions formed between stacked 2D layers offer potential advantages vis-à-vis support for large built-in electric fields and more efficient optical absorption.[252,255]

In addition to recent progress in studying the photoresponsive properties of 2D TMDs, interest has emerged in exploring TMDs in the context of integrated neuromorphic computing.[258] Memtransistors, multiterminal device hybrids of memristors and transistors, can mimic salient features of neuronal function and thereby be used to perform complex calculations.[259] 2D MoS_2 memristors and memtransistors are promising candidates for information storage and processing because of their low ON-state resistance, high-frequency switching,[260] and low leakage current.[261,262]

LEDs emit light due to electron−hole recombination that takes place at $p-n$ junctions or Schottky junctions.[247,252,263] Recently, Withers et al. demonstrated the implementation of tunnel junctions in vertically stacked van der Waals heterostructures and showed that these architectures produce emission (with EQEs of ∼10%) whose frequency could be substantially tuned by appropriate ordering of the constituent MoS_2 and WS_2 layers and appropriate configuration of contacts (Figure 12d).[264] Valley-dependent optoelectronic transitions manifest in 2D TMDs but have been difficult to realize in device applications. Zhang et al. reported a WSe_2-based ambipolar electric double layer transistor (EDLT) which produces circularly polarized electroluminescence when subjected to high electrical bias (Figure 12e).[265] This electroluminescence was ascribed to the electron−hole overlap dictated by the in-plane electric field and valley-dependent optical selection rules in 2D WSe_2. These demonstrations of electronic and optical property control in 2D TMDs open the pathway for investigating lower dimensional or mixed-dimensional TMD crystals in these and other applications.

4.3.4. Quantum Information Science. Quantum information science (QIS) seeks to harness quantum mechanical phenomena to define new directions in computation, communication, cryptography, and precision measurements. 2D materials, because of their wide range of synthetically tunable properties and capacity for supporting artificial quantum states are promising candidates on which to realize QIS goals.

Strong spin−orbit coupling and large exciton-binding energies render single-layer TMDs ideal candidates for optoelectronic[2] and valleytronic applications.[266] Structural imperfections in TMD crystals, such as ripples, grain boundaries, or atom vacancies,[35,267,268] can function as trap sites which, if properly isolated, can serve as sources of single photon emission. Single-photon emitters (SPEs) are essential pieces of hardware with which one could construct optical qubits for efficient quantum communication and quantum key distribution.

Strain engineering can be employed to tailor optical emission from 2D materials.[269] Strain-based strategies have recently demonstrated success in inducing QD-like emission from 2D TMDs and their heterostructures. In this context, Bai et al. have demonstrated modulation of the moiré potential landscape, from one comprised of arrays of quantum dots (0D) to one comprised of stripes of quantum wires (1D), through modulation of the uniaxial strain in an h-BN encapsulated $WSe_2/MoSe_2$ twisted heterobilayer (Figure 13a).[270] In another study employing a microscopic model, Carmesin et al. predicted highly localized QD-like emission from MoS_2 nanobubbles and ascribed this effect to confinement arising from an interplay of surface wrinkling and strain.[271] Building on this concept for manipulating carrier confinement in 2D TMDs, Darlington et al. recently reported strain-induced exciton localization in WSe_2 nanobubbles under ambient conditions by hyperspectral nanophotoluminescence mapping.[272] In this study, the authors identified and directly probed localized excitonic (LX) emission appearing at an energy lower than that of the primary exciton (PX) in monolayer WSe_2 (Figure 13b).[272] Realizing full control over the location and addressability of excitonic states in low-dimensional TMDs will have far-reaching consequences for use of these materials in QIS applications.

Researchers have also exploited defect centers in 2D materials as candidate sites for single-photon emission. The identification, via multiple reports in 2015,[199−202] of single-photon emission at cryogenic temperatures from defect-localized excitons in single-layer WSe_2 catalyzed interest in TMD-based SPEs (Figure 13c,d,e).[199,201,273] Single photon emission has also been observed in single-layer WS_2,[273] and $MoSe_2$,[274] and it has been suggested that TMD materials could be systematically integrated into spin qubit systems. In order to realize fully functioning quantum computers or communications devices it is necessary to define the spatial position of SPE sites precisely. In this respect, scanning probe nanolithography (SPL) has recently been suggested as a method to introduce point defects in layered materials and thereby define SPE sources with atom-scale levels of precision (Figure 13f).[275,276] Finally, the ability to electrically stimulate single photon emission in TMDs presents substantial advantages. Electrically driven single-photon emission has been demonstrated in vertically layered heterostructures comprised of

https://dx.doi.org/10.1021/acs.chemrev.0c00505
Chem. Rev. 2020, 120, 12563−12591

WSe_2 or WS_2 flakes separated by h-BN layers to facilitate tunneling of electrons and holes (Figure 13e).[273,277]

In the midst of rapidly evolving efforts in quantum information processing, it is crucial to consider the unique structural features and properties of TMDs beyond 2D and other van der Waals solids that may lead to additional breakthroughs. Several features uniquely position 1D and 0D TMD crystals to impact this growing field, including (i) the ability to incorporate electrically active and laterally confined heterojunctions, (ii) the potential to support distinct strain and defect states, and (iii) the susceptibility and tunability of the crystal to edge states. Interfacing 1D crystals with materials of higher- or lower-order dimensionality (*e.g.*, nanotube, nanowire, or quantum dot) may introduce additional and unusual strain centers or topological defects. As discussed in section 3.4, the nature and quality of edges and defects in 1D TMDs shape the crystals' optical, electronic, and magnetic properties. More research is needed to clearly understand how changes to the 1D crystal edges and defects can be directly linked to modulation of key properties. Only then will the community have access to design rules enabling the engineering of coherent quantum states in confined TMD architectures.[101−104] Finally, the remarkable advances in tuning moiré landscapes in the context of 2D materials presents a wealth of opportunities for the investigation of 1D moiré potentials in TMD nanoribbons.[270] Future research efforts will focus intensively on the bottom-up synthesis and assembly of dimensionally restricted layered TMDs to realize new device schemes for quantum information science and technology.

CONCLUSION

This review discussed recent advances and future research priorities in the transition-metal dichalcogenide (TMD) field. Our primary goal was to articulate areas of need in the preparation and analysis of TMD nanoribbons encompassing dimensionalities and morphologies beyond 2D.

In Section 2 of our review, we summarized the diverse structure−property relationships encompassed by 2D TMDs and used these points to set the stage for our subsequent discussion. In Section 3 of our review, we highlighted the many exciting research efforts underway in beyond 2D TMDs with a focus on 1D (nanoribbon) motifs. Given that major innovations in rational synthesis are required to nucleate new work in this area, we devoted much of our discussion to synthetic breakthroughs. While the preparation, manipulation, and investigation of nanoscale wide and atomically thin 1D crystals presents many challenges, the mechanical, magnetic, electronic, and optical phenomena that uniquely manifest in these beyond 2D TMDs is well worth the future scientific investment required.

In Section 4, we endeavored to present a holistic view of the research prospects and priorities in the TMD field. Aside from again emphasizing the need for breakthroughs in synthesis, we highlighted the fact that new analytical instruments and methods are needed to fuel future property discovery and analysis. We focused the bulk of our discussion in this section on providing a critical view of the priority research areas in TMD materials. We emphasized how future studies in beyond 2D materials can build on the vast body of research in optoelectronics, energy science, and quantum information science that has thus far focused on 2D TMDs. Our intent was to acknowledge the great strides made to-date while providing a clear perspective on the exciting research opportunities unique to beyond 2D TMDs, 1D nanoribbons serving as a benchmark.

This review leaves our community with several key insights and goals to work toward. First, from a synthetic standpoint, the grail would be to have a method that affords selective control over the crystal dimensionality, edge morphology, and phase with atom-levels of precision and at a scale to render device fabrication practical. Second, 1D TMDs have several unique features that contribute to the exceptionally tunable and in some cases anomalous properties they exhibit. These features include (i) a lateral confinement potential that can influence electron and/or exciton transport, (ii) a non-negligible contribution of edge states to the total material response, (iii) mechanical properties providing for new strain/defect modes. Third, harnessing atomistic control of edges and defects and implementing electronically active and laterally confined heterojunctions, some of which can be done in a 1D crystal platform, is key to realizing the potential of TMDs in photonic, electronic, and quantum information processing applications.

In conclusion, once outstanding challenges in the preparation and understanding of TMD materials encompassing all manner of topologies and phases are addressed, the transformative potential of these materials in optoelectronic, energy conversion, and quantum information science applications will be realized.

AUTHOR INFORMATION

Corresponding Author

Thomas J. Kempa − *Department of Chemistry and Department of Materials Science and Engineering, Johns Hopkins University, Baltimore 21218, United States;* orcid.org/0000-0002-1672-8325; Email: tkempa@jhu.edu

Authors

Tomojit Chowdhury − *Department of Chemistry, Johns Hopkins University, Baltimore 21218, United States*

Erick C. Sadler − *Department of Chemistry, Johns Hopkins University, Baltimore 21218, United States*

Complete contact information is available at: https://pubs.acs.org/10.1021/acs.chemrev.0c00505

Author Contributions

§T.C. and E.C.S. contributed equally.

Notes

The authors declare no competing financial interest.

Biographies

Tomojit Chowdhury received his B.Sc. and M.Sc. in Chemistry from the University of Calcutta and the Indian Institute of Technology Guwahati, respectively. He is currently a graduate student under the supervision of Prof. Thomas J. Kempa at Johns Hopkins University. His research interests include the rational design of multifunctional low-dimensional materials and the application of hybrid experimental tools to explore new mesoscopic quantum phenomena.

Erick Sadler received his B.S. degree in Chemistry from Virginia Polytechnic Institute and State University. In 2016, he joined the group of Prof. Thomas J. Kempa in the Department of Chemistry at Johns Hopkins University. His current research focuses on the synthesis and characterization of low dimensional materials.

Thomas Kempa is an Assistant Professor of Chemistry and of Materials Science and Engineering at Johns Hopkins University. After receiving his B.S. degree in Chemistry from Boston College in 2004, Tom was awarded a Marshall Scholarship and spent 2 years at Imperial College London. Returning to the United States, he began graduate studies

https://dx.doi.org/10.1021/acs.chemrev.0c00505
Chem. Rev. 2020, 120, 12563−12591

under the direction of Prof. Charles Lieber at Harvard University and earned his Ph.D. in 2012. Thereafter, Tom conducted postdoctoral studies in the laboratory of Prof. Daniel Nocera, first at MIT and then Harvard. In 2015, Tom joined Johns Hopkins University as a faculty member in the Department of Chemistry. Professor Kempa's research group develops new methods to prepare and study low-dimensional inorganic crystals from nanoparticles (0D) to few-atom thick sheets (2D) whose exceptional properties render them intriguing platforms for optoelectronic, energy conversion, and quantum science studies. His group's expertise spans the areas of physical, inorganic, and materials chemistry. Professor Kempa is the recipient of numerous awards including an NSF CAREER Award, a Toshiba Distinguished Young Investigator Award, a Dreyfus Foundation Fellowship in Environmental Chemistry, and a Hopkins Discovery Award.

ACKNOWLEDGMENTS

T.J.K. acknowledges funding from the National Science Foundation (DMR-1848046) CAREER grant, funding from the Camille and Henry Dreyfus Foundation under a grant from the Postdoctoral Program in Environmental Chemistry (EP-15-046), funding from a Toshiba Distinguished Young Investigator grant, and startup funding from Johns Hopkins University. T.C. acknowledges support from an Ernest M. Marks Award.

REFERENCES

(1) Mak, K. F.; Lee, C.; Hone, J.; Shan, J.; Heinz, T. F. Atomically Thin MoS_2: A New Direct-Gap Semiconductor. *Phys. Rev. Lett.* **2010**, *105*, 136805.
(2) Mak, K. F.; Shan, J. Photonics and Optoelectronics of 2D Semiconductor Transition Metal Dichalcogenides. *Nat. Photonics* **2016**, *10*, 216−226.
(3) Xiao, D.; Liu, G.-B.; Feng, W.; Xu, X.; Yao, W. Coupled Spin and Valley Physics in Monolayers of MoS_2 and Other Group-VI Dichalcogenides. *Phys. Rev. Lett.* **2012**, *108*, 196802.
(4) Tran, K.; Moody, G.; Wu, F.; Lu, X.; Choi, J.; Kim, K.; Rai, A.; Sanchez, D. A.; Quan, J.; Singh, A.; et al. Evidence for Moiré Excitons in van der Waals Heterostructures. *Nature* **2019**, *567*, 71−75.
(5) Butler, S. Z.; Hollen, S. M.; Cao, L.; Cui, Y.; Gupta, J. A.; Gutiérrez, H. R.; Heinz, T. F.; Hong, S. S.; Huang, J.; Ismach, A. F.; et al. Progress, Challenges, and Opportunities in Two-Dimensional Materials Beyond Graphene. *ACS Nano* **2013**, *7*, 2898−2926.
(6) Chhowalla, M.; Shin, H. S.; Eda, G.; Li, L.-J.; Loh, K. P.; Zhang, H. The Chemistry of Two-Dimensional Layered Transition Metal Dichalcogenide Nanosheets. *Nat. Chem.* **2013**, *5*, 263−275.
(7) Lin, Z.; McCreary, A.; Briggs, N.; Subramanian, S.; Zhang, K.; Sun, Y.; Li, X.; Borys, N. J.; Yuan, H.; Fullerton-Shirey, S. K.; et al. 2D Materials Advances: from Large Scale Synthesis and Controlled Heterostructures to Improved Characterization Techniques, Defects and Applications. *2D Mater.* **2016**, *3*, 042001.
(8) Mannix, A. J.; Kiraly, B.; Hersam, M. C.; Guisinger, N. P. Synthesis and Chemistry of Elemental 2D Materials. *Nat. Rev. Chem.* **2017**, *1*, 0014.
(9) Liu, Y.; Weiss, N. O.; Duan, X.; Cheng, H.-C.; Huang, Y.; Duan, X. Van der Waals Heterostructures and Devices. *Nat. Rev. Mater.* **2016**, *1*, 16042.
(10) Voiry, D.; Mohite, A.; Chhowalla, M. Phase Engineering of Transition Metal Dichalcogenides. *Chem. Soc. Rev.* **2015**, *44*, 2702−2712.
(11) Miró, P.; Audiffred, M.; Heine, T. An Atlas of Two-Dimensional Materials. *Chem. Soc. Rev.* **2014**, *43*, 6537−6554.
(12) Novoselov, K. S.; Geim, A. K.; Morozov, S. V.; Jiang, D.; Zhang, Y.; Dubonos, S. V.; Grigorieva, I. V.; Firsov, A. A. Electric Field Effect in Atomically Thin Carbon Films. *Science* **2004**, *306*, 666−669.
(13) Zhang, Y.; Tan, Y.-W.; Stormer, H. L.; Kim, P. Experimental Observation of the Quantum Hall Effect and Berry's Phase in Graphene. *Nature* **2005**, *438*, 201−204.
(14) Stankovich, S.; Dikin, D. A.; Dommett, G. H. B.; Kohlhaas, K. M.; Zimney, E. J.; Stach, E. A.; Piner, R. D.; Nguyen, S. T.; Ruoff, R. S. Graphene-Based Composite Materials. *Nature* **2006**, *442*, 282−286.
(15) Ferrari, A. C.; Meyer, J. C.; Scardaci, V.; Casiraghi, C.; Lazzeri, M.; Mauri, F.; Piscanec, S.; Jiang, D.; Novoselov, K. S.; Roth, S.; et al. Raman Spectrum of Graphene and Graphene Layers. *Phys. Rev. Lett.* **2006**, *97*, 187401.
(16) Lee, C.; Wei, X.; Kysar, J. W.; Hone, J. Measurement of the Elastic Properties and Intrinsic Strength of Monolayer Graphene. *Science* **2008**, *321*, 385−388.
(17) Castro Neto, A. H.; Guinea, F.; Peres, N. M. R.; Novoselov, K. S.; Geim, A. K. The Electronic Properties of Graphene. *Rev. Mod. Phys.* **2009**, *81*, 109.
(18) Xia, F.; Mueller, T.; Lin, Y.-m.; Valdes-Garcia, A.; Avouris, P. Ultrafast Graphene Photodetector. *Nat. Nanotechnol.* **2009**, *4*, 839−843.
(19) Geim, A. K.; Novoselov, K. S. The Rise of Graphene. *Nat. Mater.* **2007**, *6*, 183−191.
(20) Cai, J.; Pignedoli, C. A.; Talirz, L.; Ruffieux, P.; Söde, H.; Liang, L.; Meunier, V.; Berger, R.; Li, R.; Feng, X.; et al. Graphene Nanoribbon Heterojunctions. *Nat. Nanotechnol.* **2014**, *9*, 896−900.
(21) Geim, A. K.; Grigorieva, I. V. Van der Waals Heterostructures. *Nature* **2013**, *499*, 419−425.
(22) Dean, C. R.; Young, A. F.; Meric, I.; Lee, C.; Wang, L.; Sorgenfrei, S.; Watanabe, K.; Taniguchi, T.; Kim, P.; Shepard, K. L.; et al. Boron Nitride Substrates for High-Quality Graphene Electronics. *Nat. Nanotechnol.* **2010**, *5*, 722−726.
(23) Lee, K. H.; Shin, H.-J.; Lee, J.; Lee, I.-y.; Kim, G.-H.; Choi, J.-Y.; Kim, S.-W. Large-Scale Synthesis of High-Quality Hexagonal Boron Nitride Nanosheets for Large-Area Graphene Electronics. *Nano Lett.* **2012**, *12*, 714−718.
(24) Vogt, P.; De Padova, P.; Quaresima, C.; Avila, J.; Frantzeskakis, E.; Asensio, M. C.; Resta, A.; Ealet, B.; Le Lay, G. Silicene: Compelling Experimental Evidence for Graphenelike Two-Dimensional Silicon. *Phys. Rev. Lett.* **2012**, *108*, 155501.
(25) Liu, H.; Neal, A. T.; Zhu, Z.; Luo, Z.; Xu, X.; Tománek, D.; Ye, P. D. Phosphorene: An Unexplored 2D Semiconductor with a High Hole Mobility. *ACS Nano* **2014**, *8*, 4033−4041.
(26) Tran, V.; Soklaski, R.; Liang, Y.; Yang, L. Layer-Controlled Band Gap and Anisotropic Excitons in Few-Layer Black Phosphorus. *Phys. Rev. B: Condens. Matter Mater. Phys.* **2014**, *89*, 235319.
(27) Gazibegovic, S.; Badawy, G.; Buckers, T. L. J.; Leubner, P.; Shen, J.; de Vries, F. K.; Koelling, S.; Kouwenhoven, L. P.; Verheijen, M. A.; Bakkers, E. P. A. M. Bottom-Up Grown 2D InSb Nanostructures. *Adv. Mater.* **2019**, *31*, 1808181.
(28) Lauth, J.; Gorris, F. E. S.; Samadi Khoshkhoo, M.; Chassé, T.; Friedrich, W.; Lebedeva, V.; Meyer, A.; Klinke, C.; Kornowski, A.; Scheele, M.; et al. Solution-Processed Two-Dimensional Ultrathin InSe Nanosheets. *Chem. Mater.* **2016**, *28*, 1728−1736.
(29) Al Balushi, Z. Y.; Wang, K.; Ghosh, R. K.; Vilá, R. A.; Eichfeld, S. M.; Caldwell, J. D.; Qin, X.; Lin, Y.-C.; DeSario, P. A.; Stone, G.; et al. Two-Dimensional Gallium Nitride Realized via Graphene Encapsulation. *Nat. Mater.* **2016**, *15*, 1166−1171.
(30) Hung, N. T.; Nugraha, A. R. T.; Saito, R. Two-Dimensional InSe as a Potential Thermoelectric Material. *Appl. Phys. Lett.* **2017**, *111*, 092107.
(31) Mak, K. F.; He, K.; Lee, C.; Lee, G. H.; Hone, J.; Heinz, T. F.; Shan, J. Tightly Bound Trions in Monolayer MoS_2. *Nat. Mater.* **2013**, *12*, 207−211.
(32) Bellus, M. Z.; Ceballos, F.; Chiu, H.-Y.; Zhao, H. Tightly Bound Trions in Transition Metal Dichalcogenide Heterostructures. *ACS Nano* **2015**, *9*, 6459−6464.
(33) Hanbicki, A. T.; Chuang, H.-J.; Rosenberger, M. R.; Hellberg, C. S.; Sivaram, S. V.; McCreary, K. M.; Mazin, I. I.; Jonker, B. T. Double Indirect Interlayer Exciton in a $MoSe_2/WSe_2$ van der Waals Heterostructure. *ACS Nano* **2018**, *12*, 4719−4726.
(34) Mueller, T.; Malic, E. Exciton Physics and Device Application of Two-Dimensional Transition Metal Dichalcogenide Semiconductors. *npj 2D Mater. Appl.* **2018**, *2*, 29.

https://dx.doi.org/10.1021/acs.chemrev.0c00505
Chem. Rev. 2020, 120, 12563−12591

(35) Moody, G.; Tran, K.; Lu, X.; Autry, T.; Fraser, J. M.; Mirin, R. P.; Yang, L.; Li, X.; Silverman, K. L. Microsecond Valley Lifetime of Defect-Bound Excitons in Monolayer WSe_2. *Phys. Rev. Lett.* **2018**, *121*, 057403.
(36) Bollinger, M. V.; Lauritsen, J. V.; Jacobsen, K. W.; Nørskov, J. K.; Helveg, S.; Besenbacher, F. One-Dimensional Metallic Edge States in MoS_2. *Phys. Rev. Lett.* **2001**, *87*, 196803.
(37) Jaramillo, T. F.; Jørgensen, K. P.; Bonde, J.; Nielsen, J. H.; Horch, S.; Chorkendorff, I. Identification of Active Edge Sites for Electrochemical H_2 Evolution from MoS_2 Nanocatalysts. *Science* **2007**, *317*, 100−102.
(38) Kibsgaard, J.; Chen, Z.; Reinecke, B. N.; Jaramillo, T. F. Engineering the Surface Structure of MoS_2 to Preferentially Expose Active Edge Sites for Electrocatalysis. *Nat. Mater.* **2012**, *11*, 963−969.
(39) Xie, J.; Zhang, H.; Li, S.; Wang, R.; Sun, X.; Zhou, M.; Zhou, J.; Lou, X. W.; Xie, Y. Defect-Rich MoS_2 Ultrathin Nanosheets with Additional Active Edge Sites for Enhanced Electrocatalytic Hydrogen Evolution. *Adv. Mater.* **2013**, *25*, 5807−5813.
(40) Rostami, H.; Asgari, R.; Guinea, F. Edge Modes in Zigzag and Armchair Ribbons of Monolayer MoS_2. *J. Phys.: Condens. Matter* **2016**, *28*, 495001.
(41) Li, F.; Chen, L.; Liu, H.; Wang, D.; Shi, C.; Pan, H. Enhanced N_2-Fixation by Engineering the Edges of Two-Dimensional Transition-Metal Disulfides. *J. Phys. Chem. C* **2019**, *123*, 22221−22227.
(42) Xu, X.; Yao, W.; Xiao, D.; Heinz, T. F. Spin and Pseudospins in Layered Transition Metal Dichalcogenides. *Nat. Phys.* **2014**, *10*, 343−350.
(43) Mak, K. F.; McGill, K. L.; Park, J.; McEuen, P. L. The Valley Hall Effect in MoS_2 Transistors. *Science* **2014**, *344*, 1489−1492.
(44) Li, H.; Tsai, C.; Koh, A. L.; Cai, L.; Contryman, A. W.; Fragapane, A. H.; Zhao, J.; Han, H. S.; Manoharan, H. C.; Abild-Pedersen, F.; et al. Activating and Optimizing MoS_2 Basal Planes for Hydrogen Evolution Through the Formation of Strained Sulphur Vacancies. *Nat. Mater.* **2016**, *15*, 48−53.
(45) Li, H.; Wu, J.; Yin, Z.; Zhang, H. Preparation and Applications of Mechanically Exfoliated Single-Layer and Multilayer MoS_2 and WSe_2 Nanosheets. *Acc. Chem. Res.* **2014**, *47*, 1067−1075.
(46) Coleman, J. N.; Lotya, M.; O'Neill, A.; Bergin, S. D.; King, P. J.; Khan, U.; Young, K.; Gaucher, A.; De, S.; Smith, R. J.; et al. Two-Dimensional Nanosheets Produced by Liquid Exfoliation of Layered Materials. *Science* **2011**, *331*, 568−571.
(47) Liu, B.; Chen, L.; Liu, G.; Abbas, A. N.; Fathi, M.; Zhou, C. High-Performance Chemical Sensing Using Schottky-Contacted Chemical Vapor Deposition Grown Monolayer MoS_2 Transistors. *ACS Nano* **2014**, *8*, 5304−5314.
(48) Tang, H.-L.; Chiu, M.-H.; Tseng, C.-C.; Yang, S.-H.; Hou, K.-J.; Wei, S.-Y.; Huang, J.-K.; Lin, Y.-F.; Lien, C.-H.; Li, L.-J. Multilayer Graphene-WSe_2 Heterostructures for WSe_2 Transistors. *ACS Nano* **2017**, *11*, 12817−12823.
(49) Lu, X.; Utama, M. I. B.; Lin, J.; Gong, X.; Zhang, J.; Zhao, Y.; Pantelides, S. T.; Wang, J.; Dong, Z.; Liu, Z.; et al. Large-Area Synthesis of Monolayer and Few-Layer $MoSe_2$ Films on SiO_2 Substrates. *Nano Lett.* **2014**, *14*, 2419−2425.
(50) Li, H.; Lu, G.; Wang, Y.; Yin, Z.; Cong, C.; He, Q.; Wang, L.; Ding, F.; Yu, T.; Zhang, H. Mechanical Exfoliation and Characterization of Single- and Few-Layer Nanosheets of WSe_2, TaS_2, and $TaSe_2$. *Small* **2013**, *9*, 1974−1981.
(51) Chen, M.-W.; Ovchinnikov, D.; Lazar, S.; Pizzochero, M.; Whitwick, M. B.; Surrente, A.; Baranowski, M.; Sanchez, O. L.; Gillet, P.; Plochocka, P.; et al. Highly Oriented Atomically Thin Ambipolar $MoSe_2$ Grown by Molecular Beam Epitaxy. *ACS Nano* **2017**, *11*, 6355−6361.
(52) Zhang, Y.; Chang, T.-R.; Zhou, B.; Cui, Y.-T.; Yan, H.; Liu, Z.; Schmitt, F.; Lee, J.; Moore, R.; Chen, Y.; et al. Direct Observation of the Transition from Indirect to Direct Bandgap in Atomically Thin Epitaxial $MoSe_2$. *Nat. Nanotechnol.* **2014**, *9*, 111−115.
(53) Yue, R.; Barton, A. T.; Zhu, H.; Azcatl, A.; Pena, L. F.; Wang, J.; Peng, X.; Lu, N.; Cheng, L.; Addou, R.; et al. $HfSe_2$ Thin Films: 2D Transition Metal Dichalcogenides Grown by Molecular Beam Epitaxy. *ACS Nano* **2015**, *9*, 474−480.
(54) Roy, A.; Movva, H. C. P.; Satpati, B.; Kim, K.; Dey, R.; Rai, A.; Pramanik, T.; Guchhait, S.; Tutuc, E.; Banerjee, S. K. Structural and Electrical Properties of $MoTe_2$ and $MoSe_2$ Grown by Molecular Beam Epitaxy. *ACS Appl. Mater. Interfaces* **2016**, *8*, 7396−7402.
(55) Kang, K.; Xie, S.; Huang, L.; Han, Y.; Huang, P. Y.; Mak, K. F.; Kim, C.-J.; Muller, D.; Park, J. High-Mobility Three-Atom-Thick Semiconducting Films with Wafer-Scale Homogeneity. *Nature* **2015**, *520*, 656−660.
(56) Splendiani, A.; Sun, L.; Zhang, Y.; Li, T.; Kim, J.; Chim, C.-Y.; Galli, G.; Wang, F. Emerging Photoluminescence in Monolayer MoS_2. *Nano Lett.* **2010**, *10*, 1271−1275.
(57) Eda, G.; Yamaguchi, H.; Voiry, D.; Fujita, T.; Chen, M.; Chhowalla, M. Photoluminescence from Chemically Exfoliated MoS_2. *Nano Lett.* **2011**, *11*, 5111−5116.
(58) Scuri, G.; Zhou, Y.; High, A. A.; Wild, D. S.; Shu, C.; De Greve, K.; Jauregui, L. A.; Taniguchi, T.; Watanabe, K.; Kim, P.; et al. Large Excitonic Reflectivity of Monolayer $MoSe_2$ Encapsulated in Hexagonal Boron Nitride. *Phys. Rev. Lett.* **2018**, *120*, 037402.
(59) Wang, K.; De Greve, K.; Jauregui, L. A.; Sushko, A.; High, A.; Zhou, Y.; Scuri, G.; Taniguchi, T.; Watanabe, K.; Lukin, M. D.; et al. Electrical Control of Charged Carriers and Excitons in Atomically Thin Materials. *Nat. Nanotechnol.* **2018**, *13*, 128−132.
(60) Sangwan, V. K.; Jariwala, D.; Kim, I. S.; Chen, K.-S.; Marks, T. J.; Lauhon, L. J.; Hersam, M. C. Gate-Tunable Memristive Phenomena Mediated by Grain Boundaries in Single-Layer MoS_2. *Nat. Nanotechnol.* **2015**, *10*, 403−406.
(61) Najmaei, S.; Liu, Z.; Zhou, W.; Zou, X.; Shi, G.; Lei, S.; Yakobson, B. I.; Idrobo, J.-C.; Ajayan, P. M.; Lou, J. Vapour Phase Growth and Grain Boundary Structure of Molybdenum Disulphide Atomic Layers. *Nat. Mater.* **2013**, *12*, 754−759.
(62) Voiry, D.; Yamaguchi, H.; Li, J.; Silva, R.; Alves, D. C. B.; Fujita, T.; Chen, M.; Asefa, T.; Shenoy, V. B.; Eda, G.; et al. Enhanced Catalytic Activity in Strained Chemically Exfoliated WS_2 Nanosheets for Hydrogen Evolution. *Nat. Mater.* **2013**, *12*, 850−855.
(63) Alivisatos, A. P. Semiconductor Clusters, Nanocrystals, and Quantum Dots. *Science* **1996**, *271*, 933−937.
(64) Hu, J.; Odom, T. W.; Lieber, C. M. Chemistry and Physics in One Dimension: Synthesis and Properties of Nanowires and Nanotubes. *Acc. Chem. Res.* **1999**, *32*, 435−445.
(65) Dai, H.; Lieber, C. M. Scanning Tunneling Microscopy Studies of Low-Dimensional Materials: Charge Density Wave Pinning and Melting in Two Dimensions. *Annu. Rev. Phys. Chem.* **1993**, *44*, 237−263.
(66) Kempa, T. J.; Kim, S.-K.; Day, R. W.; Park, H.-G.; Nocera, D. G.; Lieber, C. M. Facet-Selective Growth on Nanowires Yields Multi-Component Nanostructures and Photonic Devices. *J. Am. Chem. Soc.* **2013**, *135*, 18354−18357.
(67) Kim, S.-K.; Song, K.-D.; Kempa, T. J.; Day, R. W.; Lieber, C. M.; Park, H.-G. Design of Nanowire Optical Cavities as Efficient Photon Absorbers. *ACS Nano* **2014**, *8*, 3707−3714.
(68) Kempa, T. J.; Cahoon, J. F.; Kim, S.-K.; Day, R. W.; Bell, D. C.; Park, H.-G.; Lieber, C. M. Coaxial Multishell Nanowires with High-Quality Electronic Interfaces and Tunable Optical Cavities for Ultrathin Photovoltaics. *Proc. Natl. Acad. Sci. U. S. A.* **2012**, *109*, 1407−1412.
(69) Kempa, T. J.; Lieber, C. M. Semiconductor Nanowire Solar Cells: Synthetic Advances and Tunable Properties. *Pure Appl. Chem.* **2014**, *86*, 13−26.
(70) Song, K.-D.; Kempa, T. J.; Park, H.-G.; Kim, S.-K. Laterally Assembled Nanowires for Ultrathin Broadband Solar Absorbers. *Opt. Express* **2014**, *22*, A992−A1000.
(71) Cohen-Karni, T.; Timko, B. P.; Weiss, L. E.; Lieber, C. M. Flexible Electrical Recording from Cells Using Nanowire Transistor Arrays. *Proc. Natl. Acad. Sci. U. S. A.* **2009**, *106*, 7309−7313.
(72) Hu, Y.; Kuemmeth, F.; Lieber, C. M.; Marcus, C. M. Hole Spin Relaxation in Ge-Si Core-Shell Nanowire Qubits. *Nat. Nanotechnol.* **2012**, *7*, 47−50.
(73) Tian, B.; Liu, J.; Dvir, T.; Jin, L.; Tsui, J. H.; Qing, Q.; Suo, Z.; Langer, R.; Kohane, D. S.; Lieber, C. M. Macroporous Nanowire

https://dx.doi.org/10.1021/acs.chemrev.0c00505
Chem. Rev. 2020, 120, 12563−12591

Nanoelectronic Scaffolds for Synthetic Tissues. *Nat. Mater.* **2012**, *11*, 986−994.
(74) Deng, J.; Su, Y.; Liu, D.; Yang, P.; Liu, B.; Liu, C. Nanowire Photoelectrochemistry. *Chem. Rev.* **2019**, *119*, 9221−9259.
(75) Su, Y.; Liu, C.; Brittman, S.; Tang, J.; Fu, A.; Kornienko, N.; Kong, Q.; Yang, P. Single-Nanowire Photoelectrochemistry. *Nat. Nanotechnol.* **2016**, *11*, 609−612.
(76) Park, H.-G.; Barrelet, C. J.; Wu, Y.; Tian, B.; Qian, F.; Lieber, C. M. A Wavelength-Selective Photonic-Crystal Waveguide Coupled to a Nanowire Light Source. *Nat. Photonics* **2008**, *2*, 622−626.
(77) Nakada, K.; Fujita, M.; Dresselhaus, G.; Dresselhaus, M. S. Edge State in Graphene Ribbons: Nanometer Size Effect and Edge Shape Dependence. *Phys. Rev. B: Condens. Matter Mater. Phys.* **1996**, *54*, 17954.
(78) Li, X.; Wang, X.; Zhang, L.; Lee, S.; Dai, H. Chemically Derived, Ultrasmooth Graphene Nanoribbon Semiconductors. *Science* **2008**, *319*, 1229−1232.
(79) Han, M. Y.; Özyilmaz, B.; Zhang, Y.; Kim, P. Energy Band-Gap Engineering of Graphene Nanoribbons. *Phys. Rev. Lett.* **2007**, *98*, 206805.
(80) Wang, X.; Dai, H. Etching and Narrowing of Graphene from the Edges. *Nat. Chem.* **2010**, *2*, 661−665.
(81) Kosynkin, D. V.; Higginbotham, A. L.; Sinitskii, A.; Lomeda, J. R.; Dimiev, A.; Price, B. K.; Tour, J. M. Longitudinal Unzipping of Carbon Nanotubes to form Graphene Nanoribbons. *Nature* **2009**, *458*, 872−876.
(82) Jiao, L.; Zhang, L.; Wang, X.; Diankov, G.; Dai, H. Narrow Graphene Nanoribbons from Carbon Nanotubes. *Nature* **2009**, *458*, 877−880.
(83) Rizzo, D. J.; Veber, G.; Cao, T.; Bronner, C.; Chen, T.; Zhao, F.; Rodriguez, H.; Louie, S. G.; Crommie, M. F.; Fischer, F. R. Topological Band Engineering of Graphene Nanoribbons. *Nature* **2018**, *560*, 204−208.
(84) Yang, X.; Dou, X.; Rouhanipour, A.; Zhi, L.; Räder, H. J.; Müllen, K. Two-Dimensional Graphene Nanoribbons. *J. Am. Chem. Soc.* **2008**, *130*, 4216−4217.
(85) Li, Y.; Zhou, Z.; Zhang, S.; Chen, Z. MoS_2 Nanoribbons: High Stability and Unusual Electronic and Magnetic Properties. *J. Am. Chem. Soc.* **2008**, *130*, 16739−16744.
(86) Wang, Z.; Li, H.; Liu, Z.; Shi, Z.; Lu, J.; Suenaga, K.; Joung, S.-K.; Okazaki, T.; Gu, Z.; Zhou, J.; et al. Mixed Low-Dimensional Nanomaterial: 2D Ultranarrow MoS_2 Inorganic Nanoribbons Encapsulated in Quasi-1D Carbon Nanotubes. *J. Am. Chem. Soc.* **2010**, *132*, 13840−13847.
(87) Zhang, J.; Soon, J. M.; Loh, K. P.; Yin, J.; Ding, J.; Sullivian, M. B.; Wu, P. Magnetic Molybdenum Disulfide Nanosheet Films. *Nano Lett.* **2007**, *7*, 2370−2376.
(88) Tongay, S.; Varnoosfaderani, S. S.; Appleton, B. R.; Wu, J.; Hebard, A. F. Magnetic Properties of MoS_2: Existence of Ferromagnetism. *Appl. Phys. Lett.* **2012**, *101*, 123105.
(89) Pan, H.; Zhang, Y.-W. Edge-Dependent Structural, Electronic and Magnetic Properties of MoS_2 Nanoribbons. *J. Mater. Chem.* **2012**, *22*, 7280−7290.
(90) Fan, D. D.; Liu, H. J.; Cheng, L.; Jiang, P. H.; Shi, J.; Tang, X. F. MoS_2 Nanoribbons as Promising Thermoelectric Materials. *Appl. Phys. Lett.* **2014**, *105*, 133113.
(91) Hicks, L. D.; Dresselhaus, M. S. Thermoelectric Figure of Merit of a One-Dimensional Conductor. *Phys. Rev. B: Condens. Matter Mater. Phys.* **1993**, *47*, 16631.
(92) Hicks, L. D.; Harman, T. C.; Sun, X.; Dresselhaus, M. S. Experimental Study of the Effect of Quantum-Well Structures on the Thermoelectric Figure of Merit. *Phys. Rev. B* **1996**, *53*, 450−453.
(93) Zan, W.; Zhang, Z.; Yang, Y.; Yao, X.; Li, S.; Yakobson, B. I. Width-Dependent Phase Crossover in Transition Metal Dichalcogenide Nanoribbons. *Nanotechnology* **2019**, *30*, 075701.
(94) Dago, A. I.; Ryu, Y. K.; Palomares, F. J.; Garcia, R. Direct Patterning of p-Type-Doped Few-layer WSe_2 Nanoelectronic Devices by Oxidation Scanning Probe Lithography. *ACS Appl. Mater. Interfaces* **2018**, *10*, 40054−40061.
(95) Wu, J.-B.; Zhao, H.; Li, Y.; Ohlberg, D.; Shi, W.; Wu, W.; Wang, H.; Tan, P.-H. Monolayer Molybdenum Disulfide Nanoribbons with High Optical Anisotropy. *Adv. Opt. Mater.* **2016**, *4*, 756−762.
(96) Chen, S.; Kim, S.; Chen, W.; Yuan, J.; Bashir, R.; Lou, J.; van der Zande, A. M.; King, W. P. Monolayer MoS_2 Nanoribbon Transistors Fabricated by Scanning Probe Lithography. *Nano Lett.* **2019**, *19*, 2092−2098.
(97) Liu, H.; Gu, J.; Ye, P. D. MoS_2 Nanoribbon Transistors: Transition From Depletion Mode to Enhancement Mode by Channel-Width Trimming. *IEEE Electron Device Lett.* **2012**, *33*, 1273−1275.
(98) Kotekar-Patil, D.; Deng, J.; Wong, S. L.; Lau, C. S.; Goh, K. E. J. Single Layer MoS_2 Nanoribbon Field Effect Transistor. *Appl. Phys. Lett.* **2019**, *114*, 013508.
(99) Watts, M. C.; Picco, L.; Russell-Pavier, F. S.; Cullen, P. L.; Miller, T. S.; Bartuś, S. P.; Payton, O. D.; Skipper, N. T.; Tileli, V.; Howard, C. A. Production of Phosphorene Nanoribbons. *Nature* **2019**, *568*, 216−220.
(100) Stanford, M. G.; Rack, P. D.; Jariwala, D. Emerging Nanofabrication and Quantum Confinement Techniques for 2D Materials Beyond Graphene. *npj 2D Materials and Applications* **2018**, *2*, 20.
(101) Cheng, F.; Xu, H.; Xu, W.; Zhou, P.; Martin, J.; Loh, K. P. Controlled Growth of 1D $MoSe_2$ Nanoribbons with Spatially Modulated Edge States. *Nano Lett.* **2017**, *17*, 1116−1120.
(102) Chen, T.; Hao, G.; Wang, G.; Li, B.; Kou, L.; Yang, H.; Zheng, X.; Zhong, J. Controlled Growth of Atomically Thin $MoSe_2$ Films and Nanoribbons by Chemical Vapor Deposition. *2D Mater.* **2019**, *6*, 025002.
(103) Poh, S. M.; Tan, S. J. R.; Zhao, X.; Chen, Z.; Abdelwahab, I.; Fu, D.; Xu, H.; Bao, Y.; Zhou, W.; Loh, K. P. Large Area Synthesis of 1D-$MoSe_2$ Using Molecular Beam Epitaxy. *Adv. Mater.* **2017**, *29*, 1605641.
(104) Chowdhury, T.; Kim, J.; Sadler, E. C.; Li, C.; Lee, S. W.; Jo, K.; Xu, W.; Gracias, D. H.; Drichko, N. V.; Jariwala, D.; Brintlinger, T. H.; Mueller, T.; Park, H.-G.; Kempa, T. J. Substrate-Directed Synthesis of MoS_2 Nanocrystals with Tunable Dimensionality and Optical Properties. *Nat. Nanotechnol.* **2020**, *15*, 29−34.
(105) Cho, B.; Bareño, J.; Foo, Y. L.; Hong, S.; Spila, T.; Petrov, I.; Greene, J. E. Phosphorus Incorporation During Si(001):P Gas-Source Molecular Beam Epitaxy: Effects on Growth Kinetics and Surface Morphology. *J. Appl. Phys.* **2008**, *103*, 123530.
(106) Kong, D.; Wang, H.; Cha, J. J.; Pasta, M.; Koski, K. J.; Yao, J.; Cui, Y. Synthesis of MoS_2 and $MoSe_2$ Films with Vertically Aligned Layers. *Nano Lett.* **2013**, *13*, 1341−1347.
(107) Yang, L.; Hong, H.; Fu, Q.; Huang, Y.; Zhang, J.; Cui, X.; Fan, Z.; Liu, K.; Xiang, B. Single-Crystal Atomic-Layered Molybdenum Disulfide Nanobelts with High Surface Activity. *ACS Nano* **2015**, *9*, 6478−6483.
(108) Yu, J. H.; Lee, H. R.; Hong, S. S.; Kong, D.; Lee, H.-W.; Wang, H.; Xiong, F.; Wang, S.; Cui, Y. Vertical Heterostructure of Two-Dimensional MoS_2 and WSe_2 with Vertically Aligned Layers. *Nano Lett.* **2015**, *15*, 1031−1035.
(109) Murthy, A. A.; Li, Y.; Palacios, E.; Li, Q.; Hao, S.; DiStefano, J. G.; Wolverton, C.; Aydin, K.; Chen, X.; Dravid, V. P. Optically Active 1D MoS_2 Nanobelts. *ACS Appl. Mater. Interfaces* **2018**, *10*, 6799−6804.
(110) Jung, Y.; Shen, J.; Liu, Y.; Woods, J. M.; Sun, Y.; Cha, J. J. Metal Seed Layer Thickness-Induced Transition From Vertical to Horizontal Growth of MoS_2 and WS_2. *Nano Lett.* **2014**, *14*, 6842−6849.
(111) Li, H.; Wu, H.; Yuan, S.; Qian, H. Synthesis and Characterization of Vertically Standing MoS_2 Nanosheets. *Sci. Rep.* **2016**, *6*, 21171.
(112) Kumar, P.; Viswanath, B. Horizontally and Vertically Aligned Growth of Strained MoS_2 Layers with Dissimilar Wetting and Catalytic Behaviors. *CrystEngComm* **2017**, *19*, 5068−5078.
(113) Chen, Y.; Cui, P.; Ren, X.; Zhang, C.; Jin, C.; Zhang, Z.; Shih, C.-K. Fabrication of $MoSe_2$ Nanoribbons via an Unusual Morphological Phase Transition. *Nat. Commun.* **2017**, *8*, 15135.
(114) Scheuschner, N.; Ochedowski, O.; Kaulitz, A.-M.; Gillen, R.; Schleberger, M.; Maultzsch, J. Photoluminescence of Freestanding

https://dx.doi.org/10.1021/acs.chemrev.0c00505
Chem. Rev. 2020, 120, 12563−12591

Single- and Few-Layer MoS_2. *Phys. Rev. B: Condens. Matter Mater. Phys.* **2014**, *89*, 125406.
(115) Li, S.; Lin, Y.-C.; Zhao, W.; Wu, J.; Wang, Z.; Hu, Z.; Shen, Y.; Tang, D.-M.; Wang, J.; Zhang, Q.; et al. Vapour-Liquid-Solid Growth of Monolayer MoS_2 Nanoribbons. *Nat. Mater.* **2018**, *17*, 535−542.
(116) Gnanasekaran, T.; Mahendran, K. H.; Kutty, K. V. G.; Mathews, C. K. Phase Diagram Studies on the Na-Mo-O system. *J. Nucl. Mater.* **1989**, *165*, 210−216.
(117) Ismach, A.; Segev, L.; Wachtel, E.; Joselevich, E. Atomic-Step-Templated Formation of Single Wall Carbon Nanotube Patterns. *Angew. Chem., Int. Ed.* **2004**, *43*, 6140−6143.
(118) Tsivion, D.; Schvartzman, M.; Popovitz-Biro, R.; von Huth, P.; Joselevich, E. Guided Growth of Millimeter-Long Horizontal Nanowires with Controlled Orientations. *Science* **2011**, *333*, 1003−1007.
(119) Jacobberger, R. M.; Murray, E. A.; Fortin-Deschênes, M.; Göltl, F.; Behn, W. A.; Krebs, Z. J.; Levesque, P. L.; Savage, D. E.; Smoot, C.; Lagally, M. G.; et al. Alignment of Semiconducting Graphene Nanoribbons on Vicinal Ge(001). *Nanoscale* **2019**, *11*, 4864−4875.
(120) Jacobberger, R. M.; Kiraly, B.; Fortin-Deschenes, M.; Levesque, P. L.; McElhinny, K. M.; Brady, G. J.; Rojas Delgado, R.; Singha Roy, S.; Mannix, A.; Lagally, M. G.; et al. Direct Oriented Growth of Armchair Graphene Nanoribbons on Germanium. *Nat. Commun.* **2015**, *6*, 8006.
(121) Kiraly, B.; Mannix, A. J.; Jacobberger, R. M.; Fisher, B. L.; Arnold, M. S.; Hersam, M. C.; Guisinger, N. P. Sub-5nm, Globally Aligned Graphene Nanoribbons on Ge(001). *Appl. Phys. Lett.* **2016**, *108*, 213101.
(122) Ma, Z.; Wang, S.; Deng, Q.; Hou, Z.; Zhou, X.; Li, X.; Cui, F.; Si, H.; Zhai, T.; Xu, H. Epitaxial Growth of Rectangle Shape MoS_2 with Highly Aligned Orientation on Twofold Symmetry a-Plane Sapphire. *Small* **2020**, *16*, 2000596.
(123) Tenne, R.; Margulis, L.; Genut, M.; Hodes, G. Polyhedral and Cylindrical Structures of Tungsten Disulphide. *Nature* **1992**, *360*, 444−446.
(124) Feldman, Y.; Wasserman, E.; Srolovitz, D. J.; Tenne, R. High-Rate, Gas-Phase Growth of MoS_2 Nested Inorganic Fullerenes and Nanotubes. *Science* **1995**, *267*, 222−225.
(125) Goldbart, O.; Cohen, S. R.; Kaplan-Ashiri, I.; Glazyrina, P.; Wagner, H. D.; Enyashin, A.; Tenne, R. Diameter-Dependent Wetting of Tungsten Disulfide Nanotubes. *Proc. Natl. Acad. Sci. U. S. A.* **2016**, *113*, 13624−13629.
(126) Qin, F.; Shi, W.; Ideue, T.; Yoshida, M.; Zak, A.; Tenne, R.; Kikitsu, T.; Inoue, D.; Hashizume, D.; Iwasa, Y. Superconductivity in a Chiral Nanotube. *Nat. Commun.* **2017**, *8*, 14465.
(127) Qin, F.; Ideue, T.; Shi, W.; Zhang, X.-X.; Yoshida, M.; Zak, A.; Tenne, R.; Kikitsu, T.; Inoue, D.; Hashizume, D.; et al. Diameter-Dependent Superconductivity in Individual WS_2 Nanotubes. *Nano Lett.* **2018**, *18*, 6789−6794.
(128) Blees, M. K.; Barnard, A. W.; Rose, P. A.; Roberts, S. P.; McGill, K. L.; Huang, P. Y.; Ruyack, A. R.; Kevek, J. W.; Kobrin, B.; Muller, D. A.; et al. Graphene Kirigami. *Nature* **2015**, *524*, 204−207.
(129) Davelou, D.; Kopidakis, G.; Kaxiras, E.; Remediakis, I. N. Nanoribbon Edges of Transition-Metal Dichalcogenides: Stability and Electronic Properties. *Phys. Rev. B: Condens. Matter Mater. Phys.* **2017**, *96*, 165436.
(130) Orlof, A.; Ruseckas, J.; Zozoulenko, I. V. Effect of Zigzag and Armchair Edges on the Electronic Transport in Single-Layer and Bilayer Graphene Nanoribbons with Defects. *Phys. Rev. B: Condens. Matter Mater. Phys.* **2013**, *88*, 125409.
(131) Yao, A. L.; Wang, X.-F.; Liu, Y.-S.; Sun, Y.-N. Electronic Structure and I-V Characteristics of InSe Nanoribbons. *Nanoscale Res. Lett.* **2018**, *13*, 107.
(132) Ataca, C.; Şahin, H.; Aktürk, E.; Ciraci, S. Mechanical and Electronic Properties of MoS_2 Nanoribbons and Their Defects. *J. Phys. Chem. C* **2011**, *115*, 3934−3941.
(133) Chen, K.; Deng, J.; Ding, X.; Sun, J.; Yang, S.; Liu, J. Z. Ferromagnetism of 1T′-MoS_2 Nanoribbons Stabilized by Edge Reconstruction and Its Periodic Variation on Nanoribbons Width. *J. Am. Chem. Soc.* **2018**, *140*, 16206−16212.
(134) Varsano, D.; Palummo, M.; Molinari, E.; Rontani, M. A Monolayer Transition-Metal Dichalcogenide as a Topological Excitonic Insulator. *Nat. Nanotechnol.* **2020**, *15*, 367−372.
(135) Huang, J.-H.; Wang, X.-F.; Liu, Y.-S.; Zhou, L.-P. Electronic Properties of Armchair Black Phosphorene Nanoribbons Edge-Modified by Transition Elements V, Cr, and Mn. *Nanoscale Res. Lett.* **2019**, *14*, 145.
(136) Sorkin, V.; Zhang, Y. W. The Structure and Elastic Properties of Phosphorene Edges. *Nanotechnology* **2015**, *26*, 235707.
(137) Chen, Q.; Li, H.; Xu, W.; Wang, S.; Sawada, H.; Allen, C. S.; Kirkland, A. I.; Grossman, J. C.; Warner, J. H. Atomically Flat Zigzag Edges in Monolayer MoS_2 by Thermal Annealing. *Nano Lett.* **2017**, *17*, 5502−5507.
(138) Ghorbani-Asl, M.; Enyashin, A. N.; Kuc, A.; Seifert, G.; Heine, T. Defect-Induced Conductivity Anisotropy in MoS_2 Monolayers. *Phys. Rev. B: Condens. Matter Mater. Phys.* **2013**, *88*, 245440.
(139) Nan, H.; Wang, Z.; Wang, W.; Liang, Z.; Lu, Y.; Chen, Q.; He, D.; Tan, P.; Miao, F.; Wang, X.; et al. Strong Photoluminescence Enhancement of MoS_2 through Defect Engineering and Oxygen Bonding. *ACS Nano* **2014**, *8*, 5738−5745.
(140) Yin, X.; Ye, Z.; Chenet, D. A.; Ye, Y.; O'Brien, K.; Hone, J. C.; Zhang, X. Edge Nonlinear Optics on a MoS_2 Atomic Monolayer. *Science* **2014**, *344*, 488−490.
(141) Zhang, Z.; Zou, X.; Crespi, V. H.; Yakobson, B. I. Intrinsic Magnetism of Grain Boundaries in Two-Dimensional Metal Dichalcogenides. *ACS Nano* **2013**, *7*, 10475−10481.
(142) Chen, Y.; Huang, S.; Ji, X.; Adepalli, K.; Yin, K.; Ling, X.; Wang, X.; Xue, J.; Dresselhaus, M.; Kong, J.; et al. Tuning Electronic Structure of Single Layer MoS_2 through Defect and Interface Engineering. *ACS Nano* **2018**, *12*, 2569−2579.
(143) Cho, K.; Pak, J.; Chung, S.; Lee, T. Recent Advances in Interface Engineering of Transition-Metal Dichalcogenides with Organic Molecules and Polymers. *ACS Nano* **2019**, *13*, 9713−9734.
(144) Hu, Z.; Wu, Z.; Han, C.; He, J.; Ni, Z.; Chen, W. Two-Dimensional Transition Metal Dichalcogenides: Interface and Defect Engineering. *Chem. Soc. Rev.* **2018**, *47*, 3100−3128.
(145) Chen, W.; Qi, D.; Gao, X.; Wee, A. T. S. Surface Transfer Doping of Semiconductors. *Prog. Surf. Sci.* **2009**, *84*, 279−321.
(146) Wang, Y.; Kim, J. C.; Wu, R. J.; Martinez, J.; Song, X.; Yang, J.; Zhao, F.; Mkhoyan, A.; Jeong, H. Y.; Chhowalla, M. Van der Waals Contacts Between Three-Dimensional Metals and Two-Dimensional Semiconductors. *Nature* **2019**, *568*, 70−74.
(147) Liu, Y.; Guo, J.; Zhu, E.; Liao, L.; Lee, S.-J.; Ding, M.; Shakir, I.; Gambin, V.; Huang, Y.; Duan, X. Approaching the Schottky-Mott Limit in van der Waals Metal-Semiconductor Junctions. *Nature* **2018**, *557*, 696−700.
(148) Cui, X.; Shih, E.-M.; Jauregui, L. A.; Chae, S. H.; Kim, Y. D.; Li, B.; Seo, D.; Pistunova, K.; Yin, J.; Park, J.-H.; et al. Low-Temperature Ohmic Contact to Monolayer MoS_2 by van der Waals Bonded Co/h-BN Electrodes. *Nano Lett.* **2017**, *17*, 4781−4786.
(149) Liu, W.; Kang, J.; Sarkar, D.; Khatami, Y.; Jena, D.; Banerjee, K. Role of Metal Contacts in Designing High-Performance Monolayer n-Type WSe_2 Field Effect Transistors. *Nano Lett.* **2013**, *13*, 1983−1990.
(150) Joo, M.-K.; Moon, B. H.; Ji, H.; Han, G. H.; Kim, H.; Lee, G.; Lim, S. C.; Suh, D.; Lee, Y. H. Understanding Coulomb Scattering Mechanism in Monolayer MoS_2 Channel in the Presence of h-BN Buffer Layer. *ACS Appl. Mater. Interfaces* **2017**, *9*, 5006−5013.
(151) Lin, Z.; Carvalho, B. R.; Kahn, E.; Lv, R.; Rao, R.; Terrones, H.; Pimenta, M. A.; Terrones, M. Defect Engineering of Two-Dimensional Transition Metal Dichalcogenides. *2D Mater.* **2016**, *3*, 022002.
(152) Zhang, S.; Wang, C.-G.; Li, M.-Y.; Huang, D.; Li, L.-J.; Ji, W.; Wu, S. Defect Structure of Localized Excitons in a WSe_2 Monolayer. *Phys. Rev. Lett.* **2017**, *119*, 046101.
(153) Qiu, H.; Xu, T.; Wang, Z.; Ren, W.; Nan, H.; Ni, Z.; Chen, Q.; Yuan, S.; Miao, F.; Song, F.; et al. Hopping Transport Through Defect-Induced Localized States in Molybdenum Disulphide. *Nat. Commun.* **2013**, *4*, 2642.

https://dx.doi.org/10.1021/acs.chemrev.0c00505
Chem. Rev. 2020, 120, 12563−12591

(154) Zhang, C.; Wang, C.; Yang, F.; Huang, J.-K.; Li, L.-J.; Yao, W.; Ji, W.; Shih, C.-K. Engineering Point-Defect States in Monolayer WSe_2. *ACS Nano* **2019**, *13*, 1595−1602.
(155) Voiry, D.; Goswami, A.; Kappera, R.; Silva, C. d. C. C. e.; Kaplan, D.; Fujita, T.; Chen, M.; Asefa, T.; Chhowalla, M. Covalent Functionalization of Monolayered Transition Metal Dichalcogenides by Phase Engineering. *Nat. Chem.* **2015**, *7*, 45−49.
(156) Bao, W.; Borys, N. J.; Ko, C.; Suh, J.; Fan, W.; Thron, A.; Zhang, Y.; Buyanin, A.; Zhang, J.; Cabrini, S.; et al. Visualizing Nanoscale Excitonic Relaxation Properties of Disordered Edges and Grain Boundaries in Monolayer Molybdenum Disulfide. *Nat. Commun.* **2015**, *6*, 7993.
(157) Zhang, H.; Abhiraman, B.; Zhang, Q.; Miao, J.; Jo, K.; Roccasecca, S.; Knight, M. W.; Davoyan, A. R.; Jariwala, D. Hybrid Exciton-Plasmon-Polaritons in van der Waals Semiconductor Gratings. *Nat. Commun.* **2020**, *11*, 3552.
(158) Jariwala, D.; Davoyan, A. R.; Tagliabue, G.; Sherrott, M. C.; Wong, J.; Atwater, H. A. Near-Unity Absorption in van der Waals Semiconductors for Ultrathin Optoelectronics. *Nano Lett.* **2016**, *16*, 5482−5487.
(159) Durr, R. A.; Haberer, D.; Lee, Y.-L.; Blackwell, R.; Kalayjian, A. M.; Marangoni, T.; Ihm, J.; Louie, S. G.; Fischer, F. R. Orbitally Matched Edge-Doping in Graphene Nanoribbons. *J. Am. Chem. Soc.* **2018**, *140*, 807−813.
(160) Pedramrazi, Z.; Chen, C.; Zhao, F.; Cao, T.; Nguyen, G. D.; Omrani, A. A.; Tsai, H.-Z.; Cloke, R. R.; Marangoni, T.; Rizzo, D. J.; et al. Concentration Dependence of Dopant Electronic Structure in Bottom-up Graphene Nanoribbons. *Nano Lett.* **2018**, *18*, 3550−3556.
(161) Rizzo, D. J.; Wu, M.; Tsai, H.-Z.; Marangoni, T.; Durr, R. A.; Omrani, A. A.; Liou, F.; Bronner, C.; Joshi, T.; Nguyen, G. D.; et al. Length-Dependent Evolution of Type II Heterojunctions in Bottom-Up-Synthesized Graphene Nanoribbons. *Nano Lett.* **2019**, *19*, 3221−3228.
(162) Price, C. C.; Frey, N. C.; Jariwala, D.; Shenoy, V. B. Engineering Zero-Dimensional Quantum Confinement in Transition-Metal Dichalcogenide Heterostructures. *ACS Nano* **2019**, *13*, 8303−8311.
(163) Fathipour, S.; Remskar, M.; Varlec, A.; Ajoy, A.; Yan, R.; Vishwanath, S.; Rouvimov, S.; Hwang, W. S.; Xing, H. G.; Jena, D.; et al. Synthesized Multiwall MoS_2 Nanotube and Nanoribbon Field-Effect Transistors. *Appl. Phys. Lett.* **2015**, *106*, 022114.
(164) Kim, I. S.; Sangwan, V. K.; Jariwala, D.; Wood, J. D.; Park, S.; Chen, K.-S.; Shi, F.; Ruiz-Zepeda, F.; Ponce, A.; Jose-Yacaman, M.; et al. Influence of Stoichiometry on the Optical and Electrical Properties of Chemical Vapor Deposition Derived MoS_2. *ACS Nano* **2014**, *8*, 10551−10558.
(165) Sagynbaeva, M.; Panigrahi, P.; Yunguo, L.; Ramzan, M.; Ahuja, R. Tweaking the Magnetism of MoS_2 Nanoribbon with Hydrogen and Carbon Passivation. *Nanotechnology* **2014**, *25*, 165703.
(166) Zhou, X. Y.; Wang, R.; Meng, L. J.; Xu, X. Y.; Hu, J. G.; Pan, J. Achieving Half-Metallicity in Zigzag MoS_2 Nanoribbon with a Sulfur Vacancy by Edge Passivation. *J. Phys. D: Appl. Phys.* **2018**, *51*, 265005.
(167) Pan, M.; Girão, E. C.; Jia, X.; Bhaviripudi, S.; Li, Q.; Kong, J.; Meunier, V.; Dresselhaus, M. S. Topographic and Spectroscopic Characterization of Electronic Edge States in CVD Grown Graphene Nanoribbons. *Nano Lett.* **2012**, *12*, 1928−1933.
(168) Li, H.; Zhang, Q.; Yap, C. C. R.; Tay, B. K.; Edwin, T. H. T.; Olivier, A.; Baillargeat, D. From Bulk to Monolayer MoS_2: Evolution of Raman Scattering. *Adv. Funct. Mater.* **2012**, *22*, 1385−1390.
(169) Mendes, R. G.; Pang, J.; Bachmatiuk, A.; Ta, H. Q.; Zhao, L.; Gemming, T.; Fu, L.; Liu, Z.; Rümmeli, M. H. Electron-Driven In Situ Transmission Electron Microscopy of 2D Transition Metal Dichalcogenides and Their 2D Heterostructures. *ACS Nano* **2019**, *13*, 978−995.
(170) Tian, X.; Kim, D. S.; Yang, S.; Ciccarino, C. J.; Gong, Y.; Yang, Y.; Yang, Y.; Duschatko, B.; Yuan, Y.; Ajayan, P. M.; et al. Correlating the Three-Dimensional Atomic Defects and Electronic Properties of Two-Dimensional Transition Metal Dichalcogenides. *Nat. Mater.* **2020**, *19*, 867−873.
(171) Lee, Y.-H.; Zhang, X.-Q.; Zhang, W.; Chang, M.-T.; Lin, C.-T.; Chang, K.-D.; Yu, Y.-C.; Wang, J. T.-W.; Chang, C.-S.; Li, L.-J.; et al. Synthesis of Large-Area MoS_2 Atomic Layers with Chemical Vapor Deposition. *Adv. Mater.* **2012**, *24*, 2320−2325.
(172) Watanabe, K.; Nagata, T.; Wakayama, Y.; Sekiguchi, T.; Erdélyi, R.; Volk, J. Band-Gap Deformation Potential and Elasticity Limit of Semiconductor Free-Standing Nanorods Characterized in Situ by Scanning Electron Microscope-Cathodoluminescence Nanospectroscopy. *ACS Nano* **2015**, *9*, 2989−3001.
(173) Fabbri, F.; Smith, M. J.; Recht, D.; Aziz, M. J.; Gradečak, S.; Salviati, G. Depth-Resolved Cathodoluminescence Spectroscopy of Silicon Supersaturated with Sulfur. *Appl. Phys. Lett.* **2013**, *102*, 031909.
(174) Kallesøe, C.; Wen, C.-Y.; Booth, T. J.; Hansen, O.; Bøggild, P.; Ross, F. M.; Mølhave, K. In Situ TEM Creation and Electrical Characterization of Nanowire Devices. *Nano Lett.* **2012**, *12*, 2965−2970.
(175) Qi, D.; Han, C.; Rong, X.; Zhang, X.-W.; Chhowalla, M.; Wee, A. T. S.; Zhang, W. Continuously Tuning Electronic Properties of Few-Layer Molybdenum Ditelluride with in Situ Aluminum Modification toward Ultrahigh Gain Complementary Inverters. *ACS Nano* **2019**, *13*, 9464−9472.
(176) Wang, X.; Yao, Z.; Hwang, S.; Pan, Y.; Dong, H.; Fu, M.; Li, N.; Sun, K.; Gan, H.; Yao, Y.; et al. In Situ Electron Microscopy Investigation of Sodiation of Titanium Disulfide Nanoflakes. *ACS Nano* **2019**, *13*, 9421−9430.
(177) Ren, J.; Camacho-Forero, L. E.; Rossi, D.; Park, Y.; Balbuena, P. B.; Son, D. H. In Situ Optical Measurement of the Rapid Li Intercalation and Deintercalation Dynamics in Colloidal 2D Layered TiS_2 Nanodiscs. *Nanoscale* **2016**, *8*, 11248−11255.
(178) Li, F.; Zou, J.; Cao, L.; Li, Z.; Gu, S.; Liu, Y.; Zhang, J.; Liu, H.; Lu, Z. In Situ Study of K^+ Electrochemical Intercalating into MoS_2 Flakes. *J. Phys. Chem. C* **2019**, *123*, 5067−5072.
(179) He, Q.; Lin, Z.; Ding, M.; Yin, A.; Halim, U.; Wang, C.; Liu, Y.; Cheng, H.-C.; Huang, Y.; Duan, X. In Situ Probing Molecular Intercalation in Two-Dimensional Layered Semiconductors. *Nano Lett.* **2019**, *19*, 6819−6826.
(180) Kumar, A.; Sebastian, A.; Das, S.; Ringe, E. In Situ Optical Tracking of Electroablation in Two-Dimensional Transition-Metal Dichalcogenides. *ACS Appl. Mater. Interfaces* **2018**, *10*, 40773−40780.
(181) Sang, X.; Li, X.; Zhao, W.; Dong, J.; Rouleau, C. M.; Geohegan, D. B.; Ding, F.; Xiao, K.; Unocic, R. R. In Situ Edge Engineering in Two-Dimensional Transition Metal Dichalcogenides. *Nat. Commun.* **2018**, *9*, 2051.
(182) Chen, J.; Ryu, G. H.; Zhang, Q.; Wen, Y.; Tai, K.-L.; Lu, Y.; Warner, J. H. Spatially Controlled Fabrication and Mechanisms of Atomically Thin Nanowell Patterns in Bilayer WS_2 Using in Situ High Temperature Electron Microscopy. *ACS Nano* **2019**, *13*, 14486−14499.
(183) Vasu, K.; Yamijala, S. S. R. K. C.; Zak, A.; Gopalakrishnan, K.; Pati, S. K.; Rao, C. N. R. Clean WS_2 and MoS_2 Nanoribbons Generated by Laser-Induced Unzipping of the Nanotubes. *Small* **2015**, *11*, 3916−3920.
(184) Tapasztó, L.; Dobrik, G.; Lambin, P.; Biró, L. P. Tailoring the Atomic Structure of Graphene Nanoribbons by Scanning Tunnelling Microscope Lithography. *Nat. Nanotechnol.* **2008**, *3*, 397−401.
(185) Koós, A. A.; Vancsó, P.; Magda, G. Z.; Osváth, Z.; Kertész, K.; Dobrik, G.; Hwang, C.; Tapasztó, L.; Biró, L. P. STM study of the MoS_2 Flakes Grown on Graphite: A Model System for Atomically Clean 2D Heterostructure Interfaces. *Carbon* **2016**, *105*, 408−415.
(186) Abbas, A. N.; Liu, G.; Liu, B.; Zhang, L.; Liu, H.; Ohlberg, D.; Wu, W.; Zhou, C. Patterning, Characterization, and Chemical Sensing Applications of Graphene Nanoribbon Arrays Down to 5 nm Using Helium Ion Beam Lithography. *ACS Nano* **2014**, *8*, 1538−1546.
(187) Fox, D. S.; Zhou, Y.; Maguire, P.; O'Neill, A.; Ó'Coileáin, C.; Gatensby, R.; Glushenkov, A. M.; Tao, T.; Duesberg, G. S.; Shvets, I. V.; et al. Nanopatterning and Electrical Tuning of MoS_2 Layers with a Subnanometer Helium Ion Beam. *Nano Lett.* **2015**, *15*, 5307−5313.
(188) Liu, X.; Xu, T.; Wu, X.; Zhang, Z.; Yu, J.; Qiu, H.; Hong, J.-H.; Jin, C.-H.; Li, J.-X.; Wang, X.-R.; Sun, L.-T.; Guo, W.; et al. Top-Down Fabrication of Sub-Nanometre Semiconducting Nanoribbons Derived from Molybdenum Disulfide Sheets. *Nat. Commun.* **2013**, *4*, 1776.

https://dx.doi.org/10.1021/acs.chemrev.0c00505
Chem. Rev. 2020, 120, 12563−12591

(189) Huang, W.; Wang, X.; Ji, X.; Zhang, Z.; Jin, C. In-Situ Fabrication of Mo_6S_6-Nanowire-Terminated Edges in Monolayer Molybdenum Disulfide. *Nano Res.* **2018**, *11*, 5849−5857.
(190) Kumar, P.; Horwath, J. P.; Foucher, A. C.; Price, C. C.; Acero, N.; Shenoy, V. B.; Stach, E. A.; Jariwala, D. Direct Visualization of Out-of-Equilibrium Structural Transformations in Atomically Thin Chalcogenides. *npj 2D Materials and Applications* **2020**, *4*, 16.
(191) Wilcoxon, J. P.; Samara, G. A. Strong Quantum-Size Effects in a Layered Semiconductor: MoS_2 Nanoclusters. *Phys. Rev. B: Condens. Matter Mater. Phys.* **1995**, *51*, 7299−7302.
(192) Arul, N. S.; Nithya, V. D. Molybdenum Disulfide Quantum Dots: Synthesis and Applications. *RSC Adv.* **2016**, *6*, 65670−65682.
(193) Zhang, X.; Lai, Z.; Liu, Z.; Tan, C.; Huang, Y.; Li, B.; Zhao, M.; Xie, L.; Huang, W.; Zhang, H. A Facile and Universal Top-Down Method for Preparation of Monodisperse Transition-Metal Dichalcogenide Nanodots. *Angew. Chem., Int. Ed.* **2015**, *54*, 5425−5428.
(194) Tan, C.; Luo, Z.; Chaturvedi, A.; Cai, Y.; Du, Y.; Gong, Y.; Huang, Y.; Lai, Z.; Zhang, X.; Zheng, L.; et al. Preparation of High-Percentage 1T-Phase Transition Metal Dichalcogenide Nanodots for Electrochemical Hydrogen Evolution. *Adv. Mater.* **2018**, *30*, 1705509.
(195) Roy, S.; Neupane, G. P.; Dhakal, K. P.; Lee, J.; Yun, S. J.; Han, G. H.; Kim, J. Observation of Charge Transfer in Heterostructures Composed of $MoSe_2$ Quantum Dots and a Monolayer of MoS_2 or WSe_2. *J. Phys. Chem. C* **2017**, *121*, 1997−2004.
(196) Zhang, S.; Liu, X.; Liu, C.; Luo, S.; Wang, L.; Cai, T.; Zeng, Y.; Yuan, J.; Dong, W.; Pei, Y.; et al. MoS_2 Quantum Dot Growth Induced by S Vacancies in a $ZnIn_2S_4$ Monolayer: Atomic-Level Heterostructure for Photocatalytic Hydrogen Production. *ACS Nano* **2018**, *12*, 751−758.
(197) Wu, H.; Yang, R.; Song, B.; Han, Q.; Li, J.; Zhang, Y.; Fang, Y.; Tenne, R.; Wang, C. Biocompatible Inorganic Fullerene-Like Molybdenum Disulfide Nanoparticles Produced by Pulsed Laser Ablation in Water. *ACS Nano* **2011**, *5*, 1276−1281.
(198) Ou, G.; Fan, P.; Ke, X.; Xu, Y.; Huang, K.; Wei, H.; Yu, W.; Zhang, H.; Zhong, M.; Wu, H.; et al. Defective Molybdenum Sulfide Quantum Dots as Highly Active Hydrogen Evolution Electrocatalysts. *Nano Res.* **2018**, *11*, 751−761.
(199) Srivastava, A.; Sidler, M.; Allain, A. V.; Lembke, D. S.; Kis, A.; Imamoğlu, A. Optically Active Quantum Dots In Monolayer WSe_2. *Nat. Nanotechnol.* **2015**, *10*, 491−496.
(200) Chakraborty, C.; Kinnischtzke, L.; Goodfellow, K. M.; Beams, R.; Vamivakas, A. N. Voltage-Controlled Quantum Light from an Atomically Thin Semiconductor. *Nat. Nanotechnol.* **2015**, *10*, 507−511.
(201) He, Y.-M.; Clark, G.; Schaibley, J. R.; He, Y.; Chen, M.-C.; Wei, Y.-J.; Ding, X.; Zhang, Q.; Yao, W.; Xu, X.; et al. Single Quantum Emitters In Monolayer Semiconductors. *Nat. Nanotechnol.* **2015**, *10*, 497−502.
(202) Koperski, M.; Nogajewski, K.; Arora, A.; Cherkez, V.; Mallet, P.; Veuillen, J. Y.; Marcus, J.; Kossacki, P.; Potemski, M. Single Photon Emitters In Exfoliated WSe_2 structures. *Nat. Nanotechnol.* **2015**, *10*, 503−506.
(203) Lu, X.; Chen, X.; Dubey, S.; Yao, Q.; Li, W.; Wang, X.; Xiong, Q.; Srivastava, A. Optical Initialization of a Single Spin-Valley in Charged WSe_2 Quantum Dots. *Nat. Nanotechnol.* **2019**, *14*, 426−431.
(204) Voiry, D.; Yang, J.; Chhowalla, M. Recent Strategies for Improving the Catalytic Activity of 2D TMD Nanosheets Toward the Hydrogen Evolution Reaction. *Adv. Mater.* **2016**, *28*, 6197−6206.
(205) Zhu, Y.; Peng, L.; Fang, Z.; Yan, C.; Zhang, X.; Yu, G. Structural Engineering of 2D Nanomaterials for Energy Storage and Catalysis. *Adv. Mater.* **2018**, *30*, 1706347.
(206) Kempa, T. J.; Bediako, D. K.; Jones, E. C.; Lieber, C. M.; Nocera, D. G. Facile, Rapid, and Large-Area Periodic Patterning of Semiconductor Substrates with Submicron Inorganic Structures. *J. Am. Chem. Soc.* **2015**, *137*, 3739−3742.
(207) Kempa, T. J.; Bediako, D. K.; Kim, S.-K.; Park, H.-G.; Nocera, D. G. High-Throughput Patterning of Photonic Structures with Tunable Periodicity. *Proc. Natl. Acad. Sci. U. S. A.* **2015**, *112*, 5309−5313.
(208) Lukowski, M. A.; Daniel, A. S.; Meng, F.; Forticaux, A.; Li, L.; Jin, S. Enhanced Hydrogen Evolution Catalysis from Chemically Exfoliated Metallic MoS_2 Nanosheets. *J. Am. Chem. Soc.* **2013**, *135*, 10274−10277.
(209) Li, Y.; Wang, H.; Xie, L.; Liang, Y.; Hong, G.; Dai, H. MoS_2 Nanoparticles Grown on Graphene: An Advanced Catalyst for the Hydrogen Evolution Reaction. *J. Am. Chem. Soc.* **2011**, *133*, 7296−7299.
(210) Tsai, C.; Li, H.; Park, S.; Park, J.; Han, H. S.; Nørskov, J. K.; Zheng, X.; Abild-Pedersen, F. Electrochemical Generation of Sulfur Vacancies in the Basal Plane of MoS_2 for Hydrogen Evolution. *Nat. Commun.* **2017**, *8*, 15113.
(211) Ouyang, Y.; Ling, C.; Chen, Q.; Wang, Z.; Shi, L.; Wang, J. Activating Inert Basal Planes of MoS_2 for Hydrogen Evolution Reaction through the Formation of Different Intrinsic Defects. *Chem. Mater.* **2016**, *28*, 4390−4396.
(212) Gao, G.; Sun, Q.; Du, A. Activating Catalytic Inert Basal Plane of Molybdenum Disulfide to Optimize Hydrogen Evolution Activity via Defect Doping and Strain Engineering. *J. Phys. Chem. C* **2016**, *120*, 16761−16766.
(213) Fang, Z.; Peng, L.; Lv, H.; Zhu, Y.; Yan, C.; Wang, S.; Kalyani, P.; Wu, X.; Yu, G. Metallic Transition Metal Selenide Holey Nanosheets for Efficient Oxygen Evolution Electrocatalysis. *ACS Nano* **2017**, *11*, 9550−9557.
(214) Fang, Z.; Peng, L.; Qian, Y.; Zhang, X.; Xie, Y.; Cha, J. J.; Yu, G. Dual Tuning of Ni-Co-A (A = P, Se, O) Nanosheets by Anion Substitution and Holey Engineering for Efficient Hydrogen Evolution. *J. Am. Chem. Soc.* **2018**, *140*, 5241−5247.
(215) Chen, Z.; Cummins, D.; Reinecke, B. N.; Clark, E.; Sunkara, M. K.; Jaramillo, T. F. Core-shell MoO_3-MoS_2 Nanowires for Hydrogen Evolution: A Functional Design for Electrocatalytic Materials. *Nano Lett.* **2011**, *11*, 4168−4175.
(216) Wang, J.; Wang, W.; Wang, Z.; Chen, J. G.; Liu, C.-j. Porous MS_2/MO_2 (M = W, Mo) Nanorods as Efficient Hydrogen Evolution Reaction Catalysts. *ACS Catal.* **2016**, *6*, 6585−6590.
(217) Shifa, T. A.; Wang, F.; Liu, K.; Cheng, Z.; Xu, K.; Wang, Z.; Zhan, X.; Jiang, C.; He, J. Efficient Catalysis of Hydrogen Evolution Reaction from $WS_{2(1-x)}P_{2x}$ Nanoribbons. *Small* **2017**, *13*, 1603706.
(218) Li, J.; Hong, M.; Sun, L.; Zhang, W.; Shu, H.; Chang, H. Enhanced Electrocatalytic Hydrogen Evolution from Large-Scale, Facile-Prepared, Highly Crystalline WTe_2 Nanoribbons with Weyl Semimetallic Phase. *ACS Appl. Mater. Interfaces* **2018**, *10*, 458−467.
(219) Zheng, Y.-R.; Wu, P.; Gao, M.-R.; Zhang, X.-L.; Gao, F.-Y.; Ju, H.-X.; Wu, R.; Gao, Q.; You, R.; Huang, W.-X.; et al. Doping-Induced Structural Phase Transition in Cobalt Diselenide Enables Enhanced Hydrogen Evolution Catalysis. *Nat. Commun.* **2018**, *9*, 2533.
(220) Aras, M.; Kılıç, Ç.; Ciraci, S. Lateral and Vertical Heterostructures of Transition Metal Dichalcogenides. *J. Phys. Chem. C* **2018**, *122*, 1547−1555.
(221) Bogaert, K.; Liu, S.; Chesin, J.; Titow, D.; Gradečak, S.; Garaj, S. Diffusion-Mediated Synthesis of MoS_2/WS_2 Lateral Heterostructures. *Nano Lett.* **2016**, *16*, 5129−5134.
(222) Zhang, X.-Q.; Lin, C.-H.; Tseng, Y.-W.; Huang, K.-H.; Lee, Y.-H. Synthesis of Lateral Heterostructures of Semiconducting Atomic Layers. *Nano Lett.* **2015**, *15*, 410−415.
(223) Choudhary, N.; Park, J.; Hwang, J. Y.; Chung, H.-S.; Dumas, K. H.; Khondaker, S. I.; Choi, W.; Jung, Y. Centimeter Scale Patterned Growth of Vertically Stacked Few Layer Only 2D MoS_2/WS_2 van der Waals Heterostructure. *Sci. Rep.* **2016**, *6*, 25456.
(224) Sahoo, P. K.; Memaran, S.; Xin, Y.; Balicas, L.; Gutiérrez, H. R. One-Pot Growth of Two-Dimensional Lateral Heterostructures Via Sequential Edge-Epitaxy. *Nature* **2018**, *553*, 63−67.
(225) Susarla, S.; Kutana, A.; Hachtel, J. A.; Kochat, V.; Apte, A.; Vajtai, R.; Idrobo, J. C.; Yakobson, B. I.; Tiwary, C. S.; Ajayan, P. M. Quaternary 2D Transition Metal Dichalcogenides (TMDs) with Tunable Bandgap. *Adv. Mater.* **2017**, *29*, 1702457.
(226) Susarla, S.; Hachtel, J. A.; Yang, X.; Kutana, A.; Apte, A.; Jin, Z.; Vajtai, R.; Idrobo, J. C.; Lou, J.; Yakobson, B. I.; et al. Thermally

https://dx.doi.org/10.1021/acs.chemrev.0c00505
Chem. Rev. 2020, 120, 12563−12591

Induced 2D Alloy-Heterostructure Transformation in Quaternary Alloys. *Adv. Mater.* **2018**, *30*, 1804218.
(227) Li, J.; Yang, X.; Liu, Y.; Huang, B.; Wu, R.; Zhang, Z.; Zhao, B.; Ma, H.; Dang, W.; Wei, Z.; et al. General Synthesis of Two-Dimensional van der Waals Heterostructure Arrays. *Nature* **2020**, *579*, 368−374.
(228) Zhao, G.; Rui, K.; Dou, S. X.; Sun, W. Heterostructures for Electrochemical Hydrogen Evolution Reaction: A Review. *Adv. Funct. Mater.* **2018**, *28*, 1803291.
(229) Voiry, D.; Shin, H. S.; Loh, K. P.; Chhowalla, M. Low-Dimensional Catalysts for Hydrogen Evolution and CO_2 Reduction. *Nat. Rev. Chem.* **2018**, *2*, 0105.
(230) Zhang, N.; Surrente, A.; Baranowski, M.; Maude, D. K.; Gant, P.; Castellanos-Gomez, A.; Plochocka, P. Moiré Intralayer Excitons in a $MoSe_2/MoS_2$ Heterostructure. *Nano Lett.* **2018**, *18*, 7651−7657.
(231) Iannaccone, G.; Bonaccorso, F.; Colombo, L.; Fiori, G. Quantum Engineering of Transistors Based on 2D Materials Heterostructures. *Nat. Nanotechnol.* **2018**, *13*, 183−191.
(232) Zhou, Y.; Dong, J.; Li, H. Electronic Transport Properties of In-Plane Heterostructures Constructed by MoS_2 and WS_2 Nanoribbons. *RSC Adv.* **2015**, *5*, 66852−66860.
(233) Deng, S.; Li, L.; Guy, O. J.; Zhang, Y. Enhanced Thermoelectric Performance of Monolayer MoSSe, Bilayer MoSSe and Graphene/MoSSe Heterogeneous Nanoribbons. *Phys. Chem. Chem. Phys.* **2019**, *21*, 18161−18169.
(234) Yang, Y.; Zhou, Y.; Luo, Z.; Guo, Y.; Rao, D.; Yan, X. Electronic Structures and Transport Properties of SnS-SnSe Nanoribbon Lateral Heterostructures. *Phys. Chem. Chem. Phys.* **2019**, *21*, 9296−9301.
(235) Yang, Z.; Pan, J.; Liu, Q.; Wu, N.; Hu, M.; Ouyang, F. Electronic Structures and Transport Properties of a MoS_2-NbS_2 Nanoribbon Lateral Heterostructure. *Phys. Chem. Chem. Phys.* **2017**, *19*, 1303−1310.
(236) Xie, S.; Tu, L.; Han, Y.; Huang, L.; Kang, K.; Lao, K. U.; Poddar, P.; Park, C.; Muller, D. A.; DiStasio, R. A.; et al. Coherent, Atomically Thin Transition-Metal Dichalcogenide Superlattices with Engineered Strain. *Science* **2018**, *359*, 1131−1136.
(237) Zhang, K.; Bersch, B. M.; Joshi, J.; Addou, R.; Cormier, C. R.; Zhang, C.; Xu, K.; Briggs, N. C.; Wang, K.; Subramanian, S.; et al. 2D Materials: Tuning the Electronic and Photonic Properties of Monolayer MoS_2 via In Situ Rhenium Substitutional Doping. *Adv. Funct. Mater.* **2018**, *28*, 1706950.
(238) Chen, J.; Wu, X.-J.; Gong, Y.; Zhu, Y.; Yang, Z.; Li, B.; Lu, Q.; Yu, Y.; Han, S.; Zhang, Z.; et al. Edge Epitaxy of Two-Dimensional $MoSe_2$ and MoS_2 Nanosheets on One-Dimensional Nanowires. *J. Am. Chem. Soc.* **2017**, *139*, 8653−8660.
(239) Choudhary, N.; Li, C.; Chung, H.-S.; Moore, J.; Thomas, J.; Jung, Y. High-Performance One-Body Core/Shell Nanowire Supercapacitor Enabled by Conformal Growth of Capacitive 2D WS_2 Layers. *ACS Nano* **2016**, *10*, 10726−10735.
(240) Han, Y.; Li, M.-Y.; Jung, G.-S.; Marsalis, M. A.; Qin, Z.; Buehler, M. J.; Li, L.-J.; Muller, D. A. Sub-Nanometre Channels Embedded in Two-Dimensional Materials. *Nat. Mater.* **2018**, *17*, 129−133.
(241) Guo, P.; Xu, J.; Gong, K.; Shen, X.; Lu, Y.; Qiu, Y.; Xu, J.; Zou, Z.; Wang, C.; Yan, H.; et al. On-Nanowire Axial Heterojunction Design for High-Performance Photodetectors. *ACS Nano* **2016**, *10*, 8474−8481.
(242) Zhou, Y.; Dong, J.; Li, H. Multifunctional Heterostructures Constructed Using MoS_2 and WS_2 Nanoribbons. *Phys. Chem. Chem. Phys.* **2016**, *18*, 27468−27475.
(243) Xu, X.; Gabor, N. M.; Alden, J. S.; van der Zande, A. M.; McEuen, P. L. Photo-Thermoelectric Effect at a Graphene Interface Junction. *Nano Lett.* **2010**, *10*, 562−566.
(244) Freitag, M.; Low, T.; Xia, F.; Avouris, P. Photoconductivity of Biased Graphene. *Nat. Photonics* **2013**, *7*, 53−59.
(245) Gan, X.; Shiue, R.-J.; Gao, Y.; Meric, I.; Heinz, T. F.; Shepard, K.; Hone, J.; Assefa, S.; Englund, D. Chip-Integrated Ultrafast Graphene Photodetector with High Responsivity. *Nat. Photonics* **2013**, *7*, 883−887.
(246) Fogler, M. M.; Butov, L. V.; Novoselov, K. S. High-Temperature Superfluidity with Indirect Excitons in van der Waals Heterostructures. *Nat. Commun.* **2014**, *5*, 4555.
(247) Ross, J. S.; Klement, P.; Jones, A. M.; Ghimire, N. J.; Yan, J.; Mandrus, D. G.; Taniguchi, T.; Watanabe, K.; Kitamura, K.; Yao, W.; et al. Electrically Tunable Excitonic Light-Emitting Diodes Based on Monolayer WSe_2 p-n Junctions. *Nat. Nanotechnol.* **2014**, *9*, 268−272.
(248) Lee, H. S.; Min, S.-W.; Chang, Y.-G.; Park, M. K.; Nam, T.; Kim, H.; Kim, J. H.; Ryu, S.; Im, S. MoS_2 Nanosheet Phototransistors with Thickness-Modulated Optical Energy Gap. *Nano Lett.* **2012**, *12*, 3695−3700.
(249) Britnell, L.; Ribeiro, R. M.; Eckmann, A.; Jalil, R.; Belle, B. D.; Mishchenko, A.; Kim, Y. J.; Gorbachev, R. V.; Georgiou, T.; Morozov, S. V.; et al. Strong Light-Matter Interactions in Heterostructures of Atomically Thin Films. *Science* **2013**, *340*, 1311−1314.
(250) Lopez-Sanchez, O.; Lembke, D.; Kayci, M.; Radenovic, A.; Kis, A. Ultrasensitive Photodetectors Based on Monolayer MoS_2. *Nat. Nanotechnol.* **2013**, *8*, 497−501.
(251) Cheng, R.; Li, D.; Zhou, H.; Wang, C.; Yin, A.; Jiang, S.; Liu, Y.; Chen, Y.; Huang, Y.; Duan, X. Electroluminescence and Photocurrent Generation from Atomically Sharp WSe_2/MoS_2 Heterojunction p-n Diodes. *Nano Lett.* **2014**, *14*, 5590−5597.
(252) Lee, C.-H.; Lee, G.-H.; van der Zande, A. M.; Chen, W.; Li, Y.; Han, M.; Cui, X.; Arefe, G.; Nuckolls, C.; Heinz, T. F.; et al. Atomically Thin p-n Junctions with van der Waals Heterointerfaces. *Nat. Nanotechnol.* **2014**, *9*, 676−681.
(253) Baugher, B. W. H.; Churchill, H. O. H.; Yang, Y.; Jarillo-Herrero, P. Optoelectronic Devices Based on Electrically Tunable p-n Diodes in a Monolayer Dichalcogenide. *Nat. Nanotechnol.* **2014**, *9*, 262−267.
(254) Pospischil, A.; Furchi, M. M.; Mueller, T. Solar-Energy Conversion and Light Emission in an Atomic Monolayer p-n Diode. *Nat. Nanotechnol.* **2014**, *9*, 257−261.
(255) Furchi, M. M.; Pospischil, A.; Libisch, F.; Burgdörfer, J.; Mueller, T. Photovoltaic Effect in an Electrically Tunable van der Waals Heterojunction. *Nano Lett.* **2014**, *14*, 4785−4791.
(256) Sze, S. M. L. M-K. *Semiconductor Devices: Physics and Technology*; Wiley, 2012.
(257) Wang, R.; Ruzicka, B. A.; Kumar, N.; Bellus, M. Z.; Chiu, H.-Y.; Zhao, H. Ultrafast and Spatially Resolved Studies of Charge Carriers in Atomically Thin Molybdenum Disulfide. *Phys. Rev. B: Condens. Matter Mater. Phys.* **2012**, *86*, 045406.
(258) Sangwan, V. K.; Hersam, M. C. Neuromorphic Nanoelectronic Materials. *Nat. Nanotechnol.* **2020**, *15*, 517−528.
(259) Sangwan, V. K.; Lee, H.-S.; Bergeron, H.; Balla, I.; Beck, M. E.; Chen, K.-S.; Hersam, M. C. Multi-terminal Memtransistors From Polycrystalline Monolayer Molybdenum Disulfide. *Nature* **2018**, *554*, 500−504.
(260) Kim, M.; Ge, R.; Wu, X.; Lan, X.; Tice, J.; Lee, J. C.; Akinwande, D. Zero-Static Power Radio-Frequency Switches Based on MoS_2 Atomristors. *Nat. Commun.* **2018**, *9*, 2524.
(261) Ge, R.; Wu, X.; Kim, M.; Shi, J.; Sonde, S.; Tao, L.; Zhang, Y.; Lee, J. C.; Akinwande, D. Atomristor: Nonvolatile Resistance Switching in Atomic Sheets of Transition Metal Dichalcogenides. *Nano Lett.* **2018**, *18*, 434−441.
(262) Beck, M. E.; Shylendra, A.; Sangwan, V. K.; Guo, S.; Gaviria Rojas, W. A.; Yoo, H.; Bergeron, H.; Su, K.; Trivedi, A. R.; Hersam, M. C. Spiking Neurons From Tunable Gaussian Heterojunction Transistors. *Nat. Commun.* **2020**, *11*, 1565.
(263) Sundaram, R. S.; Engel, M.; Lombardo, A.; Krupke, R.; Ferrari, A. C.; Avouris, P.; Steiner, M. Electroluminescence in Single Layer MoS_2. *Nano Lett.* **2013**, *13*, 1416−1421.
(264) Withers, F.; Del Pozo-Zamudio, O.; Mishchenko, A.; Rooney, A. P.; Gholinia, A.; Watanabe, K.; Taniguchi, T.; Haigh, S. J.; Geim, A. K.; Tartakovskii, A. I.; et al. Light-Emitting Diodes by Band-Structure Engineering in van der Waals Heterostructures. *Nat. Mater.* **2015**, *14*, 301−306.

https://dx.doi.org/10.1021/acs.chemrev.0c00505
Chem. Rev. 2020, 120, 12563−12591

(265) Zhang, Y. J.; Oka, T.; Suzuki, R.; Ye, J. T.; Iwasa, Y. Electrically Switchable Chiral Light-Emitting Transistor. *Science* **2014**, *344*, 725−728.
(266) Schaibley, J. R.; Yu, H.; Clark, G.; Rivera, P.; Ross, J. S.; Seyler, K. L.; Yao, W.; Xu, X. Valleytronics in 2D Materials. *Nat. Rev. Mater.* **2016**, *1*, 16055.
(267) Tran, T. T.; Bray, K.; Ford, M. J.; Toth, M.; Aharonovich, I. Quantum Emission From Hexagonal Boron Nitride Monolayers. *Nat. Nanotechnol.* **2016**, *11*, 37−41.
(268) Grosso, G.; Moon, H.; Lienhard, B.; Ali, S.; Efetov, D. K.; Furchi, M. M.; Jarillo-Herrero, P.; Ford, M. J.; Aharonovich, I.; Englund, D. Tunable and High-Purity Room Temperature Single-Photon Emission From Atomic Defects in Hexagonal Boron Nitride. *Nat. Commun.* **2017**, *8*, 705.
(269) Dai, Z.; Liu, L.; Zhang, Z. Strain Engineering of 2D Materials: Issues and Opportunities at the Interface. *Adv. Mater.* **2019**, *31*, 1805417.
(270) Bai, Y.; Zhou, L.; Wang, J.; Wu, W.; McGilly, L. J.; Halbertal, D.; Lo, C. F. B.; Liu, F.; Ardelean, J.; Rivera, P. et al. Excitons in Strain-Induced One-Dimensional Moiré Potentials at Transition Metal Dichalcogenide Heterojunctions. *Nat. Mater.* **2020**, DOI: 10.1038/s41563-020-0773-x.
(271) Carmesin, C.; Lorke, M.; Florian, M.; Erben, D.; Schulz, A.; Wehling, T. O.; Jahnke, F. Quantum-Dot-Like States in Molybdenum Disulfide Nanostructures Due to the Interplay of Local Surface Wrinkling, Strain, and Dielectric Confinement. *Nano Lett.* **2019**, *19*, 3182−3186.
(272) Darlington, T. P.; Carmesin, C.; Florian, M.; Yanev, E.; Ajayi, O.; Ardelean, J.; Rhodes, D. A.; Ghiotto, A.; Krayev, A.; Watanabe, K. et al. Imaging Strain-Localized Excitons in Nanoscale Bubbles of Monolayer WSe_2 at Room Temperature. *Nat. Nanotechnol.* **2020**, DOI: 10.1038/s41565-020-0730-5.
(273) Palacios-Berraquero, C.; Barbone, M.; Kara, D. M.; Chen, X.; Goykhman, I.; Yoon, D.; Ott, A. K.; Beitner, J.; Watanabe, K.; Taniguchi, T.; Ferrari, A. C.; Atature, M.; et al. Atomically Thin Quantum Light-Emitting Diodes. *Nat. Commun.* **2016**, *7*, 12978.
(274) Branny, A.; Wang, G.; Kumar, S.; Robert, C.; Lassagne, B.; Marie, X.; Gerardot, B. D.; Urbaszek, B. Discrete Quantum Dot Like Emitters In Monolayer $MoSe_2$: Spatial Mapping, Magneto-Optics, and Charge Tuning. *Appl. Phys. Lett.* **2016**, *108*, 142101.
(275) Liu, X.; Chen, K.-S.; Wells, S. A.; Balla, I.; Zhu, J.; Wood, J. D.; Hersam, M. C. Scanning Probe Nanopatterning and Layer-by-Layer Thinning of Black Phosphorus. *Adv. Mater.* **2017**, *29*, 1604121.
(276) Liu, X.; Hersam, M. C. 2D Materials for Quantum Information Science. *Nat. Rev. Mater.* **2019**, *4*, 669−684.
(277) Clark, G.; Schaibley, J. R.; Ross, J.; Taniguchi, T.; Watanabe, K.; Hendrickson, J. R.; Mou, S.; Yao, W.; Xu, X. Single defect light-emitting diode in a van der Waals heterostructure. *Nano Lett.* **2016**, *16*, 3944−3948.

https://dx.doi.org/10.1021/acs.chemrev.0c00505
Chem. Rev. 2020, 120, 12563−12591